

Diss. ETH No. 17446

Interacting Fermi gases and Bose-Fermi mixtures in optical lattices

A dissertation submitted to the
SWISS FEDERAL INSTITUTE OF TECHNOLOGY
ZURICH

for the degree of
Doctor of Natural Sciences

presented by

KENNETH JOHN GÜNTER

Dipl.-Phys. ETH
Swiss Federal Institute of Technology
Zurich, Switzerland

born 10.04.1978
citizen of Switzerland

accepted on the recommendation of

Prof. Dr. Tilman Esslinger, examiner
Prof. Dr. Manfred Sigrist, co-examiner

2007

To my parents.

Zusammenfassung

Wechselwirkende fermionische Quantengase sind Grundlage zahlreicher Effekte in der Festkörperphysik. Bei den in dieser Arbeit vorgestellten Experimenten wählen wir einen neuen Zugang zur Untersuchung solcher Systeme; wir laden quantenentartete atomare Fermigase und Mischungen aus bosonischen und fermionischen Atomen in dreidimensionale optische Gitter.

Die Wechselwirkung zwischen den Atomen kann in der Umgebung einer Feshbach-Resonanz beliebig zwischen stark repulsiv und stark attraktiv eingestellt werden. Dies erlaubt es, aus Paaren fermionischer Atome schwach gebundene Moleküle im Gitter zu bilden. Durch Anwenden eines tiefen Gitterpotentials kann die atomare Bewegung entweder auf eine Dimension oder auf einen einzelnen Gitterpunkt eingeschränkt werden. Im Falle negativer Streulängen sind die gebundenen Zustände allein durch den Einschluss des optischen Gitters stabilisiert.

Des Weiteren stellen wir erstmals niederdimensionale Fermigase her, die über p -Wellenstreuung wechselwirken. Indem wir den atomaren Spin relativ zur Symmetrieachse des einschliessenden Potentials ausrichten, können wir spezifische asymptotische Streuzustände aufgrund ihres anisotropen Charakters unterdrücken. Dies zeigt sich in der Abwesenheit von Atomverlusten nahe einer p -Wellen-Feshbach-Resonanz. Wir beobachten zudem eine Verschiebung der Position der Resonanz im Vergleich zum dreidimensionalen Fall infolge der erhöhten Grundzustandsenergie.

In Mischungen bosonischer und fermionischer Atome treten zahlreiche exotische Vielteilcheneffekte auf. Wir laden solche Mischungen in dreidimensionale optische Gitter und messen die Phasenkohärenz der bosonischen Wolke, indem wir den Kontrast der Materiewelleninterferenz und die Kohärenzlänge bestimmen. Wir beobachten, dass eine grössere Beimischung der fermionischen Spezies die Kohärenz reduziert. Ausserdem führt die attraktive Wechselwirkung zwischen den beiden Spezies zu einer grösseren lokalen Dichte im Gitter, die wir anhand von Dreikörperstössen nachweisen.

Diese Experimente zeigen die aussergewöhnliche Vielseitigkeit von atomaren Quantengasen in optischen Gittern und bringen die Besonderheiten der Stosswechselwirkung in solchen Potentialen zum Vorschein. Die Realisierung von stark wechselwirkenden Gasen und der direkte Zugang zu niederdimensionalen Systemen eröffnen neue Perspektiven für die Erforschung grundlegender Vielteilchenprobleme in der modernen Quantenphysik.

Abstract

Interacting fermionic quantum gases form the basis of solid state physics. In this thesis we choose a novel approach to explore such systems by creating quantum degenerate atomic Fermi gases and mixtures of bosonic and fermionic atoms in three-dimensional optical lattices. The collisional interaction between the atoms can be arbitrarily tuned between strongly repulsive and strongly attractive in the vicinity of a Feshbach resonance.

This tuneability allows us to create weakly bound molecules from pairs of fermionic atoms confined to one-dimensional motion or trapped in isolated potential wells. For negative scattering lengths the bound states are solely stabilised by the tight confinement of the optical lattice.

In a further experiment we realise low-dimensional p -wave interacting Fermi gases for the first time. By properly aligning the atomic spins with respect to the symmetry axis of the confining potential we can prohibit specific asymptotic scattering states due to their anisotropic character. The suppressed scattering manifests itself in the absence of atom losses close to the corresponding p -wave Feshbach resonance. We also observe a shift of the resonance position with respect to the three-dimensional case which is a consequence of the increased ground state energy.

A range of new phenomena becomes accessible when a mixture of bosonic and fermionic atoms is prepared. We load Bose-Fermi mixtures into three-dimensional optical lattices and probe the phase coherence of the bosonic cloud by means of the visibility of the matter wave interference pattern and the coherence length. We observe that an increasing admixture of the fermionic species diminishes the coherence. Moreover, the attractive interspecies interaction leads to an enhanced bosonic density in the lattice, which we measure by studying the three-body recombination.

These experiments demonstrate the unprecedented versatility of atomic quantum gases in optical lattices and reveal the special nature of collisional interactions in these potentials. The realisation of strongly interacting gases and the direct access to low-dimensional systems opens up new perspectives for the investigation of fundamental questions of modern quantum many-body physics.

Contents

1	Introduction	1
2	Degenerate Bose and Fermi gases	5
2.1	Bosons	5
2.1.1	Bose-Einstein condensation of an ideal gas in a harmonic trap . . .	6
2.1.2	The weakly interacting Bose-Einstein condensate	7
2.2	Fermions	10
2.2.1	The ideal Fermi gas in a harmonic trap	10
2.2.2	Interacting fermions	12
3	Optical lattices	15
3.1	Optical dipole potentials	15
3.1.1	The dipole force	16
3.1.2	Periodic potentials	18
3.1.3	Trap parameters	18
3.2	Band structure and Bloch states	20
3.3	Tunnelling in the lowest band	21
3.4	Fermions in an optical lattice	23
3.4.1	The external harmonic confinement	23
3.4.2	Quasi-momentum distribution	25
3.4.3	Momentum distribution	26
3.5	Including interactions: The Fermi-Hubbard model	28
4	Interactions in cold atomic gases	31
4.1	Scattering theory	31
4.2	Emerging length scales	33
4.3	Feshbach resonances	34
4.3.1	Bound state and BCS-BEC crossover	36
4.3.2	Resonances in ^{40}K	37
4.4	Scattering in optical lattices	39
5	Preparation of the quantum degenerate gases	43
5.1	Overview of the cooling cycle	43
5.2	^{87}Rb and ^{40}K and their cooling transitions	44
5.3	Atom sources and MOT	45

5.4	Magnetic trapping and evaporative cooling	46
5.5	Setups for the optical potentials	48
5.5.1	The first setup	48
5.5.2	The new setup	49
6	<i>s</i>-wave interacting fermions and molecules in optical lattices	55
6.1	Fermionic atoms in a three-dimensional optical lattice	55
6.1.1	Experimental procedure	56
6.1.2	Observing Fermi surfaces	56
6.1.3	Redistribution dynamics	58
6.1.4	Interaction induced coupling to higher Bloch bands	59
6.1.5	Conclusions	59
6.2	Confinement-induced molecules in one-dimensional Fermi gases	63
6.2.1	Bound states in quasi-1D systems	63
6.2.2	Molecules and rf-spectroscopy	64
6.2.3	Binding energy spectra	65
6.3	Molecules of fermionic atoms in a three-dimensional optical lattice	69
6.3.1	Two interacting atoms in a harmonic oscillator well	69
6.3.2	Molecule production and detection	70
6.3.3	Binding energy and molecular fraction	70
6.3.4	Thermometry in the lattice	75
7	<i>p</i>-wave interactions in low-dimensional Fermi gases	77
7.1	<i>p</i> -wave scattering	77
7.2	Suppression of scattering by reducing the dimensionality	79
7.3	Preparation of a spin-polarised Fermi gas	81
7.4	Three-dimensional gas	81
7.5	Two-dimensional gas	82
7.6	One-dimensional gas	82
8	Bose-Fermi mixtures in a three-dimensional optical lattice	87
8.1	Bose-Fermi mixtures in atomic quantum gases	87
8.2	Preparing and characterising the mixture in the lattice	88
8.3	Measuring the phase coherence of the superfluid	90
8.4	Adding fermions to the condensate	91
8.5	Fermion-driven condensate depletion	93
8.6	Change of the bosonic site occupation	94
8.7	Conclusions	95
9	Conclusions and outlook	97
9.1	Controlling the interactions of fermions in a lattice	97
9.2	Quantum simulation with fermions	98
9.3	Tuning the interaction between fermions and bosons	99

10 Appendix	101
10.1 Singlet and triplet character of the scattering length	101
10.2 Atomic properties	103
10.2.1 Fermionic potassium ^{40}K	103
10.2.2 Bosonic rubidium ^{87}Rb	103
10.3 Publications	106
Bibliography	107
Acknowledgements	125
Curriculum vitae	127

1 Introduction

Matter at low temperatures exhibits many fascinating properties which are of wide physical and technological interest. Especially intriguing are strongly correlated quantum phases, as for instance the Mott insulating phase or some superfluid phases, which are governed by interaction. Gaining deeper insight into quantum many-body systems and their underlying microscopic mechanism is therefore a central objective of modern physics. This is usually a rather difficult task, however: theoretical models which are believed to describe the relevant features are hard to solve. In addition, testing these models in solid-state systems is often unfeasible since the physical parameters cannot be adjusted independently. For instance, a complete explanation of how high-temperature superconductivity arises has so far eluded scientists, despite intensive research since its discovery in cuprate compounds over 20 years ago [1].

In our experiment we choose a novel approach towards the study of interacting many-body systems in periodic potentials and their quantum phases. We prepare cold atomic Fermi gases and Bose-Fermi mixtures in the artificial crystal structure of an optical lattice. The periodic potential of the crystal is generated by the intensity pattern formed by the interference of counter-propagating laser beams. While this system bears striking resemblance to electrons in a solid crystal, it also provides a very clean setting with unprecedented controllability. All relevant parameters—the lattice filling, the tunnelling amplitude, and the interaction strength—can be tuned in a continuous way, enabling the investigation of static and dynamic properties in different parameter regimes. Cold atoms in optical lattices thus constitute a toolkit to implement and test fundamental many-body models pertinent to solid state physics. In particular, the study of regimes where the interaction energy dominates over the kinetic energy may shed new light on strongly correlated phases which are extremely challenging for condensed matter theory. In this respect, our system can serve as a quantum simulator to reproduce and explore the physics of other quantum systems.

The recent investigation of cold atomic Fermi gases in weakly confining harmonic traps has given new insight into the many-body physics of fermions. In the strongly interacting regime, for instance, the character of superfluidity in the BCS-BEC crossover has been studied extensively [2, 3, 4, 5]. This thesis describes the first experiments carried out with quantum degenerate fermions in optical lattices with the additional freedom of a tuneable interaction strength. Previous studies have been restricted to ideal fermions in one-dimensional lattices, where many particles reside in the same potential minimum [6]. In our setup we are able to load ^{40}K atoms into a three-dimensional lattice and directly image the Fermi surface. We can adjust the filling of the lattice and therefore

observe the dynamics of the transition from a metallic phase to a band insulator, where the lattice sites contain one atom per spin state. These achievements are promising for the exploration of complex many-body quantum states in a lattice.

The objective of gaining insight into the physics of strongly correlated quantum phases demands a precise understanding of the interactions on a microscopic scale. By exploiting a so-called Feshbach resonance we can realise gases with almost any interaction strength, ranging from strongly attractive to strongly repulsive. This allows us to investigate the unique scattering properties in the presence of strong confinement. An optical lattice potential significantly alters the atomic scattering states by introducing new length scales in the system, which have to be compared with those of the interatomic potential.

A manifestation of the influence of the strong confinement on the scattering properties is the existence of novel two-body bound states. Weakly bound diatomic molecules have been produced in harmonic traps by sweeping the magnetic field over a Feshbach resonance to the side where the scattering length is positive [7, 8]. In sharp contrast, a bound state appears also for negative scattering lengths in periodic potentials. In our experiments we form weakly bound molecules in optical lattices of different dimensions, confirming theoretical predictions of their binding energies. The molecules can exhibit bosonic character and play an important role for the realisation of the BCS-BEC crossover in those geometries [9, 10]. Furthermore, the molecule formation efficiency in a deep three-dimensional lattice directly reflects the double occupancy of the lattice sites. Measuring this quantity provides us with a valuable tool to determine the temperature of the Fermi gas in the lattice.

An appealing possibility offered by deep optical lattices is the realisation of low-dimensional systems. The atoms can be trapped in the isolated potential minima of the laser standing wave(s) such that their motion is restricted to the dimensions of weak confinement. The study of p -wave scattering in low dimensions is particularly interesting due to its anisotropic character. Moreover, spin-aligned strongly attracting fermions confined to one-dimensional motion can be mapped to non-interacting bosons (“bosonisation”) and represent the fermionic analogue of a Tonks gas [11]. We load a spin-polarised Fermi gas interacting via the p -wave into an optical lattice for the first time and observe that scattering into states oriented along the direction of strong confinement is kinematically suppressed. Our findings are important for the realisation of exotic p -wave superfluid phases, which have been predicted to occur [12].

The high degree of control over the relevant parameters in these experiments demonstrates that fermionic atoms in optical lattices can be used as a model system for electrons in a solid. We can for instance implement the Fermi-Hubbard model [13], which is essential in solid state physics. It is probably the simplest model that captures the relevant many-body physics of strongly correlated fermions. For repulsive interaction its phase diagram contains a Mott insulating and an antiferromagnetic phase as well as d -wave superconductivity [14]. By accessing the regime of strong interactions we can also study physics beyond the single-band Hubbard model.

The range of accessible phenomena can be extended if bosonic atoms are loaded into the lattice in addition to the fermions. The interplay between two species of fundamentally different quantum statistics in the presence of intra- and interspecies interaction

entails thrilling effects beyond those of purely bosonic or fermionic particles to be discovered. Theorists have already predicted a wealth of strongly correlated quantum phases, including supersolidity [15], boson-induced superfluidity [16] and a polaronic phase [17]. We prepare a Bose-Fermi mixture consisting of bosonic ^{87}Rb and fermionic ^{40}K atoms in a three-dimensional optical lattice, thereby implementing a Bose-Fermi Hubbard Hamiltonian. The coherence properties of the bosonic cloud for different admixtures of fermions and the analysis of three-body losses give valuable information on the mutual interaction effects of the two species.

Ultracold Fermi gases and Bose-Fermi mixtures in optical lattices provide a versatile environment for the exploration of quantum many-body phenomena. The present studies of the interaction specific to these systems are an important step towards the rich world of strongly correlated quantum phases. In the future the excellent control over the system should allow an “engineering” of the many-body wave function.

Outline of this thesis

In the first part of this thesis a brief theoretical framework for Fermi gases in optical lattices is developed. Chapter two covers cold bosonic and fermionic atoms in harmonic traps. Chapter three then treats fermions in optical lattices, while the specific nature of interactions in these systems is pointed out in chapter four.

An overview of our apparatus and the experimental sequence to produce degenerate Fermi gases and Bose-Fermi mixtures in optical lattices is given in chapter five. The modifications in the setup of the optical potentials to optimise the lattice filling are emphasised.

The sixth chapter presents our experiments with ideal and s -wave interacting fermions in optical lattices. Our measurements include the observation of Fermi surfaces, interaction-induced coupling to higher bands, confinement-induced molecules in quasi-1D systems as well as molecule formation in a three-dimensional optical lattice.

In chapter seven I report on our experiments with spin-polarised, p -wave interacting fermions. I show how in low-dimensional systems specific scattering channels can be deliberately suppressed due to the anisotropic character of the interaction.

I describe our measurements with Bose-Fermi mixtures in a three-dimensional optical lattice in chapter eight. The influence of the fermionic admixture on the bosonic phase coherence is investigated.

Finally, I discuss future perspectives for our experimental setup in chapter nine. In addition, I give a review of our latest transport measurements with attractively interacting fermions.

2 Degenerate Bose and Fermi gases

At ultralow temperatures the physics of an ensemble of particles is governed by its quantum statistics, which makes a sharp distinction between bosons and fermions. Indistinguishable particles have a many-body wave function which is either symmetric or antisymmetric under the exchange of two particles. Over half a century ago Wolfgang Pauli unveiled the connection between the quantum statistics and the spin, known as the spin-statistics theorem [18]: The wave function has to be totally antisymmetric for particles with half-integral spin (fermions) and totally symmetric for particles with integral spin (bosons). Although this is popularly understood as a postulate, the anti-commutation relation for fermions and the commutation relation for bosons can be shown to be requisite in the framework of relativistic quantum mechanics [19]. They follow from the requirements that energy must be positive and that observables on different space-time points with a space-like distance commute [20].

In the common system of an atomic gas the quantum statistics has not been revealed before the observation of a Bose-Einstein condensate in 1995 [21, 22]. This breakthrough marked the starting point for a very fruitful research activity in the field of ultracold atomic gases, which is driven by the ambition to gain deeper insight into macroscopic quantum phenomena like superfluidity or superconductivity in complex systems. The study of cold Fermi gases is especially promising since the building blocks of matter around us—electrons, protons and neutrons—are all fermions. However, cooling fermionic alkali atoms to quantum degeneracy is more challenging than cooling bosonic ones due to the limitations set by the Pauli principle. Nevertheless, four years after the realisation of a Bose-Einstein condensate in an atomic gas, a degenerate Fermi gas of potassium atoms was produced for the first time [23], and presently over a dozen of laboratories have reached the degenerate regime with fermionic gases of ^{40}K [23, 24, 25, 26, 27, 28], ^6Li [29, 30, 31, 32, 33, 34], ^3He [35] or ^{173}Yb [36] atoms.

2.1 Bosons

Already in 1925 Einstein predicted, based on a work by Bose on photons, that at low temperatures massive bosonic particles macroscopically occupy the ground state of a given potential and form a coherent matter wave. Today, Bose-Einstein condensates (BECs) are routinely produced and investigated in many laboratories around the world. In most of the experiments presented in this thesis a bosonic cloud is solely used in the preparation sequence to cool the fermionic cloud sympathetically. Only the studies of chapter 8, where the coherence of a BEC in the presence of fermions was probed, actually

involve a Bose gas. The relevant properties in this context are summarised in the present section. For a detailed theoretical description of atomic BECs the reader is referred to refs. [37, 38, 39].

2.1.1 Bose-Einstein condensation of an ideal gas in a harmonic trap

In experiments with ultracold gases the atoms are confined either in a magnetic or an optical trap. At low temperatures the atoms only experience the bottom of the trapping potential which can to very good accuracy be approximated harmonically. In the following we will therefore consider atoms of mass m in a three-dimensional harmonic potential

$$V_{\text{trap}}(\mathbf{r}) = \frac{m}{2} (\omega_x^2 x^2 + \omega_y^2 y^2 + \omega_z^2 z^2), \quad (2.1)$$

where $\mathbf{r} = (x, y, z)$ and ω_x , ω_y and ω_z are the trapping frequencies in the x -, y - and z -direction, respectively. We also define the characteristic trapping frequency $\bar{\omega} = (\omega_x \omega_y \omega_z)^{1/3}$. The energy levels of this system are characterised by the quantum numbers $\{n_x, n_y, n_z\}$ and are given by

$$\epsilon_{n_x, n_y, n_z} = \left(\frac{1}{2} + n_x\right) \hbar \omega_x + \left(\frac{1}{2} + n_y\right) \hbar \omega_y + \left(\frac{1}{2} + n_z\right) \hbar \omega_z, \quad (2.2)$$

with \hbar being the reduced Planck constant.

In the grand-canonical ensemble the quantum statistics of bosonic particles is described by the Bose-Einstein occupation number [40]

$$f_{\text{BE}}(E) = \frac{1}{e^{(E-\mu)/k_B T} - 1}. \quad (2.3)$$

Here, μ is the chemical potential, T the temperature and k_B the Boltzmann constant. $f_{\text{BE}}(E)$ is the statistical probability for a boson to occupy a state with energy E . The total particle number is obtained by summing the occupation number (2.3) over the discrete energy spectrum (2.2). It is convenient to split off the population N_0 of the ground state with energy $\epsilon_0 \equiv \epsilon_{0,0,0} = \frac{1}{2} \hbar (\omega_x + \omega_y + \omega_z)$ and to write

$$N = \frac{1}{e^{(\epsilon_0 - \mu)/k_B T} - 1} + \sum_{n_x n_y n_z \neq 0} \frac{1}{e^{(\epsilon_{n_x, n_y, n_z} - \mu)/k_B T} - 1} = N_0 + N_T, \quad (2.4)$$

where N_T denotes the number of thermal atoms in higher lying energy states. At low values of the chemical potential μ the ground state occupation N_0 is on the order of one. However, upon increasing μ —for example by adding particles to the system at constant temperature— N_0 will diverge as the maximum value $\mu \rightarrow \epsilon_0$ is reached, while the number of atoms in the excited states N_T remains finite. This is the origin of Bose-Einstein condensation where the ground state occupation becomes macroscopically large, i. e. on the order of the total number of atoms N . Temperatures in typical experiments are much higher than the level spacing of the harmonic trap, $k_B T \gg \hbar \bar{\omega}$. The sum over

the discrete single-particle spectrum in expression (2.4) may therefore be replaced by an integral over a continuum whose density of states is

$$\rho(E) = \int d\mathbf{r} \frac{d\mathbf{p}}{(2\pi\hbar)^3} \delta\left(E - \frac{\mathbf{p}^2}{2m} - V_{\text{trap}}(\mathbf{r})\right) = \frac{1}{2} \frac{E^2}{(\hbar\bar{\omega})^3} \quad (2.5)$$

(semi-classical approximation). Very close to or below the phase transition one may set $\mu = \epsilon_0$ [39] and the integration yields the number of thermal atoms

$$N_T = \int_{\epsilon_0}^{\infty} dE \frac{\rho(E)}{e^{(E-\epsilon_0)/k_B T} - 1} = \frac{1}{2(\hbar\bar{\omega})^3} (k_B T)^3 \Gamma(3) \zeta(3), \quad (2.6)$$

where the integral has been replaced by the product of the Gamma function $\Gamma(s) = \int_0^{\infty} dt t^{s-1} e^{-t}$ and the Riemann Zeta function $\zeta(s) = \Gamma(s)^{-1} \int_0^{\infty} d\varepsilon \varepsilon^{s-1} / (\exp(\varepsilon) - 1)$. The critical temperature T_c for the BEC phase transition, at which the ground state just starts to become macroscopically populated, is now found by equating eqn. (2.6) with the total atom number, $N = N_T$. Evaluating $\Gamma(3) = 2$ the result reads

$$k_B T_c = \left(\frac{N}{\zeta(3)} \right)^{1/3} \hbar\bar{\omega}, \text{ with } \zeta(3) = 1.202... \quad (2.7)$$

Below T_c eqns (2.6) and (2.7) can be applied to determine the condensate fraction

$$\frac{N_0}{N} = 1 - \frac{N_T}{N} = 1 - \left(\frac{T}{T_c} \right)^3. \quad (2.8)$$

2.1.2 The weakly interacting Bose-Einstein condensate

In real Bose gases the interaction between atoms cannot be neglected in the physical description of the gas. Typically, weak interactions dominate the physics by affecting the phase space distribution and the excitation spectrum of the condensate. A striking consequence is the appearance of superfluidity, one of the most fascinating quantum phenomena that can be observed macroscopically. These topics, starting with the Gross-Pitaevskii equation which successfully describes weakly interacting Bose-Einstein condensates, will be addressed in this section.

The Gross-Pitaevskii equation and the Thomas-Fermi limit

The many-body problem of interacting condensed bosons can be appreciably simplified if the interactions are weak, as is normally the case in experiments. Starting from the Schrödinger equation in second quantisation two major steps are taken [39]. First, the interatomic potential is modelled by an effective potential parameterised by the scattering length a which allows the application of the Born approximation (see chapter 4). The interactions are then characterised by the mean-field coupling constant $g = 4\pi\hbar^2 a/m$. Second, the bosonic field operator $\hat{\Psi}(\mathbf{r}) = \phi_0(\mathbf{r})\hat{a}_0 + \sum_{i \neq 0} \phi_i(\mathbf{r})\hat{a}_i$ is replaced by the classical field $\Psi_0(\mathbf{r}) = \sqrt{N_0}\phi_0(\mathbf{r})$ for the ground state mode. This Bogoliubov prescription

corresponds to neglecting the non-commutability of the field operator, which is reasonable at low temperatures where the ground state is occupied by a large number $N_0 \gg 1$ of bosons. We then arrive at the illustrious time-dependent Gross-Pitaevskii equation describing a weakly interacting condensate

$$i\hbar \frac{\partial}{\partial t} \Psi_0(\mathbf{r}, t) = \left(-\frac{\hbar^2 \nabla^2}{2m} + V_{\text{trap}}(\mathbf{r}, t) + g|\Psi_0(\mathbf{r}, t)|^2 \right) \Psi_0(\mathbf{r}, t). \quad (2.9)$$

Despite the similarity to a Schrödinger equation, eqn. (2.9) describes a classical field $\Psi_0(\mathbf{r}, t)$, which plays the role of the condensate wave function and is the order parameter of the system. It is straightforward to show that the time dependence of the stationary solution is governed by the chemical potential $\mu = \partial E / \partial N$, with $\Psi_0(\mathbf{r}, t) = \Psi_0(\mathbf{r}) e^{-i\mu t / \hbar}$. Inserting this into eqn. (2.9) leads to the time-independent Gross-Pitaevskii equation

$$\left(-\frac{\hbar^2 \nabla^2}{2m} + V_{\text{trap}}(\mathbf{r}) - \mu + g|\Psi_0(\mathbf{r})|^2 \right) \Psi_0(\mathbf{r}) = 0. \quad (2.10)$$

From atom number conservation $N_0 = \int d\mathbf{r} |\Psi_0(\mathbf{r})|^2$ we can deduce the condensate density $n_0(\mathbf{r}) = |\Psi_0(\mathbf{r})|^2$.

A further simplification can be made in the so-called Thomas-Fermi limit: The kinetic energy term is neglected if it is small compared to the interaction term, which leads to a simple formula for the density distribution:

$$n_{\text{TF}}(\mathbf{r}) = \frac{1}{g} (\mu_{\text{TF}} - V_{\text{trap}}(\mathbf{r})), \quad (2.11)$$

where the ground state chemical potential $\mu_{\text{TF}} = \frac{\hbar\bar{\omega}}{2} (15Na/a_{\text{ho}})^{2/5}$, with $a_{\text{ho}} = \sqrt{\hbar/m\bar{\omega}}$ the harmonic oscillator length, is calculated within the Bogoliubov theory (see below). The condensate—having the shape of an inverted parabola—reflects the trapping potential, while the remaining thermal atoms have a Gaussian profile leading to a bimodal total distribution. During expansion the condensate will eventually reverse its aspect ratio due to the mean-field interaction $U_{\text{MF}} = gn_{\text{TF}}$ which acts as an additional potential that is proportional to the density [41].

Coherence and superfluidity

Above we have seen that in a BEC all the atoms occupy the ground state, and we may write the condensate wave function as

$$\Psi_0 = \sqrt{n_0} e^{iS}, \quad (2.12)$$

up to a constant phase factor, with S being a real number. This reflects the fact that all the atoms in the condensate have the same phase and form a coherent matter wave, a property which was demonstrated in an eminent interference experiment [42]. The coherence manifests itself in the long-range order of the one-body density matrix $n^{(1)}(\mathbf{r}, \mathbf{r}') = \langle \hat{\Psi}^\dagger(\mathbf{r}) \hat{\Psi}(\mathbf{r}') \rangle$, which remains finite at large distances $|\mathbf{r} - \mathbf{r}'|$ [43].

Contrary to the phase coherence, which also emerges in an ideal gas, superfluidity is only enabled by interactions. Superfluid flow without dissipation requires an excitation spectrum $\epsilon(\mathbf{p})$ defining a finite critical velocity

$$v_c = \min_{\mathbf{p}} \frac{\epsilon(\mathbf{p})}{p}. \quad (2.13)$$

In a fluid flowing with velocity v relative to a potential the creation of an excitation with momentum \mathbf{p} is then energetically unfavourable (in the frame of the static potential) if Landau's criterion,

$$v < v_c, \quad (2.14)$$

is satisfied. As shown below, in a weakly interacting BEC these requirements can indeed be met and the superfluid velocity is identified with the gradient of the phase of the order parameter, $v_s = \frac{\hbar}{m} \nabla S$ [39].

Bogoliubov excitations and quantum depletion

The excitation spectrum of the weakly interacting gas can be obtained within the Bogoliubov prescription mentioned above. In the interaction term of the Hamiltonian one retains the quadratic terms of the particle operator $\hat{a}_{\mathbf{p}}$ with momentum $\mathbf{p} \neq 0$ [39]. This corresponds to going one order beyond the Born approximation of the interatomic potential. After applying the so-called Bogoliubov transformation $\hat{a}_{\mathbf{p}} \rightarrow \hat{b}_{\mathbf{p}}$ the original system of interacting particles is described by a Hamiltonian of non-interacting quasi-particles $\hat{b}_{\mathbf{p}}$. Diagonalisation is then straightforward and leads to the dispersion relation

$$\epsilon(p) = \sqrt{\frac{gn}{m}p^2 + \left(\frac{p^2}{2m}\right)^2}. \quad (2.15)$$

Long-wavelength excitations ($p \ll mc$) are phonon-like, $\epsilon(p) \simeq cp$, with a sound velocity $c = \sqrt{gn/m}$. The critical velocity (2.13) below which the condensate flows without dissipation is determined to be $v_c = c$, showing that the condensate is indeed superfluid.

In the presence of interactions quantum fluctuations will deplete the condensate, even at $T = 0$. Reversing the Bogoliubov transformation to calculate $n_0 = \langle \hat{a}_{\mathbf{p}=0}^\dagger \hat{a}_{\mathbf{p}=0} \rangle$ yields the condensate density

$$n_0 = n \left(1 - \frac{8}{3\sqrt{\pi}} \sqrt{na^3} \right), \quad (2.16)$$

where n is the total density. The reduction of the condensed fraction is fixed by the parameter $\sqrt{na^3}$ and is called quantum depletion.

2.2 Fermions

Electrically neutral alkali atoms with an even mass number are composed of an uneven number of electrons, protons and neutrons. They therefore possess a half-integral total spin and are fermions obeying Fermi-Dirac statistics [40]

$$f_{\text{FD}}(E) = \frac{1}{e^{(E-\mu)/k_B T} + 1}. \quad (2.17)$$

Comparing this function with the bosonic occupation number (2.3) the only difference is the sign in the denominator. Yet, at low temperatures this has striking consequences, as is illustrated by the example of liquid helium. While the bosonic species ^4He undergoes Bose-Einstein condensation and becomes superfluid at 2.17 K, this is not possible for the fermionic isotope ^3He . Although ^3He is also superfluid below ~ 1 mK, the microscopic mechanism is completely different. In fact, at weak attractive interactions the fermions form Cooper pairs, which are bosonic in nature and ultimately condense.

In this chapter the main properties of normal (not superfluid) Fermi gases trapped in a harmonic potential are described.

2.2.1 The ideal Fermi gas in a harmonic trap

Any quantum-mechanical ensemble of fermions must obey Pauli's exclusion principle. It states that indistinguishable atoms cannot occupy the same state, which follows directly from the spin-statistics theorem. At $T = 0$ N atoms with equal spin thus populate the N lowest energy levels up to the so-called Fermi energy E_F (ground state). The Fermi energy also defines the Fermi wave number by $\hbar^2 k_F^2 / (2m) = E_F$, which sets the smallest length scale $\sim k_F^{-1}$ in the system.

The calculation of physical quantities of the gas in equilibrium is most conveniently carried out in a local density approximation (LDA) [39]. This is equivalent to a semi-classical approach where the quantised energy levels of the potential are incorporated in a density of states, similar to the case of thermal bosons in paragraph 2.1.1. In the LDA or Thomas-Fermi approximation [44] one introduces the distribution function

$$f_{\text{TF}}(\mathbf{r}, \mathbf{p}) = \frac{1}{e^{(\mathbf{p}^2/2m + V_{\text{trap}}(\mathbf{r}) - \mu)/k_B T} + 1}. \quad (2.18)$$

Accordingly, the gas is assumed to have locally the same properties as the homogeneous gas at temperature T with a chemical potential $\mu_{\text{LDA}} = \mu - V_{\text{trap}}$ and a local Fermi wave vector $k_0(\mathbf{r})$ defined by $\mu_{\text{LDA}} = \hbar^2 k_0(\mathbf{r})^2 / 2m$ [45]. This requires the external potential to vary weakly over the correlation length $\sim k_0^{-1}$ of the homogeneous gas, which is admissible for large (and not too anisotropic) systems whose typical dimensions R_x , R_y and R_z fulfill the conditions $1/k_0(\mathbf{r}) \ll R_x, R_y, R_z$. At the borders of a trapped cloud, where k_0 tends to zero, the approximation fails to give accurate results.

The chemical potential $\mu(N, T)$ is fixed by the normalisation condition for the total

particle number. Employing the density of states (2.5) to integrate over energy, it reads

$$N = \frac{1}{(2\pi\hbar)^3} \int d\mathbf{r} d\mathbf{p} f_{\text{TF}}(\mathbf{r}, \mathbf{p}) = \int_0^\infty dE \rho(E) f_{\text{FD}}(E) = \frac{1}{2(\hbar\bar{\omega})^3} \int_0^\infty dE \frac{E^2}{e^{(E-\mu)/k_B T} + 1}. \quad (2.19)$$

While this equation is generally solved numerically, analytical solutions can be derived

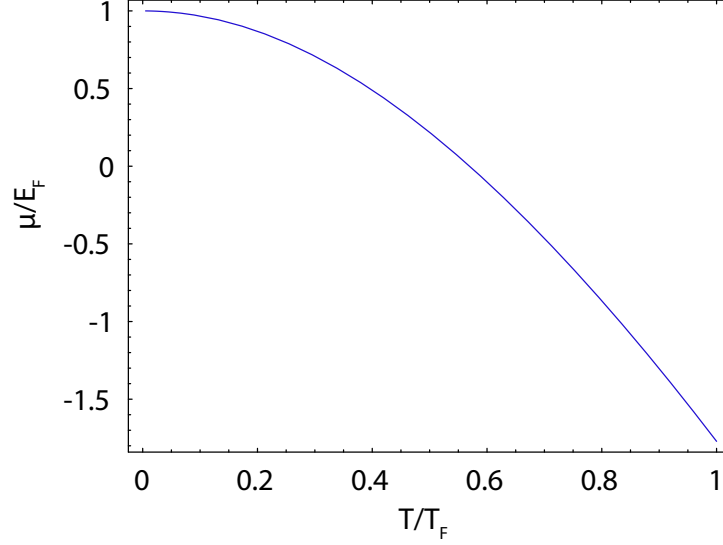


Figure 2.1: The normalised chemical potential μ/E_F of non-interacting fermions in a harmonic trap as a function of the reduced temperature T/T_F . The curve was calculated by numerically solving eqn. (2.19).

in the limits $T \ll T_F$ and $T \gg T_F$ [44], where $T_F = E_F/k_B$ is the Fermi temperature. In Fig. 2.1 the chemical potential in units of the Fermi energy is plotted as a function of the reduced temperature T/T_F . For values $T/T_F \gtrsim 0.55$ it is negative because adding particles at constant entropy will effectively annihilate holes fairly deep in the Fermi sea such that the energy in the system decreases. Expression (2.19) also delivers the Fermi energy by means of its definition

$$E_F \equiv \mu(T = 0) = (6N)^{1/3} \hbar\bar{\omega}. \quad (2.20)$$

Typical values of the Fermi temperature T_F for $N = 10^5$ atoms in our experiment (trapping frequencies $\bar{\omega} \sim 2\pi \cdot 100$ Hz) are a few hundred nK.

For $T = 0$ it is straightforward to calculate the physical quantities of the ideal gas. With the total energy $E = \int_0^\infty dE E \rho(E) f_{\text{FD}}(E) = (6N)^{4/3} \hbar\bar{\omega}/8$ the average energy per atom evaluates to

$$\frac{E}{N} = \frac{3}{4} E_F. \quad (2.21)$$

The extension of the cloud in each direction $i = x, y, z$, the so-called Thomas-Fermi lengths R_i , can be determined by setting $E_F = V_{\text{trap}}(R_i)$. One finds

$$R_i^{T=0} = (48N)^{1/6} \sqrt{\frac{\hbar}{m\omega_i}}. \quad (2.22)$$

Experimentally physical quantities describing the Fermi gas are most often obtained by measuring the spatial distribution of the atoms with absorption imaging. The cloud—either in the trap or after some expansion time—is illuminated with a resonant laser beam with a weak intensity I_0 , and its transmission $I/I_0 = e^{-OD}$ is measured on a CCD (Charge-Coupled Device) camera. The optical density OD at each position is proportional to the atomic column density. From theoretical fits to the measured distribution (which is integrated along the line of sight) the total atom number and the temperature are inferred. The atomic density and momentum distributions in the trap are calculated by integrating the function (2.18) over momentum or position space, respectively. These integrals can be brought to the form

$$\int_0^\infty d\varepsilon \frac{\varepsilon^s}{z^{-1}e^\varepsilon + 1} = -\Gamma(s+1)\text{Li}_{s+1}(z) \quad (2.23)$$

with $s = 1/2$, where $\text{Li}_s(z)$ is the polylogarithmic function (also called Fermi-Dirac integral). For the density distribution one finds

$$n(\mathbf{r}) = \int \frac{d\mathbf{p}}{(2\pi\hbar)^3} f_{\text{TF}}(\mathbf{r}, \mathbf{p}) = -\frac{1}{4\pi^2} \left(\frac{2k_B T m}{\hbar^2} \right)^{3/2} \Gamma(3/2) \text{Li}_{3/2}(-\tilde{z}(\mathbf{r}, T)) \quad (2.24)$$

with $\tilde{z}(\mathbf{r}, T) = \exp \frac{\mu(N, T) - m/2(x^2\omega_x^2 + y^2\omega_y^2 + z^2\omega_z^2)}{k_B T}$. Equivalently, integration over position space yields the momentum distribution

$$n(\mathbf{p}) = \int \frac{d\mathbf{r}}{(2\pi\hbar)^3} f_{\text{TF}}(\mathbf{r}, \mathbf{p}) = -\frac{1}{4\pi^2} \left(\frac{2k_B T}{\hbar^2 \bar{\omega}^2 m} \right)^{3/2} \Gamma(3/2) \text{Li}_{3/2}(-\tilde{z}(\mathbf{p}, T)) \quad (2.25)$$

with $\tilde{z}(\mathbf{p}, T) = \exp [(\mu(N, T) - \mathbf{p}^2/2m)/k_B T]$. The shape of both distributions, (2.24) and (2.25), is determined by the function $\text{Li}_{3/2}(-\tilde{z})$, as shown in Fig. 2.2. As a consequence of the semi-classical behaviour the cloud is isotropic in momentum space; a non-interacting cloud of fermions looks spherical in time-of-flight absorption imaging.

In a gas with more than one spin component the quantities derived above hold for each component separately. For instance, if interactions are neglected, an equal spin mixture of spin up and spin down atoms is denser and smaller than a spin-polarised sample containing the same total number of atoms at the same temperature.

2.2.2 Interacting fermions

In contrast to a spin-polarised Fermi gas, in a spin mixture of ultracold fermionic atoms particles in different spin states can interact via s -wave scattering. In the experiments discussed in this thesis, spin mixtures are usually composed of two clouds in different

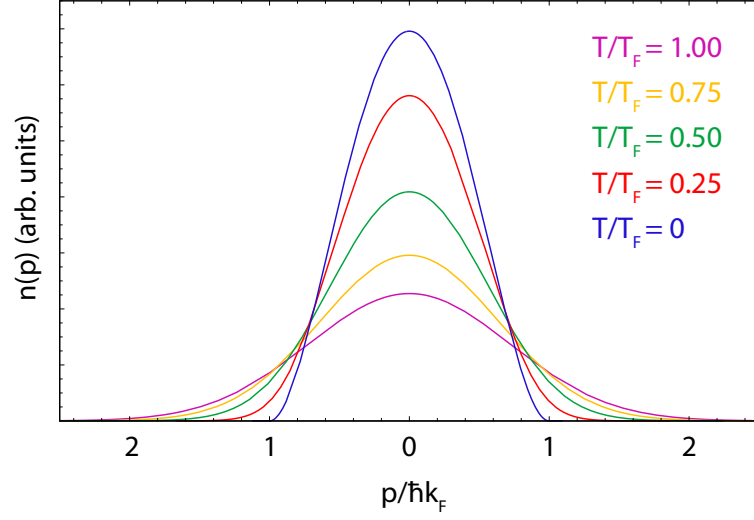


Figure 2.2: The momentum distribution of non-interacting fermions in a harmonic trap for different temperatures T . The plot shows a central cut through the density integrated along the line of sight.

magnetic hyperfine states with equal atom number. For such a gas the ratio of the expectation value of the interaction energy in the ground state of the ideal gas E_{int} to the corresponding value of the harmonic potential E_{ho} is [39]

$$\frac{E_{\text{int}}}{E_{\text{ho}}} = 0.29 k_F a. \quad (2.26)$$

Accordingly, the relevance of the interaction in a harmonic trap is determined by the dimensionless parameter $k_F a$. If this quantity is small the equilibrium distributions do not change much compared to the non-interacting case. Using a contact potential, mean-field theory has been applied to a Fermi gas in a harmonic trap [46]. Generally, interacting fermions in the normal state are described by Landau's theory of Fermi liquids [47]. According to this, when the interaction is turned on, a fermion disturbs the surrounding ones locally, forming together with the disturbance a quasi-particle. The (interacting) quasi-particles have the same spin and momentum as the initially non-interacting fermions, and their number is equal [48]. They therefore behave very similarly to non-interacting fermions which makes their description rather simple. This picture is valid under the assumption that no symmetry-breaking phase transition occurs under the influence of the interaction. The one-dimensional analogue of a Fermi liquid is the Luttinger liquid [49, 50] with its characteristic spin-charge separation [51].

As we will see in chapter 4, the scattering length in cold atomic gases can be adjusted in the vicinity of a Feshbach resonance by means of a magnetic field, providing access to the strongly interacting regime ($k_F a \gtrsim 1$). Owing to the Fermi pressure, a cloud of fermionic atoms is stable also for attractive interactions, in contrast to a Bose-Einstein condensate [52]. Superfluidity of fermionic atoms as well as of weakly bound diatomic

molecules can therefore be studied. In potassium this has been done in the experiments of refs. [2, 53].

In the following chapter 3 I discuss Fermi gases in optical lattices, where the importance of interactions in a two-component spin mixture can be significantly enhanced.

3 Optical lattices

The concept of creating lattice potentials with light goes back to an idea by Letokhov who proposed in 1968 to narrow the Doppler width of spectral lines by subjecting the atoms to the potential produced by a standing laser wave [54, 55]. In the early days of cold atom physics, standing light waves were mainly employed in laser cooling methods, where dissipative light forces require frequencies close to the atomic resonance [56]. Meanwhile, the study of quantum degenerate gases confined in the potential of far-detuned optical lattices has become an important branch of cold atom research [57].

A major motivation of this activity is the exploration of systems reminiscent of solid state physics. Fermionic atoms are especially promising in this respect because of their similarity to electrons in a solid crystal. In contrast to a solid, however, the parameters of an optical crystal are tuneable, making fermionic atoms in optical lattices an ideal playground to test and simulate fundamental models from solid state theory. One can therefore hope to get new insight into interesting phenomena, as for instance insulating behaviour, magnetic order or superconductivity. Another intriguing possibility is the realisation and study of low-dimensional systems by employing deep optical lattices. A two-dimensional lattice, for instance, produces an array of potential tubes as shown in Fig. 3.1. If the atomic motion in the strongly confined dimensions of the tubes is “frozen out”, one effectively deals with an array of one-dimensional systems [58].

Ideal Fermi gases subject to a single standing wave have been studied in the group of Inguscio [6]. Our experiments are the first ones carried out with interacting fermions and Bose-Fermi mixtures in one-, two- and three-dimensional lattices. In this chapter some basics for the theoretical description of such systems are developed. We will first derive an expression for the dipole force and then address the subject of atoms in periodic potentials, including interactions and the external trapping confinement.

3.1 Optical dipole potentials

Alkali atoms in the intensity gradient of a laser beam far-detuned from the atomic resonance are subject to the conservative light force, called the dipole force, making it possible to confine atoms in the potential of focused laser beams. In 1986, long before far-detuned optical lattices were used, Steven Chu and collaborators trapped cold sodium atoms for the first time in a tightly focused beam [59]. Since then the far-off resonant trap (FORT) has become a widely used tool to trap and cool atoms. Evaporative cooling by lowering the laser intensity has allowed to reach Bose-Einstein condensation [60] as well as degeneracy in a Fermi gas [31] in an all-optical way. Compared to magnetic



Figure 3.1: An array of tube potentials is created by a deep two-dimensional lattice. If the transverse ground state of a tube is populated only, the system is effectively one-dimensional.

traps, optical potentials have the great advantage of being independent of the magnetic sub-state, allowing for the trapping of atoms in high-field seeking states (see chapter 5). This is essential in order to access Feshbach resonances which typically occur between such states.

3.1.1 The dipole force

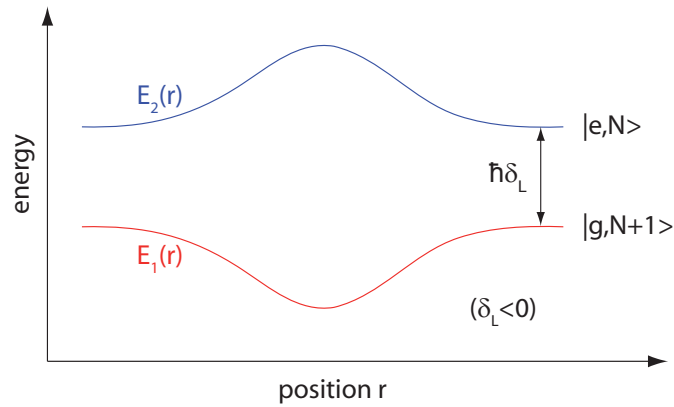


Figure 3.2: Light shifts in a two-level system and a laser beam with a Gaussian intensity profile red-detuned from the atomic resonance.

To illustrate how the dipole force arises, we will calculate it here in the dressed state picture for the simple case of a two-level atom [61, 62]. Depending on the actual

parameters, several assumptions can be made in order to determine realistic experimental parameters. The different approaches are covered in the review of ref. [63].

Consider an atom in a laser beam with intensity $I(\mathbf{r})$ and frequency $\omega_L = \omega_0 + \delta_L$ detuned by δ_L from the atomic resonance ω_0 . We start with the two unperturbed states $|g, N+1\rangle$ and $|e, N\rangle$ describing an atom in the ground state with $N+1$ photons present and an atom in the excited state with N photons present, respectively. The laser field couples these states, which in the dipole approximation is expressed by the operator $\hat{H}_{\text{dip}} = -\hat{\mathbf{d}} \cdot \hat{\mathbf{E}}$, where $\hat{\mathbf{E}}$ is the electric field operator and $\hat{\mathbf{d}} = e\hat{\mathbf{r}}$ the electric dipole operator. Coupling to other, non-resonant states, such as $|e, N+1\rangle$ or $|g, N-1\rangle$, will be disregarded (rotating-wave approximation). For the moment we will also neglect spontaneous emission. Setting the zero of energy to lie between the energies of the two unperturbed states (i. e. $\hat{H}_0|g, N+1\rangle = -\hbar\delta_L/2$ and $\hat{H}_0|e, N\rangle = \hbar\delta_L/2$), the Hamiltonian in this basis reads

$$\hat{H} = \hat{H}_0 + \hat{H}_{\text{dip}} = \frac{\hbar}{2} \begin{pmatrix} -\delta_L & \Omega_1(\mathbf{r}) \\ \Omega_1(\mathbf{r}) & \delta_L \end{pmatrix}. \quad (3.1)$$

Here we have defined the Rabi frequency $\Omega_1(\mathbf{r}) = (2/\hbar) |\langle e, N | \hat{H}_{\text{dip}}(\mathbf{r}) | g, N+1 \rangle|$. The eigenvectors of \hat{H} are $|1\rangle = \sin\theta|g, N+1\rangle + \cos\theta|e, N\rangle$ and $|2\rangle = \cos\theta|g, N+1\rangle - \sin\theta|e, N\rangle$ where the angle θ is defined by $\tan 2\theta = -\Omega_1/\delta_L$. These states describe the atoms as being dressed by the photons ('dressed states'), and their energies

$$E_{2,1} \equiv \pm \hbar\Omega(\mathbf{r}) = \pm \hbar\sqrt{\Omega_1^2(\mathbf{r}) + \delta_L^2/4} \quad (3.2)$$

are shifted from the bare energies by the so-called light shift or ac-Stark shift. Due to their spatial dependence they can be regarded as potentials with associated forces $\mathbf{F}_1 = -\mathbf{F}_2 = -\nabla E_1(\mathbf{r}) \propto \nabla I(\mathbf{r})$ (Fig. 3.2). Now, spontaneous emission gives rise to transitions between the two dressed states, occurring randomly on the time scale of the atom's decay rate $\Gamma^{-1} = 3\pi\epsilon_0\hbar c^3/\omega_L^3 \cdot |\langle e | \mathbf{d} | g \rangle|^{-2}$ (c is the velocity of light and ϵ_0 the electric constant) and causes the force to abruptly change sign. The net dipole force is calculated by weighting \mathbf{F}_1 and \mathbf{F}_2 by the average times the atom is found in the corresponding states $|1\rangle$ and $|2\rangle$. These times are proportional to the stationary populations Π_1^{st} and Π_2^{st} , respectively, and we obtain for the dipole force

$$\mathbf{F} = \Pi_1^{\text{st}}\mathbf{F}_1 + \Pi_2^{\text{st}}\mathbf{F}_2 = (\Pi_1^{\text{st}} - \Pi_2^{\text{st}})\mathbf{F}_1 = -\frac{\hbar\delta_L}{4} \frac{\nabla(\Omega_1^2)}{\delta_L^2 + \Omega_1^2/2}. \quad (3.3)$$

In the limit $\Omega_1 \ll \delta_L$ (which is usually true in the experiment) the dipole potential takes the simple form

$$U_{\text{dip}}(\mathbf{r}) = \frac{\hbar\delta_L}{2} \ln \frac{\Omega_1^2 + \delta_L^2}{\delta_L^2} \approx \frac{\hbar}{2} \frac{\Omega_1^2}{\delta_L} = \frac{3\pi c^2}{2\omega_0^3} \frac{\Gamma}{\delta_L} I(\mathbf{r}). \quad (3.4)$$

The dipole potential is proportional to the light intensity $I = 2\epsilon_0 c |\mathbf{E}|^2$ and adopts the sign of the detuning δ_L . Therefore, atoms are attracted to the intensity maximum of a red-detuned laser beam and expelled from a blue-detuned beam.

An important quantity in the context of dipole potentials is the photon scattering rate of an atom which is given by [63]

$$\Gamma_{\text{sc}} = \frac{3\pi c^2}{2\hbar\omega_0^3} \frac{\Gamma^2}{\delta_L^2} I. \quad (3.5)$$

Photon scattering has to be minimised in order to reduce the heating and decoherence of the atoms associated with spontaneous emission.

3.1.2 Periodic potentials

A one-dimensional optical lattice is created by two intersecting laser beams. The interference between the beams leads to a standing wave and produces a potential with a periodicity of $d = \lambda/2$ along the beam axis, where λ is the laser wavelength. In a red-detuned lattice atoms are attracted to the antinodes by the dipole force. The potential depth V_0 is controlled by the light intensity and is usually expressed in units of the atom's recoil energy, $E_r = \hbar^2 k_L^2 / 2m$. \hbar is Planck's constant, $k_L = 2\pi/\lambda$ the wave vector of the lattice laser and m the atomic mass.

Two- or three-dimensional optical lattices are produced by two or three intersecting standing waves. If cross-dimensional interference is to be avoided, the standing waves need to have mutually perpendicular polarisations. Additionally, one can choose differing frequencies so that any residual interference due to imperfect polarisation are averaged out on the timescale of the atomic motion.

Besides the periodic potential the standing waves of an optical lattice also produce a weak external potential, which is due to the geometric shape of the beams. Moreover, in order to provide enough confinement for the atoms, an additional optical or magnetic trap is often used in experiments. The potential inhomogeneity breaks the translational symmetry of the lattice and controls the atomic distribution. However, if the length scale of the additional confinement is much larger than the lattice spacing, we may still consider a homogeneous system when calculating local quantities like nearest-neighbour tunnelling or on-site interaction.

3.1.3 Trap parameters

In our current experimental setup the atoms in the optical lattice are additionally confined by an independent FORT consisting of two perpendicularly intersecting laser beams in the horizontal (x, y) plane. We first derive the parameters of this external trapping potential before we consider the total optical potential including the lattice. We assume that the Gaussian beams of the FORT have equal geometries characterised by the $1/e^2$ radii w_h in the horizontal and w_v in the vertical direction, respectively. The trapping potential of this configuration can be written as

$$V_T(\mathbf{r}) = -V_{T,x} \exp\left(-2\frac{y^2}{w_h^2} - 2\frac{z^2}{w_v^2}\right) - V_{T,y} \exp\left(-2\frac{x^2}{w_h^2} - 2\frac{z^2}{w_v^2}\right) + mgz, \quad (3.6)$$

where $V_{T,x}$ and $V_{T,y}$ are the potential depths of the two beams. The term proportional to the gravitational acceleration g is responsible for a sag z_0 of the atomic cloud with

respect to the vertical beam centre. For strongly confining traps it is given by $z_0 \approx -mgw_v^2 / (4(V_{T,x} + V_{T,y}))$. For distances not far from the cloud's equilibrium position ($x = 0, y = 0, z = z_0$) the potential (3.6) can be approximated to be harmonic:

$$V_T(\mathbf{r}) \simeq \frac{1}{2}m(\omega_{T,x}^2 x^2 + \omega_{T,y}^2 y^2 + \omega_{T,z}^2 (z - z_0)^2). \quad (3.7)$$

For the trapping frequencies one finds

$$\begin{aligned} \omega_{T,x} &= \frac{2}{w_h} \sqrt{\frac{V_{T,y} \exp\left(-2\frac{z_0^2}{w_v^2}\right)}{m}}, \\ \omega_{T,y} &= \frac{2}{w_h} \sqrt{\frac{V_{T,x} \exp\left(-2\frac{z_0^2}{w_v^2}\right)}{m}}, \\ \omega_{T,z} &= \frac{2}{w_v} \sqrt{\frac{(V_{T,x} + V_{T,y}) \left(1 - \frac{4z_0^2}{w_v^2}\right) \exp\left(-2\frac{z_0^2}{w_v^2}\right)}{m}}. \end{aligned} \quad (3.8)$$

Let us now turn to the cubic optical lattice created by three mutually perpendicular red-detuned standing waves with equal $1/e^2$ waists w_L . Its dipole potential reads

$$\begin{aligned} V_L(\mathbf{r}) = & -V_{L,x} \exp\left(-2\frac{y^2+z^2}{w_L^2}\right) \sin^2(k_L x) \\ & -V_{L,y} \exp\left(-2\frac{x^2+z^2}{w_L^2}\right) \sin^2(k_L y) \\ & -V_{L,z} \exp\left(-2\frac{x^2+y^2}{w_L^2}\right) \sin^2(k_L z). \end{aligned} \quad (3.9)$$

Since the lattice beams are usually adjusted to be symmetric with respect to the cloud's equilibrium position in the underlying trap, we do not have to include gravity here (z can simply be replaced by $z + z_0$). Each of the lattice beams induces an additional external confinement in the directions perpendicular to it. Furthermore, due the Gaussian beam shape, the lattice wells are shallower away from the trap centre, such that the trapping frequency of an individual lattice site is reduced:

$$\omega_{\text{site},x}(y, z) \simeq 2\frac{E_r}{\hbar} \sqrt{\frac{V_{L,x}}{E_r}} \cdot \left(1 - \frac{y^2 + z^2}{w_L^2}\right), \quad (3.10)$$

and accordingly for $\omega_{\text{site},y}$ and $\omega_{\text{site},z}$. Although this correction is small, the spatially varying ground state energy of the sites results in a non-negligible effective reduction of the external confinement [64]. Including this effect, the trapping frequencies due to the lattice beams are

$$\omega_L = \sqrt{\frac{4E_r}{mw_L^2} \left(2\frac{V_0}{E_r} - \sqrt{\frac{V_0}{E_r}}\right)}, \quad (3.11)$$

where we have assumed a lattice with equal beams in all three directions, i. e. $V_{L,x} = V_{L,y} = V_{L,z} \equiv V_0$.

Figure 5.5 shows plots of the combined potential of a crossed-beam dipole trap and a 3D optical lattice. The trapping frequencies of the total external harmonic confinement in this situation are simply calculated as

$$\omega_i = \sqrt{\omega_{T,i}^2 + \omega_L^2}, \quad (3.12)$$

for $i = x, y, z$.

In the following two sections we will neglect the inhomogeneity of the lattice. The effect of the additional potential will be discussed in section 3.4.

3.2 Band structure and Bloch states

The general quantum-mechanical characteristics of particles in a periodic potential are well known from solid state physics. The eigenstates are described by Bloch wave functions, which in one dimension read [65]

$$\psi_{n,q}(x) = u_{n,q}(x)e^{-iqx}, \quad (3.13)$$

where $u_{n,q}(x+d) = u_{n,q}(x)$ has the same periodicity as the potential. For a lattice with N_s sites contained in a box of length L , the parameter q can take the discrete and equally spaced values $q = z \cdot 2\pi/L$ with $(z = 0, \pm 1, \dots, \pm N_s - 1)$ and $\hbar q$ is called quasi- or crystal momentum. The additional quantum number $n = 1, 2, \dots$ is known as the band index. To unambiguously define the wave functions (3.13), we choose their global phase such that $\psi_{n,q}(0)$ is real and positive for all crystal wave vectors q .

In the case of a one-dimensional optical lattice the periodic potential is given by

$$V_L(x) = -V_0 \sin^2 k_L x. \quad (3.14)$$

It is straightforward to calculate the energy spectrum and the Bloch states by expressing the Hamiltonian in terms of plane waves and diagonalising it numerically [66]. The result of such a calculation is shown in Fig. 3.3: The energy spectrum is split into Bloch bands corresponding to the band indices n , separated by energetically forbidden gaps. With increasing lattice depth the bands become narrower and the gaps between them larger. In the limit $V_0 \rightarrow \infty$ the energy levels coincide with harmonic oscillator levels, each lattice site becoming similar to a harmonic oscillator well.

Generalisation to a two- or three-dimensional lattice is straightforward since the problem is separable in the different dimensions. In a square or cubic lattice higher bands ($n > 1$) are (partly) degenerate, as is easily understood when looking at Fig. 3.4 which illustrates the two-dimensional case: The two lowest bands of each *one*-dimensional lattice, with band indices $n_x = 1$ and $n_x = 2$ for the x -direction, and $n_y = 1$ and $n_y = 2$ for the y -direction, form together two square-symmetric surfaces. The surface at lower energy corresponds to the second band, $n = 2$, of the *two*-dimensional lattice, the one at higher energy to the third band, $n = 3$, and both cover the same energy range. Similarly, the next three higher bands are created by the configurations $(n_x = 1, n_y = 3)$, $(n_x = 3, n_y = 1)$ and $(n_x = 2, n_y = 2)$ and also overlap in energy space.

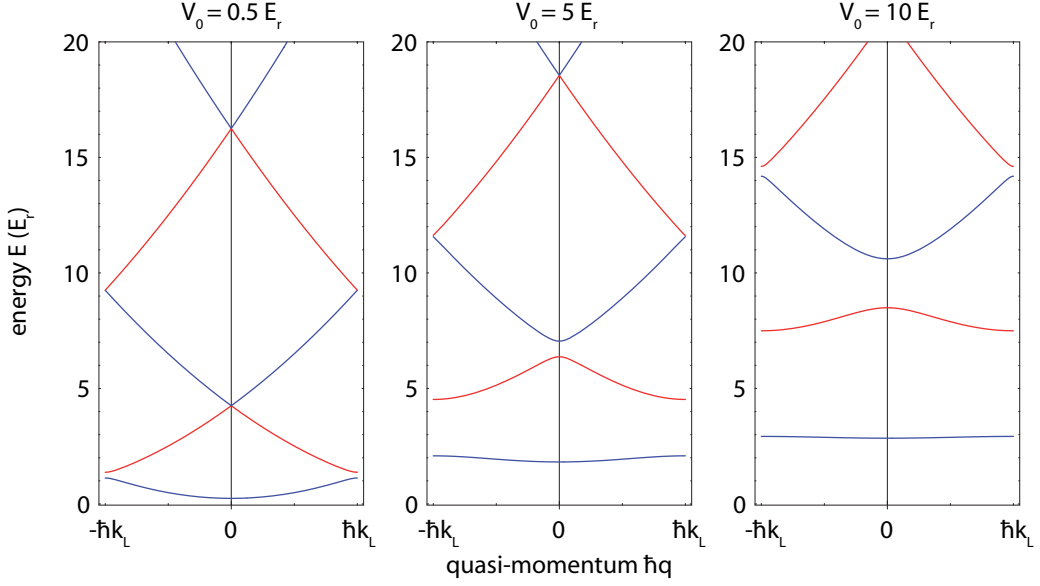


Figure 3.3: The lowest Bloch bands of a one-dimensional optical lattice of different depths in the reduced zone scheme. It should be noted that atoms in states with an energy exceeding the sum of the lattice depth and the external confinement are not trapped.

3.3 Tunnelling in the lowest band

The motion in a lattice is restrained but the atoms can still move through the periodic potential by tunnelling between the sites. In what follows, we derive expressions for the matrix elements responsible for this process and show how the tunnelling relates with the band structure of the energy spectrum.

The Hamiltonian for a homogeneous system of non-interacting atoms in second quantisation reads

$$\hat{H}_{\text{hop}} = \sum_{\sigma} \int dx \hat{\psi}_{\sigma}^{\dagger}(x) \left(-\frac{\hbar^2 \nabla^2}{2m} + V_L(x) \right) \hat{\psi}_{\sigma}(x). \quad (3.15)$$

For later convenience, we have summed over the spin index $\sigma \in \{\uparrow, \downarrow\}$ to include two spin components. In the following we will restrict ourselves to the lowest Bloch band $n = 1$ which is the only band relevant in most of the experiments since higher bands are usually not populated. The field operator $\hat{\psi}_{\sigma}(x)$ is expanded in the corresponding Wannier functions,

$$\hat{\psi}_{\sigma}(x) = \sum_i w(x - x_i) \hat{c}_{i,\sigma}. \quad (3.16)$$

The creation and annihilation operators $\hat{c}_{i,\sigma}^{\dagger}$ and $\hat{c}_{i,\sigma}$ for a fermion with spin σ at a site i obey the usual anti-commutation relations. The normalised Wannier function $w(x - x_i)$

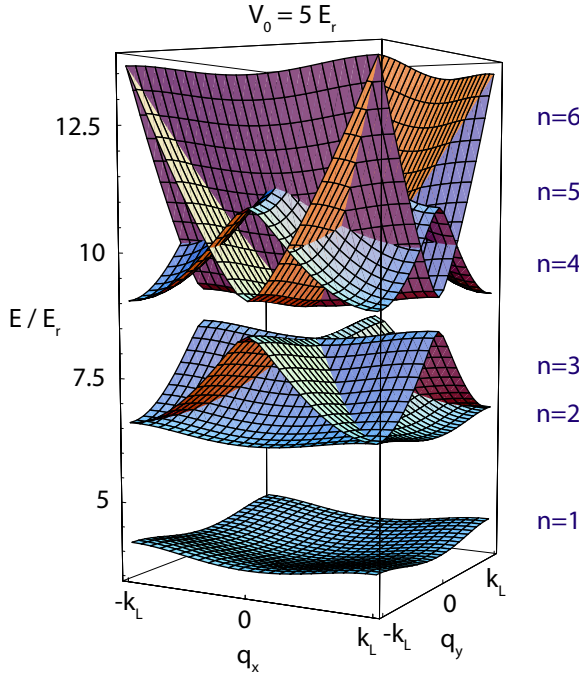


Figure 3.4: The lowest six Bloch bands of a two-dimensional optical lattice. Higher bands are (partly) degenerate, i. e. their energy ranges overlap.

localised on the lattice site i is given by

$$w(x - x_i) = \frac{1}{\sqrt{N_s}} \sum_q \psi_{n=1,q}(x) e^{iqx_i} \quad (i = 1, 2, \dots, N_s). \quad (3.17)$$

For all available sites i in the system the Wannier functions constitute a complete orthonormal set of wave functions describing particles localised in the potential wells. Inserting the expansion (3.16) of the field operator into (3.15), the hopping Hamiltonian can be written as

$$\hat{H}_{\text{hop}} = - \sum_{\sigma} \sum_{i,j} J_{ij} \hat{c}_{i,\sigma}^{\dagger} \hat{c}_{j,\sigma}. \quad (3.18)$$

The tunnelling matrix elements

$$J_{ij} = - \int dx w_i^*(x) \left(-\frac{\hbar^2 \nabla^2}{2m} + V_L(x) \right) w_j(x) = -\frac{1}{N_s} \sum_q E(q) e^{i(x_i - x_j)q} \quad (3.19)$$

include the kinetic energy as well as the periodic potential and describe the hopping of an atom from the site i to the site j . Through this tunnelling process the atoms can lower their kinetic energy. From the second part of the equation, which is obtained by inserting the definition (3.17) of the Wannier functions, it is obvious that the matrix elements J_{ij} are the Fourier coefficients of the band structure $E(q)$ [67]. We thus find the dispersion relation of the lowest band,

$$E(q) = -J_0 - 2 \sum_{n>0} J_n \cos(nqd). \quad (3.20)$$

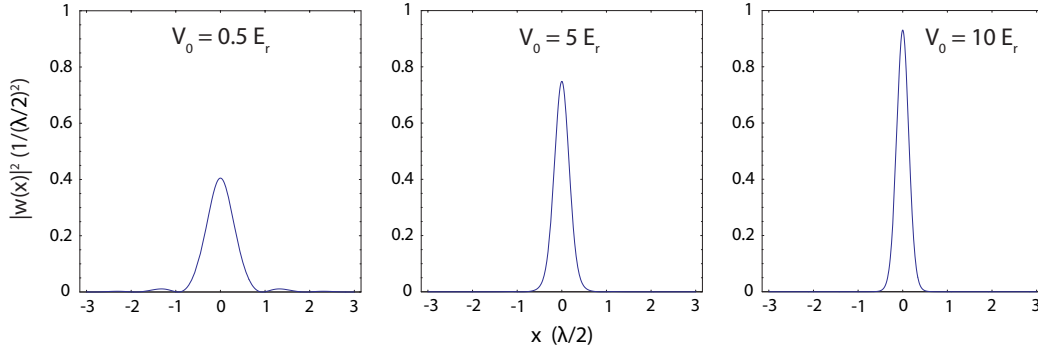


Figure 3.5: Absolute square of the Wannier functions $w(x)$ of the lowest Bloch band for different lattice depths V_0 .

The sum adds up all orders of tunnelling terms $J_n \equiv J_{i(j=i+n)}$ between sites separated by the distance nd ($n = 1, 2, \dots$). From this formula we derive a useful relation between the tunnelling elements and the bandwidth, $\Delta E = 4 \sum_{n \text{ odd}} J_n$. Note that higher order tunnelling terms become less and less important in a deeper lattice as the overlap between distant Wannier functions vanishes.

For a given crystal wave vector q the dispersion relation of the lowest band can be harmonically approximated. Comparing with the parabolic dispersion of free particles one can then define an effective mass m^* by

$$\frac{\hbar^2}{m^*} = \frac{\partial^2}{\partial q^2} E(q). \quad (3.21)$$

For $q = 0$ this approximation yields $m^* = \hbar^2/(2J_1 d^2)$ or $m^*/m = E_r/(\pi^2 J_1)$, while m^* diverges for $q \rightarrow \pm \hbar k_L/2$. Atoms in shallow lattices can often be described in a simple picture, where they are considered as free particles with a mass given by the effective mass. For instance, the lower frequencies of dipole oscillations in the lattice as compared to a pure harmonic trap are a consequence of effectively heavier atoms [68].

3.4 Fermions in an optical lattice

Condensed bosonic atoms accumulate in the lowest energy state of the lattice having zero quasi-momentum. The ground state of indistinguishable fermions looks very different: The Pauli principle admits only one atom per spin component in each quasi-momentum state of the lowest band. In this paragraph we discuss the implications of the fermionic quantum statistics on the measurable atomic distributions, which are significantly influenced by the confining potential present in experiments.

3.4.1 The external harmonic confinement

In all experiments to date the trapped atoms are subject to an external harmonic potential $V_T(x)$ due to the shape of the lattice laser beams and often also due to an additional

optical or magnetic trap. The external confinement determines the atomic distributions and has important consequences for the energy spectrum and for the temperature of the gas when it is loaded into the optical lattice.

Figure 3.6 shows illustrations of the combined potential of a lattice and an underlying trap. Locally the system can still be regarded as homogeneous and energy bands may be defined as above. However, the underlying harmonic confinement leads to a position-dependent filling-factor of the optical lattice, usually decreasing towards the edges of the trap. As a consequence, in certain regimes different phases may be simultaneously present in different regions of the trap [69, 70, 71]. In order to investigate the filling in the lattice it is instructive to look at the energy spectrum in position space [72]. In such a picture the Bloch bands are bent in space, as shown in Fig. 3.7.

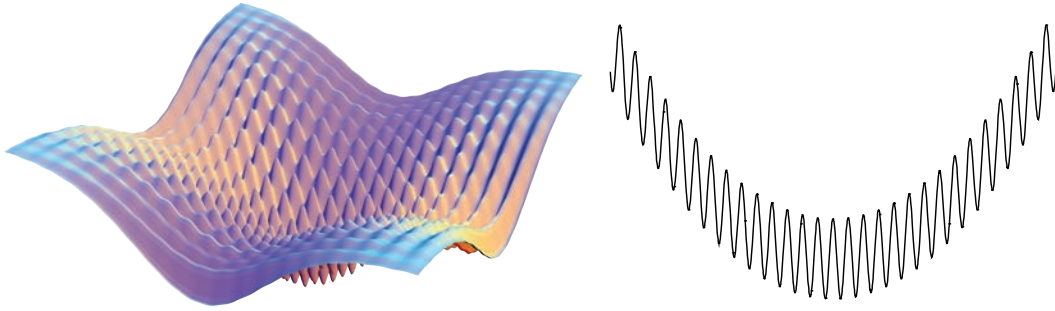


Figure 3.6: Drawings of the combined potential of an optical lattice and a weak harmonic trap (not to scale).

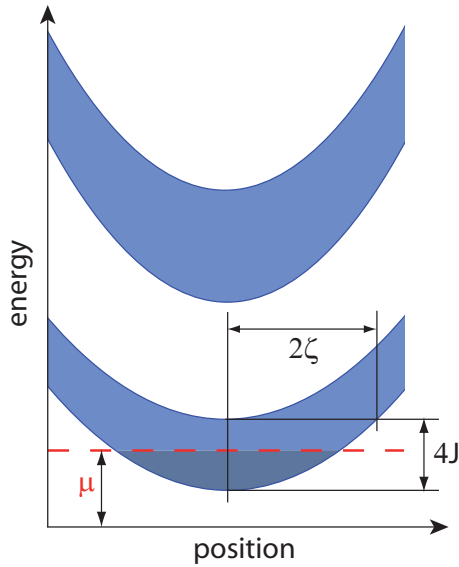


Figure 3.7: Illustration of the energy spectrum in position space for an optical lattice in the presence of an additional harmonic potential. The “bending” of the Bloch bands leads to a position-dependent filling factor of the optical lattice.

In the case of an ideal Fermi gas Rigol et al. have found a simple way to specify the atomic distribution in an inhomogeneous lattice considering a tight-binding Hamiltonian

[73]. One defines a characteristic length ζ_i for each lattice direction $i = x, y, z$, which is the distance from the centre of the trap at which the energy offset due to the harmonic confinement balances the tunnelling energy $J = J_1$ (higher order tunnelling terms are neglected here). It has been shown numerically that the density distribution scaled by ζ_i and the momentum distribution of the atoms in the lattice at $T = 0$ only depend on the (dimensionless) characteristic density ρ_c :

$$\frac{1}{2}m\omega_i^2\zeta_i^2 = J, \quad (3.22a)$$

$$\rho_c = \frac{N}{\zeta_x\zeta_y\zeta_z/d^3} = N\bar{\omega}^3d^3\left(\frac{m}{2J}\right)^{3/2}. \quad (3.22b)$$

Here, N is the atom number per spin state. As a result, systems with the same characteristic density have the same typical filling (e.g. filling in the trap centre). A specific filling factor in the lattice can be achieved by tuning either of the following three parameters: the particle number N , the trapping frequency $\bar{\omega}$ or the tunnelling J . This has been exploited in the experiment of section 6.1, where samples with different fillings have been prepared to observe the transition to a band-insulating phase.

In a translationally invariant potential particles cannot localise in the lattice wells in the absence of interactions or disorder. In contrast, atoms in a lattice with underlying confinement become localised when the energy offset between two neighbouring sites, $V_T(x_i) - V_T(x_{i+1})$, exceeds the tunnelling energy, which is more likely to happen away from the trap centre [72, 74]. More localisation is attained by increasing either the lattice depth (decreasing J) or the external confinement. In the tight binding limit, where all atomic states are assumed to be localised, the density of states for the lowest band of a three-dimensional lattice can be derived analytically [75, 76],

$$g^{(\text{tb})}(E) = 16\pi \left(\frac{2}{m\bar{\omega}^2\lambda^2} \right)^{3/2} \sqrt{E}, \quad (3.23)$$

where λ is the wavelength of the lattice laser. From this one easily obtains the Fermi energy

$$E_F^{(\text{tb})} = \left(\frac{3N}{2\pi} \right)^{2/3} \frac{m\bar{\omega}^2\lambda^2}{16}. \quad (3.24)$$

Due to the different densities of states in the lattice with underlying confinement, the entropy $S \propto T/T_F$ is only half as large as compared to a harmonic trap [see eqn. (2.20)]. Loading the fermions adiabatically (at constant S) from a harmonic trap into the lattice is therefore accompanied by an increase of the ratio T/T_F by a factor of 2 [75]. This effect is in contrast to what happens in the lowest band of a homogeneous lattice, where T/T_F remains constant [77]. In that case T drops with $T_F \propto m^{*-1/2}$ while the lattice is ramped up adiabatically because the effective mass m^* defined in eqn. (3.21) increases.

3.4.2 Quasi-momentum distribution

In the ground state of non-interacting particles in a homogeneous lattice the Bloch levels are occupied each by one fermion (of each spin state) up to the Fermi energy E_F . The

surface separating the occupied levels from the unoccupied levels in quasi-momentum space is called the Fermi surface. Its shape depends on the lattice filling, as is shown in the upper row of Fig. 3.8 for a simple cubic lattice. At low fillings the Fermi surface has the form of a sphere and gradually develops extensions towards the Bragg planes of the first Brillouin zone as the filling increases [65]. When the lowest band is completely filled, the Fermi surface coincides with the cube defining the first Brillouin zone.

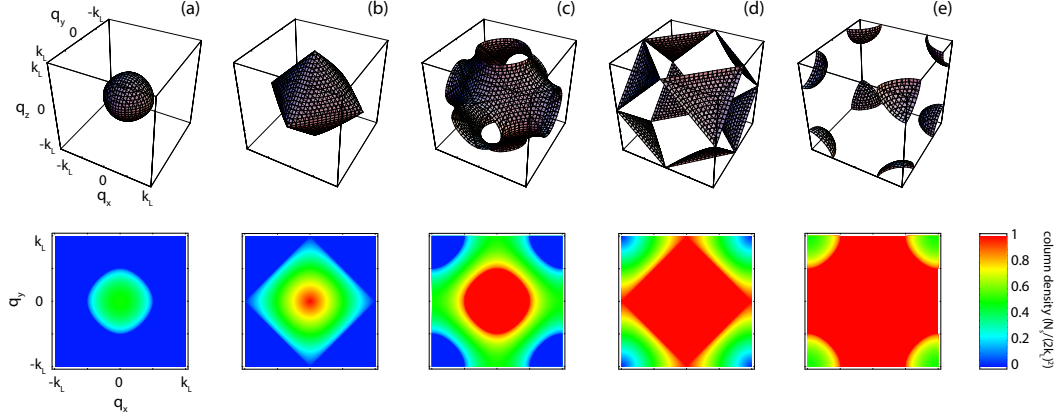


Figure 3.8: Fermi surfaces (upper row) and quasi-momentum distributions (lower row) in a homogeneous simple cubic lattice in the tight binding limit for different fillings. The distributions in the lower row have been integrated along one lattice direction. The fillings correspond to $E_F/\Delta E$ equal to (a) 1/6, (b) 1/3, (c) 1/2, (d) 2/3 and (e) 5/6, where ΔE is the bandwidth of the lowest Bloch band.

At zero temperature the quasi-momentum distribution in a homogeneous system is a function evaluating to one inside the Fermi surface and to zero outside. Integration along one lattice direction yields the distributions plotted in the lower row of Fig. 3.8. In the case of trapped fermions where the filling factor is position-dependent a Fermi surface can, strictly speaking, only be defined locally. The trapping potential modifies the global quasi-momentum distribution which can be thought of as the local distributions integrated over the extension of the trap. Experimental data therefore do not feature the sharp borders visible in the calculated distributions of Fig. 3.8.

The possibility to control the lattice potential makes a direct measurement of the quasi-momentum distribution possible. For this purpose the potential is reduced adiabatically such that the quasi-momentum is conserved and eventually mapped onto the real momentum [78, 79]. The time scale for turning off the lattice is on the order of 1 ms, which is too fast for the many-body wave function to follow, but still slow enough to avoid inter-band excitations.

3.4.3 Momentum distribution

All the information contained in the quasi-momentum distribution is also encoded in the real momentum distribution. The latter is obtained experimentally by switching off all

confining potentials (lattice and trap) quickly and letting the atomic cloud expand. If the interaction between the atoms is small compared to the kinetic energy, then after long enough time of flight the momentum distribution is mapped to position space and can be measured with absorption imaging. Since a state with a quasi-momentum $\hbar q$ is a superposition of plane waves with momenta $\hbar(q \pm n \cdot 2k_L)$ (n integer), each q will produce peaks separated by $2\hbar k_L$ in the momentum distribution. This can also be viewed as an interference between the wave function components on different lattice sites. Condensed bosons, for instance, occupy only the $q = 0$ state and therefore give rise to an interference pattern with sharp peaks. A gas of normal fermions, on the other hand, always has a finite width in quasi-momentum space and produces accordingly wide peaks.

An expression for the atomic momentum distribution is readily obtained in second quantisation [80, 81]:

$$n(k) = \langle \hat{\psi}^\dagger(k) \hat{\psi}(k) \rangle = \int dx dx' e^{-ik(x-x')} \rho(x, x') \quad (3.25)$$

with the one-body density matrix

$$\rho(x, x') = \langle \hat{\psi}^\dagger(x') \hat{\psi}(x) \rangle, \quad (3.26)$$

and using the expansion (3.16) one obtains

$$n(k) = |\tilde{w}(k)|^2 \sum_{i,j} e^{-ik(x_i - x_j)} \langle \hat{c}_i^\dagger \hat{c}_j \rangle. \quad (3.27)$$

This corresponds to the Fourier transform of the correlation function $\langle \hat{c}_i^\dagger \hat{c}_j \rangle$ enveloped by the absolute square of the Fourier transform $\tilde{w}(k)$ of the Wannier function. Evaluating the momentum distribution for the ground state $(\prod_{q=-q_{\max}}^{q_{\max}} \hat{c}_q^\dagger) |0\rangle$ with fermions filled up to the quasi wave vector q_{\max} we obtain

$$n(k) = |\tilde{w}(k)|^2 \sum_{i,j} \sum_{q=-q_{\max}}^{q_{\max}} e^{-i(k+q)(x_i - x_j)}. \quad (3.28)$$

Distributions for different values of q_{\max} are shown in Fig. 3.9 for a potential depth of $V_0 = 15E_r$. For fillings $q_{\max}/k_L < 1$ an interference pattern is visible. As the filling increases, the widths of the momentum peaks grow, reflecting the broader quasi-momentum distribution. When the lowest band is completely filled (band-insulating state), the patterns of the individual atoms complement each other and only the envelope function is observed. In a deeper lattice the number of interference peaks contained within the envelope is larger

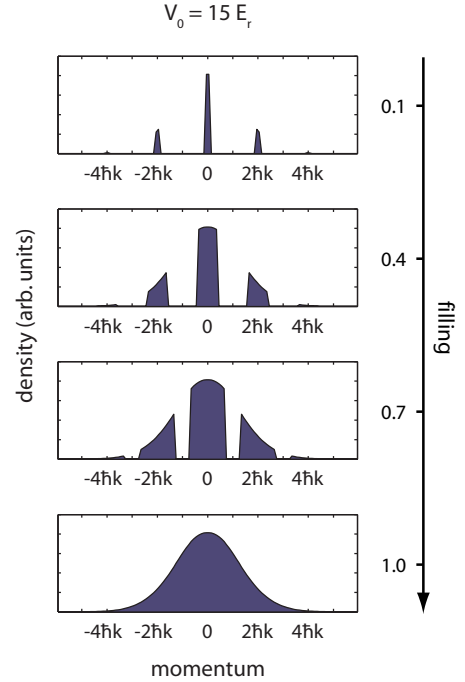


Figure 3.9: Zero-temperature momentum distribution of non-interacting fermions in a homogeneous one-dimensional optical lattice with depth $15E_r$ for different fillings.

because the Wannier functions are more localised and thus spectrally broader. As in position or quasi-momentum space, the harmonic confinement smoothes out the distribution relative to the homogeneous case. Therefore, sharpness and contrast of experimentally observed interference patterns are reduced.

3.5 Including interactions: The Fermi-Hubbard model

In 1963 J. Hubbard introduced a model to describe interacting electrons in a single energy band of a lattice [82]. In solid state physics it attracted the interest of many theorists, not only because of its simplicity but also because it is expected to support high-temperature superconductivity [14]. Cold alkali atoms in optical lattices constitute a clean implementation of the single-band Hubbard model [13, 83]. The model accurately describes the short-range two-body interactions between alkali atoms, and its restriction to the lowest Bloch band is most often justified by the low energy scales in these systems. A seminal experimental demonstration of the model's applicability to atoms in optical lattices was the observation of the superfluid to Mott insulator transition of bosonic atoms in 2002 [84].

The Hubbard model can be derived in a second quantisation approach starting from the full many-body Hamiltonian including local two-body interactions [85]. In the following this is done for a two-component Fermi gas consisting of atoms with spin σ which can take the values \uparrow and \downarrow :

$$\begin{aligned} \hat{H} = & \sum_{\sigma} \int dx \hat{\psi}_{\sigma}^{\dagger}(x) \left(-\frac{\hbar^2 \nabla^2}{2m} + V_L(x) + V_T(x) \right) \hat{\psi}_{\sigma}(x) \\ & + \frac{g}{2} \sum_{\sigma, \sigma'} \int dx \hat{\psi}_{\sigma'}^{\dagger}(x) \hat{\psi}_{\sigma}^{\dagger}(x) \hat{\psi}_{\sigma}(x) \hat{\psi}_{\sigma'}(x). \end{aligned} \quad (3.29)$$

Here, we have used a zero-range interatomic potential $V_{\text{int}}(x - x') = g\delta(x - x')$ with the coupling parameter $g = 4\pi\hbar^2 a/m$ and a being the s -wave scattering length. $V_T(x)$ is an external trapping potential which varies on a length scale much larger than the lattice spacing d . Assuming that the atoms do not occupy higher Bloch bands, we can again use the expansion (3.16) for the field operator to express the Hamiltonian in terms of Wannier functions:

$$\hat{H} = - \sum_{\sigma} \sum_{i,j} J_{ij} \hat{c}_{i,\sigma}^{\dagger} \hat{c}_{j,\sigma} + \sum_{\sigma, \sigma'} \sum_{i,j,k,l} \frac{U_{ijkl}}{2} \hat{c}_{i,\sigma'}^{\dagger} \hat{c}_{j,\sigma}^{\dagger} \hat{c}_{k,\sigma} \hat{c}_{l,\sigma'} + \sum_{\sigma} \sum_i V_T(x_i) \hat{c}_{i,\sigma}^{\dagger} \hat{c}_{i,\sigma}. \quad (3.30)$$

In addition to the hopping (first term) and the external potential (third term) we get an interaction term which is determined by the matrix elements

$$U_{ijkl} = g \int dx w_i^*(x) w_j^*(x) w_k(x) w_l(x). \quad (3.31)$$

Taking into account only the on-site interaction $U \equiv U_{iiii} = g \int dx w(x)^4$ between two fermions (with different spins) residing on the same lattice site and the nearest-neighbour

tunnelling $J \equiv J_1$ leads to the Fermi-Hubbard Hamiltonian:

$$\hat{H}_{\text{FH}} = -J \sum_{\sigma} \sum_{\langle i,j \rangle} \hat{c}_{i,\sigma}^{\dagger} \hat{c}_{j,\sigma} + U \sum_i \hat{n}_{i,\uparrow} \hat{n}_{i,\downarrow} + \sum_{\sigma} \sum_i V_T(x_i) \hat{n}_{i,\sigma}, \quad (3.32)$$

where $\langle i,j \rangle$ denotes the sum over nearest neighbours (including double counting) and $\hat{n}_{i,\sigma} = \hat{c}_{i,\sigma}^{\dagger} \hat{c}_{i,\sigma}$ is the fermionic number operator for atoms at the site i with spin σ . The Hubbard model is a tight-binding description [65] and can be applied when the optical lattice is not too shallow. At a lattice depth $V_0 = 5E_r$ J_2 is already more than an order of magnitude smaller than J_1 , such that the Hubbard approximation is justified. The lowest band then has the typical cosine shape $E_0(q) = -J_0 - 2J \cos(qd)$. Another limitation is the restriction to the lowest band. If the Fermi energy E_F , the interaction energy U or the thermal energy $k_B T$ exceeds the gap to the next higher band, the picture is not appropriate anymore and a multi-band model should be applied [86]. A detailed analysis of the validity of the Fermi Hubbard model is found in ref. [87].

Analytic formulas for U and J can be obtained in the limit of large lattice depths [80], which for a cubic lattice read:

$$U = \sqrt{\frac{8}{\pi}} k_L a E_r \left(\frac{V_0}{E_r} \right)^{3/4} \quad (3.33)$$

$$J = \frac{4}{\sqrt{\pi}} E_r \left(\frac{V_0}{E_r} \right)^{3/4} \exp \left(-2 \sqrt{\frac{V_0}{E_r}} \right). \quad (3.34)$$

J is exponentially suppressed with growing lattice depth. The time scale associated with the tunnelling process is given by $\tau = \hbar/2zJ$, with z being the number of nearest neighbours ($z = 6$ for a simple cubic lattice).

The physical relevance of the interaction in the Hubbard model is specified by the ratio U/J between interaction and kinetic energy. Its value determines for example if the system is in the Mott insulating phase or not [13, 80]. U/J can be tuned over a wide range by changing the lattice potential depth (which mainly affects J) or by adjusting U by use of a Feshbach resonance (see section 4.3), as can be seen in the plot of Fig. 3.10. For a given lattice depth V_0/E_r the parameter U/J is fully determined by the product $k_L a$ of the lattice wave vector and the scattering length. Within the validity range of the Hubbard model, the physics is thus governed by the two length scales a and λ . New effects come into play when the scattering length a becomes of the order of the extension of the Wannier function in a well. In the following chapter we will see how this affects the atomic scattering.

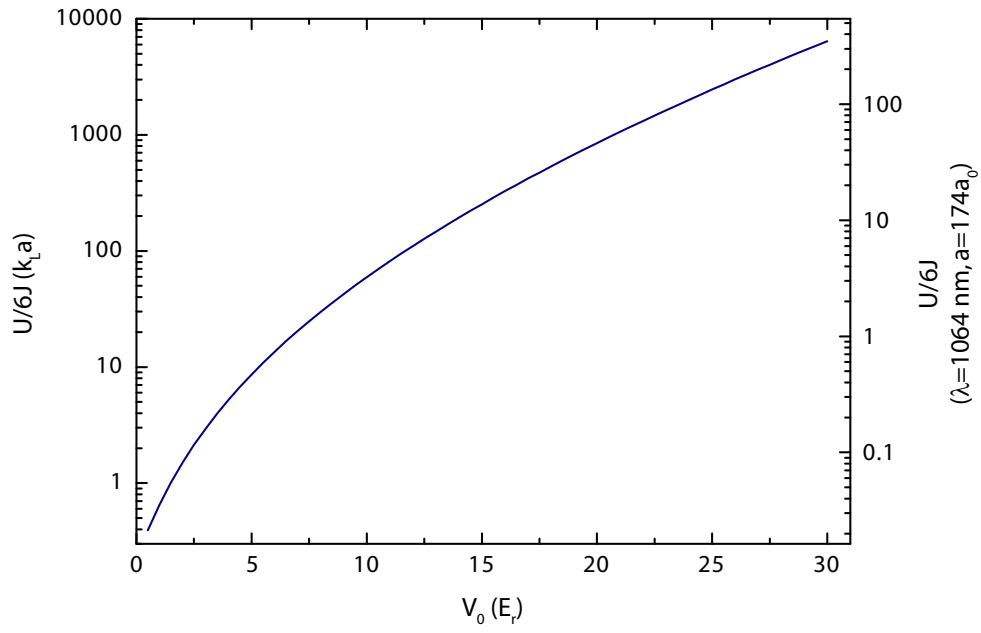


Figure 3.10: The ratio $U/6J$ as a function of the potential depth of a cubic optical lattice. The on-site interaction energy U and the tunnelling energy J have been calculated numerically. In this plot J denotes the total tunnelling, which at very small lattice depths differs noticeably from the nearest-neighbour tunnelling.

4 Interactions in cold atomic gases

The phase-space distribution of an ideal quantum gas is self-evident since the independent atoms simply occupy the single-particle eigenstates of the trapping potential according to the quantum statistical requirements. Interactions, on the other hand, lead to nontrivial correlations between the atoms and give birth to exciting quantum many-body states. Such systems become accessible with cold atomic gases by taking advantage of Feshbach resonances.

Strongly correlated states in optical lattices are especially intriguing. The periodic potential squeezes the kinetic energy and enhances the importance of the interaction. The minute structure of an optical lattice can also directly influence the scattering between atoms on a microscopic scale. The lattice potential can modify the wave function on length scales comparable to those of the interatomic potential, and its effect is of great importance for the understanding of interacting gases in optical lattices.

This chapter first revisits the subject of scattering between ultracold atoms, pointing out the relevance of the length scales involved. The second part addresses Feshbach resonances, and finally, the particularities of scattering under strong confinement are summarised.

4.1 Scattering theory

We consider two atoms interacting through a potential $V(\mathbf{r})$ with a range r_0 , where \mathbf{r} is the relative coordinate [88]. The stationary wave function is described by the Schrödinger equation

$$\left(\frac{\hbar^2}{2m} \nabla^2 + E_k \right) \psi_{\mathbf{k}}(\mathbf{r}) = V(\mathbf{r}) \psi_{\mathbf{k}}(\mathbf{r}). \quad (4.1)$$

The wave vector \mathbf{k} defines the direction of the incoming wave as well as the energy $E_k = \hbar^2 k^2 / m$ ($k = |\mathbf{k}|$) in the center of mass frame. The asymptotic ($r = |\mathbf{r}| \gg r_0$) solution can be written as the sum of the ingoing plane wave and the scattered wave,

$$\psi_{\mathbf{k}}(\mathbf{r}) = e^{i\mathbf{k} \cdot \mathbf{r}} + \frac{e^{ir}}{r} f(\mathbf{k}, \mathbf{k}') \quad (4.2)$$

with $\mathbf{k}' = k\mathbf{r}/r$ being the wave vector of the outgoing wave. The scattering amplitude f is given by the implicit expression $f(\mathbf{k}, \mathbf{k}') = - (m/2\pi\hbar^2) \int d\mathbf{r}' e^{-i\mathbf{k}' \cdot \mathbf{r}'} V(\mathbf{r}') \psi_{\mathbf{k}}(\mathbf{r}')$ and can be treated in first order in V for weak potentials. This is known as the first Born approximation. Replacing $\psi_{\mathbf{k}}(\mathbf{r})$ by its zeroth order approximation $\exp(i\mathbf{k} \cdot \mathbf{r})$ yields

$$f(\mathbf{k}, \mathbf{k}') = -\frac{m}{2\pi\hbar^2} \tilde{V}(\mathbf{k} - \mathbf{k}'), \quad (4.3)$$

where $\tilde{V}(\mathbf{k})$ is the Fourier transform of $V(\mathbf{r})$. Integrating the absolute square of the scattering amplitude over the solid angle results in the total scattering cross section:

$$\sigma = \int d\Omega |f(\mathbf{k}, \mathbf{k}')|^2. \quad (4.4)$$

For a spherically symmetric potential $V(r)$ the angular part of the wave function ψ is expanded in partial waves given by the Legendre polynomials $P_l(\cos(\theta))$ of order $l \in \{0, 1, \dots\}$. The radial part $u_l(r)/r$ obeys the 1D Schrödinger equation for each l with an effective potential

$$\frac{\hbar^2}{2m} (\partial_r^2 + k^2) u_l(r) = V_{\text{eff}} u_l(r), \quad (4.5a)$$

$$V_{\text{eff}}(r) = V(r) + \frac{\hbar^2 l(l+1)}{2mr^2}. \quad (4.5b)$$

In the limit of very low energies ($k \rightarrow 0$) the atoms cannot overcome the centrifugal barrier appearing in (4.5b), and scattering into partial waves other than the isotropic s -wave ($l = 0$) is suppressed. For $r \gg r_0$ eqn. (4.5a) reduces to $u_0''(r) = 0$ and the asymptotic scattering wave function reads

$$\psi_{\mathbf{k} \rightarrow 0}(\mathbf{r}) \sim \frac{u_0(r)}{r} \propto \frac{r-a}{r}. \quad (4.6)$$

This is equivalent to $f \rightarrow -a$ ($k \rightarrow 0$) as can be seen from eqn. (4.2). The s -wave scattering length a determines the intercept of the asymptotic scattering wave function. More precisely, for potentials vanishing fast enough for large r , the low k expansion of the s -wave scattering amplitude reads

$$f_k^{(s)} = -\frac{1}{a^{-1} + ik - \frac{1}{2}k^2 r_e + \dots}, \quad (4.7)$$

defining the effective range r_e of the potential [89, 90]. The optical theorem $\sigma(k) = (4\pi/k) \text{Im}[f(k)]$ then gives the cross section for distinguishable particles

$$\sigma = \frac{4\pi a^2}{1 + a^2 k^2} \quad (4.8)$$

in the limit $k \rightarrow 0$.

It is worthwhile noting that the spatial part of the two-body wave function is symmetric for even l and antisymmetric for odd l , resulting from the parity of the Legendre polynomials. Hence, in order to fulfill quantum statistics, two fermions with equal spin can only interact via odd partial waves. Since at low temperatures only the symmetric s -wave is important, indistinguishable, spin-polarised fermions—having an antisymmetric spatial wave function—do not interact with each other. An exception constitutes a spin-polarised gas close to a p -wave Feshbach resonance for which the p -wave interactions are drastically enhanced. This topic will be discussed in chapter 7.

4.2 Emerging length scales

Quantum degenerate atomic gases are not thermodynamically stable in the strict sense. In fact, the interatomic potential supports many bound states below the continuum with energies much smaller than the studied temperatures [91]. However, three-body recombination processes, in which two atoms form a deeply bound state and a third one carries away the remaining kinetic energy, are largely suppressed due to the low density. Indeed, the density of a degenerate Fermi gas is of the order k_F^{-3} [see eqns (2.20) and (2.22)], and the typical range $r_0 = \beta_6$ of the van der Waals potential* is much smaller than the inter-particle spacing $\sim k_F^{-1}$ [45]:

$$k_F \beta_6 \ll 1. \quad (4.9)$$

As a result, in the absence of any scattering resonance collisions occur predominantly as a two-body process. Another important consequence is that the scattering state can be described by its expression in the asymptotic regime. The macroscopic properties of the interacting many-body state thus only depend on the scattering amplitude [92], which at low temperatures is usually fully determined by the scattering length a . The latter is true in the so-called zero-range limit, where

$$k^2 |r_e| \ll |a^{-1} + ik|, \quad (4.10)$$

as is seen from eqn. (4.7). In very tight potentials such as an optical lattice this condition may be violated. This issue will be discussed below.

Calculating the exact interatomic potential is very complicated and the Born approximation can usually not be applied [93]. Yet, the above considerations allow to replace $V(r)$ by Fermi's zero-range pseudo-potential [40]

$$\hat{V}_{\text{pseudo}}(\mathbf{r}) = g \delta(\mathbf{r}) \partial_r r \quad (4.11)$$

with the coupling constant

$$g = \frac{4\pi\hbar^2}{m} a. \quad (4.12)$$

It involves as the only interaction parameter the scattering length a , which has to be determined experimentally. The regularising operator $\partial_r r$ in (4.11) removes the divergence of wave functions which behave as $1/r$ for $r \rightarrow 0$. Comparing the scattering amplitude $f_k^{\text{pseudo}} = -a/(1 + ika)$ of the pseudo-potential with the more general expression (4.7) it is clear that the application of (4.11) is restricted to s -wave scattering in the zero-range limit. Advantageously, for a small gas parameter $k_F |a| \ll 1$ the pseudo-potential is treatable in the Born approximation and permits mean-field approaches.

In the vicinity of a Feshbach resonance the scattering length can take arbitrarily large values. An interesting regime accessible in experiments is the unitary limit: for $a \rightarrow \infty$ the cross section is constrained to its maximum value $\sigma = 4\pi/k^2$ [see eqn. (4.8)]. The

*The length scale $\beta_6 = (C_6 m / \hbar^2)^{1/4}$ of the van der Waals potential $V_{\text{vdW}} = -C_6/r^6$ is defined through the equation $\hbar^2/m\beta_6^2 = C_6/\beta_6^6$.

last remaining length scale characterising the interatomic potential, a , then drops out of the problem and the physics of the strongly interacting Fermi gas becomes universal, i. e. independent of the microscopic details of the atomic species under consideration.

4.3 Feshbach resonances

In ultracold atomic physics Feshbach resonances serve as a powerful tool to control the interaction between atoms. The scattering length can be tuned to arbitrary values by varying an external magnetic bias field [94], and via an adiabatic sweep weakly bound diatomic molecules can be formed. In a degenerate Fermi gas this has enabled the study of the crossover between BCS type and BEC type superfluidity [95, 96, 5]. In optical lattices Feshbach resonances for atoms give independent control over the on-site interaction U , allowing to vary the parameter U/J over a large range. The formation of molecules in lattices reveals the special nature of bound states in periodic and quasi low-dimensional systems.

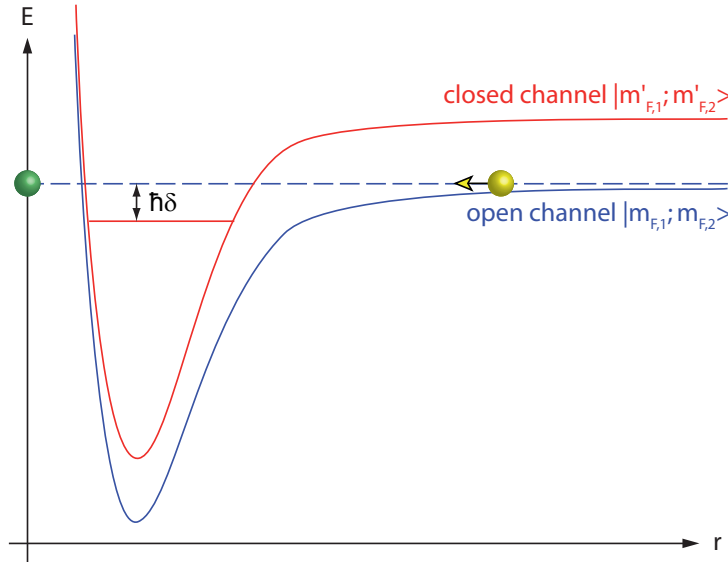


Figure 4.1: The coupling between the open entrance channel and the closed channel potentials leads to a Feshbach resonance when the detuning $\hbar\delta \rightarrow 0$ by applying a magnetic field.

The underlying mechanism of the enhanced Feshbach scattering is the resonant coupling of the collisional entrance channel to one or several other channels. In the following we consider two atoms in the hyperfine states $|F, m_{F,1}\rangle$ and $|F, m_{F,2}\rangle$ colliding at low energy. The two-body state is in general a superposition of a spin singlet and a spin triplet, and the corresponding interatomic potential determines the value of the background scattering length a_{bg} (see appendix 10.1). Since the energy of the atoms lies slightly above the continuum threshold, the entrance channel is referred to as open. Denoting the posi-

tions of the atoms \mathbf{r}_1 and \mathbf{r}_2 and their electronic spins \mathbf{s}_1 and \mathbf{s}_2 , the central part of the interatomic potential can be written as the sum of a spin-independent interaction term V_c and a spin-spin interaction term proportional to V_{ss} [97, 98]:

$$V(\mathbf{r}_1 - \mathbf{r}_2) = V_c(\mathbf{r}_1 - \mathbf{r}_2) + V_{ss}(\mathbf{r}_1 - \mathbf{r}_2)\mathbf{s}_1 \cdot \mathbf{s}_2. \quad (4.13)$$

At short distances V couples the entrance channel weakly to other two-body states with equal total spin $M_F = m_{F,1} + m_{F,2}$. Suppose that the open channel is coupled to a single closed channel with different internal states $|F', m'_{F,1}\rangle$ and $|F', m'_{F,2}\rangle$, as illustrated in Fig. 4.1. A Feshbach resonance arises when this inter-channel coupling is resonantly enhanced by tuning the highest vibrational bound state of the closed channel into degeneracy with the continuum threshold energy of the open channel. Since in general the magnetic moments of the two channels differ by an amount $\Delta\mu$, the detuning $\hbar\delta = \Delta\mu(B - B_0)$ can be changed by applying a magnetic field. At resonance, $B = B_0$, the atoms virtually populate the closed channel bound state in a second order process before flying apart in their original internal states. This leads—in the case of an s -wave resonance—to a divergence of the scattering length.

This behaviour is reminiscent of a basic (single-channel) problem in quantum mechanics, namely a square well potential with varying depth. In this case, the value of the scattering length is increased by making the potential deeper. At some depth the well supports a new bound state, and the scattering length a diverges to $+\infty$. As the potential is lowered further, a increases again from $-\infty$ and the binding energy of the bound state increases. Likewise, in the multichannel problem of a Feshbach resonance the divergence of the scattering length is linked to the emergence of a weakly bound state, which is discussed in the next paragraph. It should be noted that single-channel models can be applied to broad resonances only, whereas two-channel models [99] also successfully describe narrow resonances.

The magnetic field dependence of the scattering length takes the generic form [100, 101]

$$a(B) = a_{\text{bg}} \left(1 - \frac{\Delta B}{B - B_0} \right), \quad (4.14)$$

where ΔB is the width of the resonance and $a_{\text{bg}} = a(0)$ the background scattering length at zero magnetic field. Examples are shown in Fig. 4.4. In Fig. 4.2 it can be seen that the physically relevant resonance position B_0 does not exactly coincide with the value B_{res} where the closed channel bound state and the dissociation threshold are degenerate. In fact, an avoided crossing between the closed channel bound state and the highest vibrational bound state of the entrance channel results in a significant shift [102]. The resonance width ΔB depends on the inter-channel coupling as well as on the background scattering properties [45]: $\Delta\mu\Delta B = 2\hbar^2/mr_e a_{\text{bg}}$. We will see in the next paragraph that the width is of great significance when it comes to strongly correlated many-body physics. A resonance is considered as broad if the effective range r_e of the interaction potential is of similar (or smaller) magnitude as the van der Waals length β_6 : From the diluteness of the gas [eqn. (4.9)] it then follows directly that the condition (4.10) for the zero-range limit is fulfilled. In the opposite case one deals with a narrow resonance.

4.3.1 Bound state and BCS-BEC crossover

As mentioned above, a diverging scattering length is associated with the appearance of a bound state below the continuum threshold. A weakly bound molecular state indeed exists on the side of the Feshbach resonance where the scattering length is positive (so-called BEC side), as can be seen in Fig. 4.2. By tuning the magnetic field such that the resonance is crossed starting from the side of negative scattering lengths, two colliding atoms can be adiabatically converted into a weakly bound Feshbach molecule [103]. Its binding energy near the resonance is given by the Wigner formula [88]

$$E_b(B) = -\frac{\hbar^2}{ma(B)^2} \quad (4.15)$$

(see inset of Fig. 4.2). This formula coincides with the energy of the only bound state supported by the pseudo-potential. An expression extending its validity towards smaller values of a has been derived taking into account the long-range van der Waals tail $-C_6/r^6$ of the background scattering potential [104, 105]:

$$E_b(B) = -\frac{\hbar^2}{2m(a(B) - \bar{a})^2}, \quad (4.16)$$

where $\bar{a} = \beta_6 \cdot 0.478\dots$ is the so-called mean scattering length. In the range of parameters exploited in current experiments with ^{40}K eqn. (4.16) agrees well with one- or two-channel calculations [102]. It is noteworthy that the molecular wave function for a broad Feshbach resonance has only a small amplitude in the closed channel state, meaning that the Feshbach molecule is quite different from the unperturbed bound state. A particularly appealing feature of molecules composed of two fermions is the long lifetime close to the resonance. Since their size on the order of a is large compared to the interatomic distance, the constituent atoms still experience each other as independent fermions and three-body recombination is suppressed by the Pauli principle [106]. Farther away from resonance, the lifetime is much shorter as the molecules become more strongly bound and smaller in size.

Due to their bosonic nature the molecules can undergo a phase transition to a Bose-Einstein condensate, which has been observed in groundbreaking experiments [53, 107, 108, 96]. On the side of the resonance where a is negative (so-called BCS side), no weakly bound two-body state exists in a shallow confinement. However, in the regime of weak attractive interaction, Cooper pairs form if the temperature is low enough and the many-body state is described by the BCS theory of superfluidity [109]. The BCS and the BEC side are connected by a crossover where the scattering length is very large. In this regime resonance superfluidity of pairs [110] occurs at temperatures which are experimentally achievable [2, 3]. Furthermore, in the unitary limit the inter-atomic distance $n^{-1/3}$ is left as the only relevant length scale, such that the gas exhibits universal thermodynamic behaviour [111]. Owing to this remarkable property, the physics of other strongly interacting Fermi systems such as neutron stars or quark-gluon plasmas, can be investigated in experiments with cold atoms.

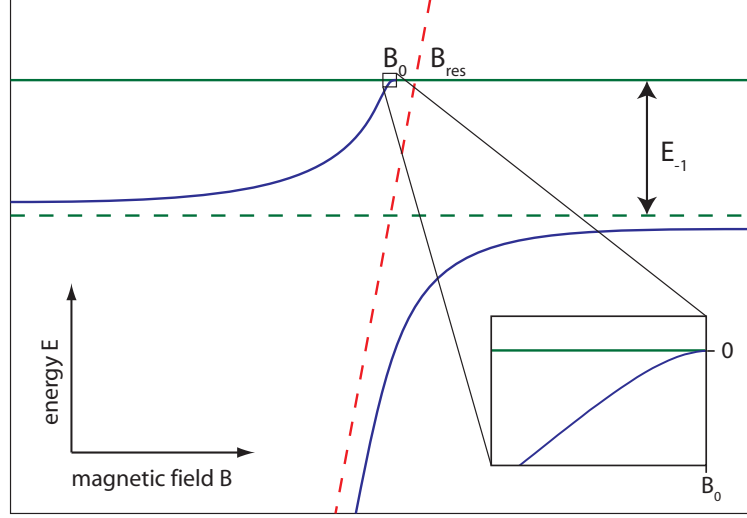


Figure 4.2: Energies of the coupled channels as a function of magnetic field. The green horizontal lines correspond to the dissociation threshold (solid) and the highest vibrational bound state (dashed) of the open channel and the red tilted line (dashed) to the highest vibrational bound state of the closed channel. The inter-channel coupling results in the energy states shown in blue. The inset magnifies the region of small binding energies of the Feshbach molecule where expression (4.15) is valid.

Reaching the unitary limit requires a broad Feshbach resonance fulfilling the zero-range limit condition and the condition $k_F r_e \ll 1$, which ensures that the entire Fermi gas is in the same interaction regime (the effective range r_e characterises the energy width of the resonance, see above) [90, 45].

4.3.2 Resonances in ^{40}K

For ^{40}K two broad s -wave Feshbach resonances and one p -wave Feshbach resonance are known for the lowest hyperfine manifold $F = 9/2$. They can all be easily accessed in experiments owing to the moderate magnetic field values of their positions:

$\{m_{F,1}, m_{F,2}\}$	<i>partial wave</i>	<i>position [G]</i>	<i>width [G]</i>	<i>references</i>
$-9/2, -7/2$	s	202.1 ± 0.1	7.8	[112, 2]
$-9/2, -5/2$	s	224.21 ± 0.05	9.7 ± 0.6	[113]
$-7/2, -7/2$	p	$\sim 198.8 \pm 0.5$ ($T = 0$)		[114]

Table 4.1: Parameters of the Feshbach resonances in ^{40}K used in our experiments.

The s -wave resonance at 202.1 G is the most utilised in experiments and is described in some more detail in the following. It involves the two lowest magnetic hyperfine

levels $|F = 9/2, m_F = -9/2\rangle$ and $|9/2, -7/2\rangle$ (Fig. 4.3) which do not suffer from spin-exchange collisions [115]. In appendix 10.1 it is shown that the atoms in these states are in an almost pure triplet configuration. For this reason the background scattering length $a_{\text{bg}} = 174a_0$ is nearly identical to the triplet scattering length [116]. The *positive* value is due the fact that the highest vibrational level of the background scattering potential lies an amount of $E_1 = h \cdot 8.75 \text{ MHz}$ *below* the dissociation threshold (see Fig. 4.2) [102]. It is this state which is responsible for the shift of the resonance position of $B_0 - B_{\text{res}} = -9.274 \text{ G}$. To get an idea of the origin of the Feshbach resonance we can consider the potential (4.13) for the spin-spin interaction. Since it conserves the total spin projection $M_F = m_{F,1} + m_{F,2} = m'_{F,1} + m'_{F,2} = -8$, the only possible coupling is between the $|9/2, -7/2\rangle$ atom and an atom in the state $|7/2, -7/2\rangle$ [97]. Owing to the difference in magnetic moment of $\Delta\mu \approx 14/9 \mu_B$, the bound state of the closed channel can be brought into resonance with the entrance channel by applying a magnetic field. Feshbach molecules created at this resonance have a fraction of at most 8% associated with the closed channel.

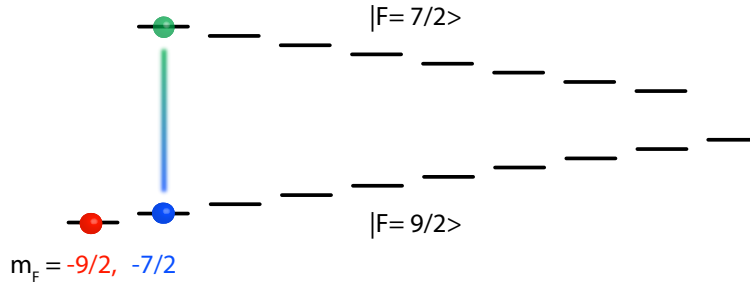


Figure 4.3: Level scheme of the lowest hyperfine states of ^{40}K at nonzero magnetic field. The quantum number m_F increases from left to right. The vertical line indicates the Feshbach coupling between the channels.

As described in chapter 5, we prepare our degenerate Fermi gas on the BCS side of the resonance (see Fig. 4.4). From there we can lower the magnetic field to access arbitrary negative values of the scattering length, or increase it to approach the background value. On the other hand, it is not obvious how large positive scattering lengths can be achieved since crossing the resonance would result in the formation of molecule. In this respect, the existence of a second resonance at 224 G is very helpful: we can transfer the atoms from the state $|9/2, -7/2\rangle$ to the state $|9/2, -5/2\rangle$ using a radio-frequency pulse and access the BEC side of that resonance from magnetic fields lying below. In this way, the experimentally accessible range of positive values of the scattering lengths is not limited by the background value a_{bg} .

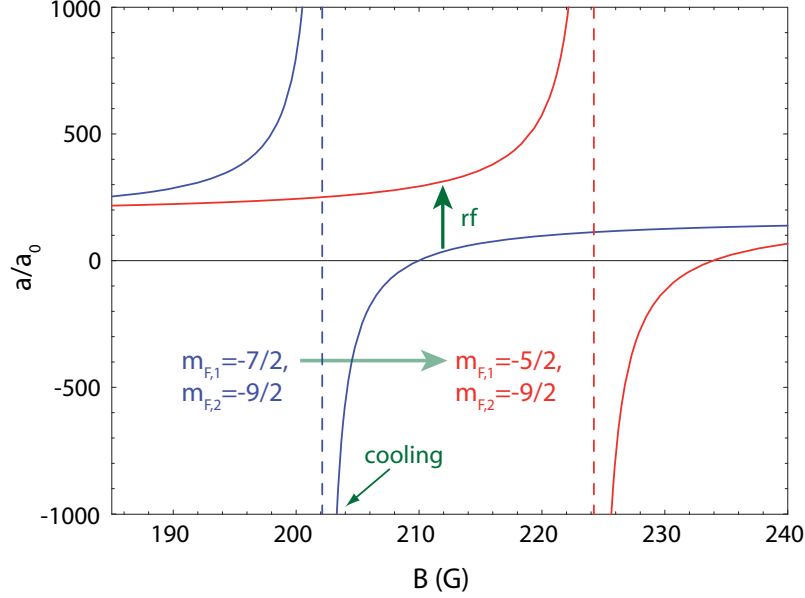


Figure 4.4: The scattering length (in units of the Bohr radius) as a function of magnetic field for the two s -wave Feshbach resonances in the $F = 9/2$ hyperfine manifold of ^{40}K . We cool our Fermi gas at the indicated point and can then—after applying an rf-pulse—access large scattering lengths.

4.4 Scattering in optical lattices

Whilst interactions are the source of fascinating many-body phenomena predicted to occur for a Fermi gas in an optical lattice, the two-body interaction itself already entails impressive features when the particles are subject to a tight confinement. Hence, it is instructive to examine the scattering between atoms in deep lattices, where the sites are isolated and can be regarded as harmonic potential wells with frequency ω_{\perp} in the strongly confined direction(s). In such a well the ground state energy $\sim \hbar\omega_{\perp}$ is considerable and the extension of the atomic wave functions along the standing waves are constrained to the harmonic oscillator length $a_{\perp} = \sqrt{\hbar/m\omega_{\perp}}$. When these quantities are of the same order of magnitude as the energy and length scales of the interatomic interaction new scattering effects, which are not encountered in weakly confining potentials, can be observed.

A unique system is realised when the temperature and the chemical potential of the gas are much smaller than the level spacing in the strongly confined dimension:

$$\mu, k_B T \ll \hbar\omega_{\perp}. \quad (4.17)$$

In this case the atoms basically only occupy the Gaussian ground state in the transverse directions, effectively reducing the system to two, one or “zero” dimensions. An example

of the kinematic restriction in low-dimensional systems is the suppression of specific anisotropic scattering channels in a gas interacting through p -wave scattering, as will be shown in chapter 7. Let us first focus on the less exotic s -wave problem in one dimension, i. e. a system with two perpendicular strong standing waves. The interaction strength can be parameterised by an effective 1D coupling parameter g_{1D} in the limit of small scattering lengths (or weak confinement), $|a| \ll a_{\perp}$ [117]. By averaging the 3D pseudo-potential (4.11) over the radial ground state density profile one obtains $g_{1D} = 2\hbar\omega_{\perp} \cdot a$. Near a Feshbach resonance where $a > a_{\perp}$ a more rigorous approach is required to solve the scattering problem. Olshanii found the following behaviour for the coupling strength in the resonant case ($|a| \ll r_e$) [118]:

$$g_{1D} = \frac{2\hbar^2}{ma_{\perp}^2} a \left(1 - C\sqrt{2}\frac{a}{a_{\perp}} \right)^{-1} \quad (4.18)$$

with $C = -\zeta(1/2) = 1.4603\dots$, where ζ denotes the Riemann zeta function. If a becomes of the same magnitude as a_{\perp} , a divergence leads to a so-called confinement-induced resonance. This is similar to a Feshbach resonance, the transverse modes of the confinement playing the roles of open and closed scattering channels [119]. An exceptional feature here is the existence of a two-body bound state also for negative values of the scattering length $a < 0$, which is solely stabilised by the confinement. Our experiment demonstrating confinement-induced molecules will be described in chapter 6.2.

In the case of a deep three-dimensional lattice, one can consider the problem of two interacting particles in a three-dimensional harmonic well with frequency ω_{site} . For a pseudo-potential interaction this has been solved analytically in ref. [120], and the eigenenergies depend on the scattering length via

$$\frac{\Gamma(-E/2\hbar\omega)}{\Gamma(-E/2\hbar\omega - 1/2)} = \frac{1}{\sqrt{2}} \frac{a_{\text{ho}}}{a}, \quad (4.19)$$

where $\Gamma(x)$ denotes the Gamma function and $a_{\text{ho}} = \sqrt{\hbar/m\omega_{\text{site}}}$. The energy spectrum as a function of a/a_{ho} is plotted in Fig. 4.5. For $a = 0$ the energy levels coincide with the unperturbed harmonic oscillator states, and the effect of the interaction is a coupling between these states. The lowest branch of the spectrum contains a molecular bound state for positive values of a , which can be accessed by crossing a Feshbach resonance to tune the scattering length from negative values over its singularity to positive values. Section 6.3 reports on the formation and detection of molecules in a deep 3D lattice. From Fig. 4.5 it is also apparent what happens if a Feshbach resonance is crossed in the opposite direction: tuning the scattering length from $a > 0$ to $a < 0$ two initially non-interacting atoms in the ground state can be adiabatically transferred into the first excited state. In the language of the periodic lattice potential this means that atoms in the lowest Bloch band shift to the next highest band. It is then obvious that the validity of the single-band Hubbard model introduced in the previous chapter breaks down as soon as the interaction energy U becomes comparable to the level spacing, $U \sim \hbar\omega$ [86]. The interaction-induced coupling of Bloch bands has been observed in our experiment described in section 6.1.

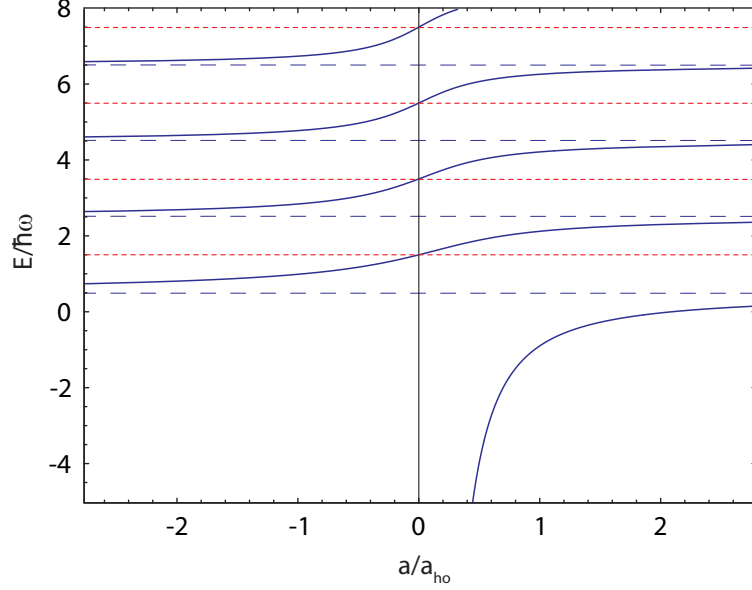


Figure 4.5: Energy spectrum of the relative motion of two interacting particles in a 3D harmonic potential as a function of the scattering length in units of the harmonic oscillator length. The blue dashed lines correspond to the energies on resonance and the red short-dashed lines to the eigenenergies of the non-interacting system.

In shallow lattices the atoms are delocalised over several sites and the scattering states are again different. A molecular state then exists below a critical negative value of the scattering length which depends on the dimension of the lattice and its potential depth [121].

So far we have quietly assumed that the interaction is well described by a pseudo-potential. However, this assumption is not obvious since the new length scale a_{\perp} (or a_{ho}) introduced by the optical lattice could violate the assumptions made in section 4.2. The energy scale $\hbar^2 k_{\text{typ}}^2 / m = \hbar \omega_{\perp}$ associated with the harmonic oscillator redefines the typical wave vector $k_{\text{typ}} = a_{\text{ho}}^{-1}$. For very tight lattice confinement the product $k_{\text{typ}} \beta_6$ can be on the order of 1 or larger such that the condition (4.9) (with k_F replaced by k_{typ}) is not satisfied. In that case the scattering wave function is not in the asymptotic regime, which questions the application of the usual pseudo-potential [122]. Furthermore, close to a Feshbach resonance the diverging scattering length drops out in the condition (4.10) for the zero-range limit. One must then check that the harmonic oscillator length of a site a_{ho} is larger than the effective range r_e . Otherwise one has to employ an energy-dependent (three-dimensional) pseudo-potential beyond the zero-range limit by replacing the scattering length a by the effective range expansion [123, 124]

$$a_E = \left(\frac{1}{a} - \frac{1}{2} k^2 r_e \right)^{-1}, \quad (4.20)$$

where $k = \sqrt{mE}/\hbar$ is the usual scattering wave number (see section 4.1). As we will see in chapter 6.1, in our experiments we have $a_{\text{ho}} \gg (\beta_6, r_e)$, such that the usual energy-independent pseudo-potential models the interaction fairly well.

5 Preparation of the quantum degenerate gases

For the experiments described in this thesis we used a state-of-the-art apparatus to cool bosonic rubidium (^{87}Rb) and fermionic potassium (^{40}K) atoms to quantum degeneracy and to load them into an optical dipole trap and a three-dimensional optical lattice. It was built, starting in 2001, with the goal to combine the research fields of ultracold fermions and three-dimensional optical lattices [125, 58]. The setup consists of two main parts, complemented by a considerable amount of electronic control devices: the ultrahigh vacuum system (UHV) and the laser system. An excellent vacuum is necessary to thermally isolate the trapped atoms as well as possible. The lasers deliver the coherent light at different wavelengths used to cool, trap, manipulate and detect the atoms. All lasers are situated on a separate optical table, together with the optical and electro-optical elements necessary to control their frequencies and intensities. The beams are then input coupled into polarisation-maintaining optical fibres and guided to another optical table which supports the vacuum system and the optics used to direct the light through the chamber and the glass cell. The original design of the vacuum system integrating a magnetic transport is due to M. Greiner [126] and allows for excellent optical access to the cell where experiments in a three-dimensional lattice are performed.

This chapter gives an overview of the experimental setup and the parameters used to prepare the quantum degenerate gases, attaching more importance to the parts in the setup which have been implemented or changed during my PhD. More details on the original apparatus and its components can be found in the theses of my predecessors, T. Stöferle [125] and H. Moritz [58].

5.1 Overview of the cooling cycle

In the first chamber of the vacuum system (pressure 10^{-8} mbar) about 10^7 fermionic ^{40}K atoms and 2×10^9 bosonic ^{87}Rb atoms are trapped and cooled to a temperature of roughly $100\ \mu\text{K}$ in a three-dimensional double-species magneto-optical trap (MOT). The magnetic quadrupole field is then switched off to perform further polarisation gradient cooling in an optical molasses before the atoms are optically pumped into low-field seeking Zeeman sub-states. At this stage the clouds are recaptured in a purely magnetic trap, allowing for their magnetic transportation from the MOT vacuum chamber to the glass cell (pressure $\sim 10^{-11}$ mbar), see Fig. 5.1. In a magnetic trap microwave (MW) evaporative cooling is applied on the rubidium atoms to bring the gases to quantum-degeneracy. The fermionic cloud is thereby cooled sympathetically by the thermal contact with the bosons. When the bosonic species is removed completely, we are left with $(1-1.5) \times 10^6$ spin-polarised ^{40}K

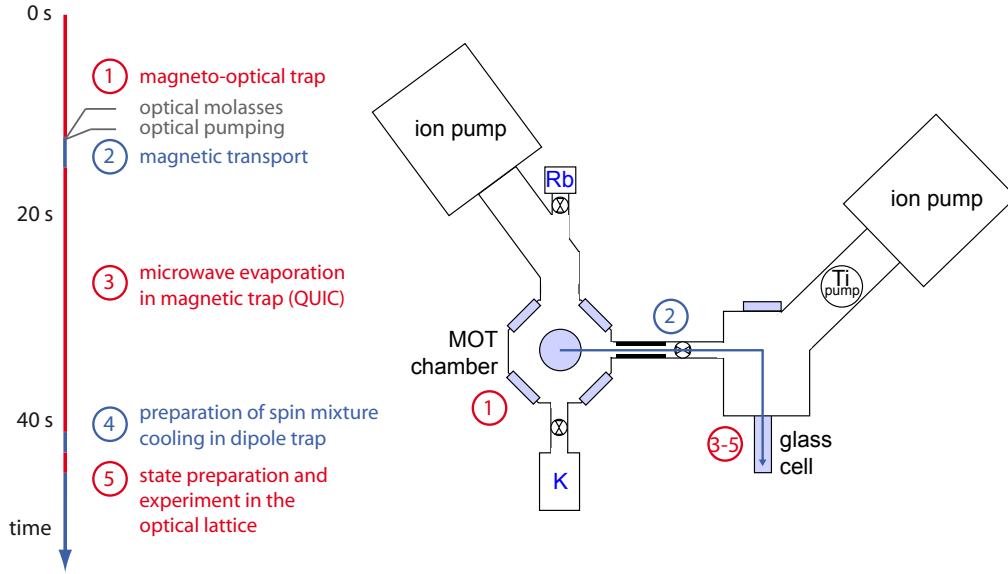


Figure 5.1: Timeline of the experimental sequence and scheme of the vacuum system.

atoms at a temperature of $0.35 T_F$. In order to cool the fermions further, it is necessary to prepare a spin mixture, thereby allowing for s -wave collisions between atoms with different spin. This is accomplished in a crossed-beam dipole trap into which the atoms are first transferred. By lowering the intensity of the beams, the hottest atoms are evaporated from the trap, ultimately obtaining a fermionic cloud of $(1-2) \times 10^5$ atoms at a degeneracy of $(0.15-0.25) T/T_F$. After the preparation of the desired spin states and adjustment of the magnetic bias field, the atoms are loaded into the optical lattice. This concludes the preparation stage, and the actual experiments can be pursued subsequently.

5.2 ^{87}Rb and ^{40}K and their cooling transitions

Cooling alkali gases with laser light works well thanks to the simple electronic structure of the atoms. For the single electron in the outermost shell, closed optical transitions exist, reducing the atom effectively to a two-level system under certain conditions.

Figure 5.2 shows the hyperfine structure relevant for the D_1 and the D_2 transitions of ^{40}K and ^{87}Rb . The D_2 transitions indicated by thick arrows are those used for laser cooling. Atoms accidentally escaping the transition cycle are repumped by lasers resonant with the transitions indicated by the thin arrows. The hyperfine structure of ^{40}K is somewhat special in the sense that it is inverted (the level with the largest hyperfine quantum number $F = 9/2$ has the lowest energy) and that it has a rather small splitting. The reason for this is in the relatively small nuclear magnetic moment which is antiparallel to the nuclear spin I . In particular, the small hyperfine splitting in the $4^2P_{3/2}$ manifold makes sub-Doppler cooling very difficult [127]. More details about the atomic species can be found in appendix 10.2.

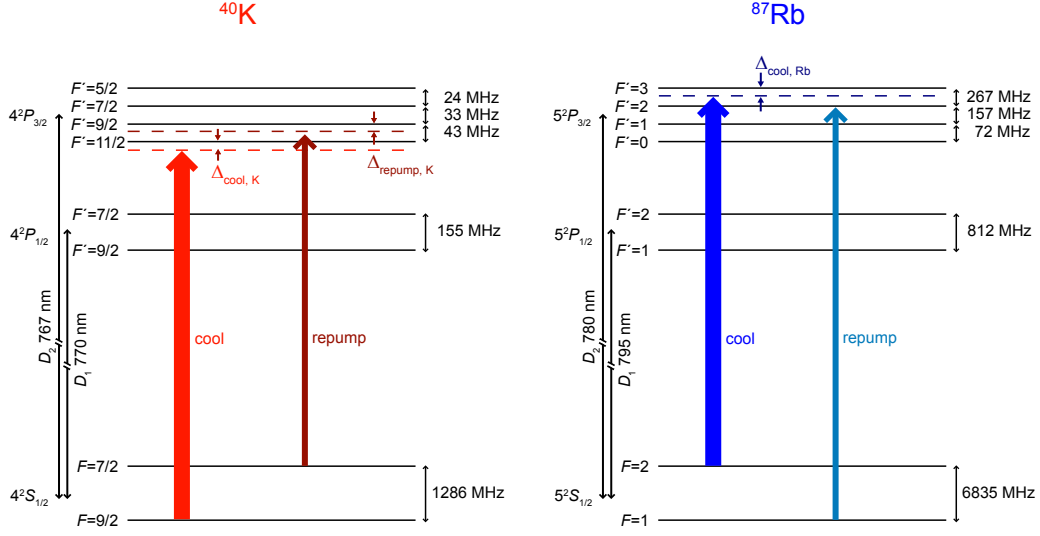


Figure 5.2: Schemes of the hyperfine level structures of ^{40}K and ^{87}Rb and of the optical transitions in the D_2 -lines used for laser cooling. Energies are not to scale.

In our experiment all (near-)resonant light sources used for cooling and optical pumping are provided by grating stabilised external cavity diode lasers and tapered amplifiers. Their frequencies are stabilised to features of the atomic absorption spectra by performing frequency modulation spectroscopy [128] on rubidium and potassium vapour cells.

5.3 Atom sources and MOT

The ^{87}Rb source consists of an ampul filled with 2 g rubidium placed in an heatable extension of the vacuum chamber. Due to the vapour pressure, which we control by the temperature, atoms diffuse into the MOT chamber where they can be captured. The low natural abundance of ^{40}K requires an enriched source in order to capture sufficiently large clouds at reasonably low pressures. Initially we were using dispensers built following a design by DeMarco et al. [129], which, when heated by an electric current, produce ^{40}K atoms from a reaction between potassium chloride salt enriched in ^{40}K and calcium. When we exchanged the dispensers for the first time, we also installed an ampul of 50 mg potassium enriched to 7% ^{40}K *. After a few days of heating at temperatures of up to 80 °C we were able to load a large number of atoms from the background vapour into the MOT. Currently, we heat the ampul to 40–60 °C in continuous mode during operation of our cold atom machine, without operating the dispensers.

A MOT constitutes the first cooling stage in experiments with ultra-cold atoms [130].

*The potassium chloride powder was bought from Trace Sciences International Corp., Richmond Hill, Canada. The metallic potassium was obtained by distillation into a quartz glass ampul by Technical Glass, Inc., Aurora, USA.

5 PREPARATION OF THE QUANTUM DEGENERATE GASES

Atoms are cooled by the dissipative light forces of three mutually perpendicular pairs of counter-propagating beams. The frequency of the beams is red-detuned from the cooling transition and the Doppler effect makes the force velocity-dependent. In addition, a magnetic quadrupole field introduces a position-dependence via the Zeeman effect, confining the atoms in the centre region. After the MOT phase, we switch off the magnetic field and increase the frequency detuning to apply polarisation gradient cooling in an optical molasses [131]. The cooling light for both atomic species and the repumping light for potassium (produced by an electro-optical modulator) is input coupled into a single optical fibre and follows the same optical path, while another fibre guides the repumping beam for rubidium. The following table summarises the parameters of the double-species MOT and the optical molasses:

<i>parameter</i>	^{40}K	^{87}Rb
cooling power (fibre output)	550 mW	140 mW
repumping power (fibre output)	120 mW	5 mW
cooler detuning Δ_{cool}	-5.75 Γ	-3 Γ
repumper detuning Δ_{repump}	-5.75 Γ	0 Γ
magnetic field gradients	(-5, -5, 10) G/cm	(-5, -5, 10) G/cm
loading duration	11.5 s	3 s
atom number	$\sim 10^7$	2×10^9
molasses detuning	-3 Γ	-10 Γ
molasses duration	6 ms	6 ms

Table 5.1: Summary of the parameters for the sequence of the MOT and the optical molasses cooling.

5.4 Magnetic trapping and evaporative cooling

After completion of the laser cooling stage the atoms are transferred to a magnetic trap for evaporative cooling.

The concept of magnetic trapping of neutral atoms is based on the atom's interaction with a spatially varying magnetic field $\mathbf{B}(\mathbf{r})$. An atom in a hyperfine state $|F, m_F\rangle$ has a dipole moment $\boldsymbol{\mu} = \mu_B g_F \mathbf{F}/\hbar$ (Zeeman regime) leading to a magnetic energy $E_m(\mathbf{r}) = -\boldsymbol{\mu} \cdot \mathbf{B}(\mathbf{r})$, where g_F is the Landé factor and μ_B the Bohr magneton. If $\boldsymbol{\mu}$ is antiparallel to \mathbf{B} , the atom is called a low-field seeker because the force $\mathbf{F}_m = -\nabla E_m$ pushes it towards smaller values of $|\mathbf{B}|$. Low-field seeking neutral atoms can therefore be confined in the proximity of a minimum of a magnetic field $\mathbf{B}(\mathbf{r})$. The field of a magnetic trap is usually produced by a combination of several magnetic coils [132].

In our experiment the atoms are after the molasses phase optically pumped into low-field seeking states by σ^+ -polarised light resonant with the $F = 2$ to $F' = 2$ D_2 -transition for rubidium and with the $F = 9/2$ to $F' = 9/2$ D_2 -transition for potassium, while a small constant magnetic field provides the quantisation axis. After 1.8 ms almost all rubidium and potassium atoms have ended up in the maximally polarised states $|F = 2, m_F = 2\rangle$

and $|F = 9/2, m_F = 9/2\rangle$, respectively, and can be trapped magnetically. For this purpose, the current in the MOT coils is switched on again, producing a quadrupole field which is mode-matched to the size of the atomic clouds. A sequence of magnetic coil pairs in anti-Helmholtz configuration is then consecutively turned on to transport the clouds through a narrow tube over a distance of 40 cm around the corner into the glass cell (see (2) in Fig. 5.1). The glass cell and the surrounding coils are enclosed in a mu-metal box for magnetic shielding. The narrow tube between the MOT chamber and the UHV chamber provides a differential pumping stage. A 75 l/s ion pump and a titanium getter pump maintain a UHV pressure of about 10^{-11} mbar. The resulting cloud lifetime is long enough to perform evaporative cooling (see stage (3) in Fig. 5.1).

A prerequisite for reaching quantum degeneracy is a large enough cross section for elastic collisions between atoms, which ensures thermal equilibrium during the cooling of the gas. However, we saw in chapter 4 that spin-aligned fermions do not collide in at ultralow temperatures: the minimal distance between two equal fermions given by the de Broglie wavelength is very large compared the range of the interatomic potential. Elastic collisions which are essential for evaporative cooling thus have a negligible cross section. The presence of bosonic atoms circumvents this problem since thermalisation of the fermions is ensured by inter-species collisions. This so-called sympathetic cooling works nicely in our experiment owing to the favourable collisional properties between the ^{87}Rb and the ^{40}K atoms [133]. During the evaporative cooling the clouds are confined by the harmonic potential of a magnetic trap in the quadrupole-Ioffe configuration, known as QUIC-trap [134]. A field minimum of $B_0 = 3.1$ G avoids losses due to Majorana spin flips [135]. The hottest ^{87}Rb atoms are selectively removed from the trap, whereas the remaining ones thermalise at a lower temperature—the fermions ^{40}K are cooled sympathetically by thermal contact with the bosons. The evaporation is carried out by microwave radiation at approximately 6.8 GHz which transfers rubidium atoms from the state $|2, 2\rangle$ to the anti-trapped high-field seeking state $|1, 1\rangle$ while the potassium atoms remain unaffected. Because of the Zeeman shift the microwave is resonant only for atoms at a certain magnetic field and therefore determines a shell in the trap where evaporation occurs. A large shell corresponding to a high microwave frequency, for instance, is solely traversed by the trajectories of hot atoms. By lowering the frequency exponentially in time, the temperature of the gas is continuously decreased during a total time of 26 s. At the same time, the trap is slightly decompressed to reduce inelastic three-body losses. We also apply an additional MW-field of constant frequency to remove atoms in the state $|2, 1\rangle$ at the trap bottom which appear during evaporation and cause unfavourable collisions with the fermionic atoms leading to loss. The final frequency of the sweep determines how many cold bosons are kept for the experiment with the fermions. For instance, we can produce a Bose-Einstein condensate of $(3\text{--}5) \times 10^5$ ^{87}Rb atoms in the presence of up to 10^6 ^{40}K atoms at a degeneracy of $T/T_F = 0.35$. The final trapping frequencies of the QUIC are $\omega_x = 2\pi \cdot 29$ Hz, $\omega_y = 2\pi \cdot 180$ Hz and $\omega_z = 2\pi \cdot 183$ Hz for potassium and accordingly scaled by the mass scaling factor $\sqrt{m_K/m_{\text{Rb}}} \approx 0.68$ for rubidium (neglecting the difference in the gravitational sag).

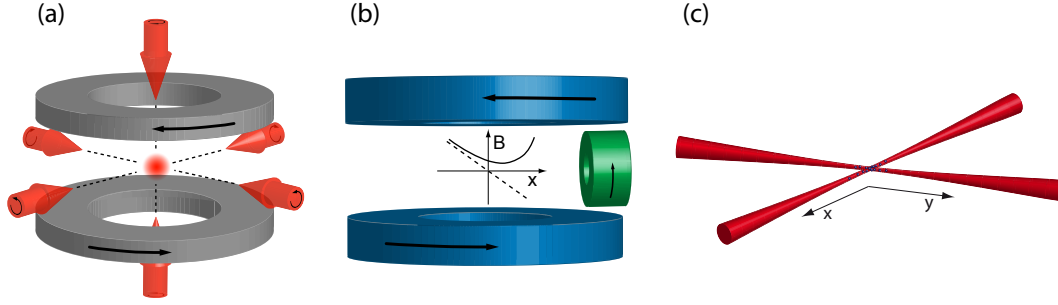


Figure 5.3: The atom traps used at the different stages of the experimental sequence: (a) magneto-optical trap (MOT), (b) magnetic QUIC trap, and (c) crossed-beam dipole trap (FORT).

5.5 Setups for the optical potentials

To be able to access a Feshbach resonance, the atoms have to be prepared in the magnetic hyperfine states of the corresponding entrance scattering channel. Since these are high-field seeking states which cannot be trapped magnetically, the atoms are first transferred from the magnetic trap into an optical dipole trap (FORT) consisting of two perpendicular laser beams in the horizontal plane intersecting at the position of the cloud. The atoms are attracted to the intensity maximum of the far red-detuned light and trapped independent of their spin state (see paragraph 3.1). In the next step the atoms are loaded into an optical lattice.

For our most recent experiments, including our studies of Bose-Fermi mixtures presented in chapter 8 of this thesis, our original setup of the FORT and the optical lattice has been modified. In the following I will describe both the previous and the new configuration.

5.5.1 The first setup

In our first as well as in our new setup, the laser beams for the dipole trap are derived from two tapered amplifiers seeded by a single diode laser at a wavelength of 826 nm, which can be stabilised to a high-finesse cavity yielding a line width of about 10 kHz. Their frequencies are offset with respect to each other by several tens of MHz in order to avoid cross-dimensional interference. In the previous configuration they were focused to waists of approximately $50 \mu\text{m}$ (x -axis) and $70 \mu\text{m}$ (y -axis), respectively. The maximum trapping frequencies for potassium were $\omega_{T,x} = 2\pi \cdot 93 \text{ Hz}$, $\omega_{T,y} = 2\pi \cdot 154 \text{ Hz}$ and $\omega_{T,z} = 2\pi \cdot 157 \text{ Hz}$.

To transfer the atoms from the magnetic to the optical trap, the intensities of the two beams are ramped up to 80 mW in 100 ms. Next, the currents in the QUIC coils are turned off in 100 ms, whereas a magnetic bias field of 13 G produced by two large coils centred on the x -axis is maintained. A short radio-frequency (rf) sweep drives a Landau-Zener transition transferring all ^{40}K atoms from the state $|F = 9/2, m_F = 9/2\rangle$

to the state $|F = 9/2, m_F = -9/2\rangle$. An equal incoherent spin mixture of $|9/2, -9/2\rangle$ and $|9/2, -7/2\rangle$ atoms is produced by a 200 ms long rf-pulse resonant with the transition between the two states at a bias field of 232.9 G. At this field well above the Feshbach resonance located at 202.1 G [112] the scattering length has a value of about $130a_0$, and the gas can be further cooled evaporatively by lowering the laser intensities [136] by approximately a factor of three. After 2 s we end up with a spin mixture of up to 2×10^5 atoms at $T/T_F = 0.2$ – 0.25 .

Previously, the laser beams of the FORT were subsequently used to create the standing waves for the optical lattice in the horizontal plane. Together with an additional standing wave along the vertical z -direction (waist $70 \mu\text{m}$) they created the simple cubic lattice. Prior to loading the atoms into the optical lattice we tuned the magnetic field to the zero-crossing at (210 ± 0.1) G of the Feshbach resonance, where the scattering length between the two states vanishes. Then the standing wave along the vertical direction is turned on. After ramping down the intensity of the trapping beam along the y -axis, the mechanical shutter in front of a retro-reflecting mirror is opened, and the intensity is ramped up again resulting a standing wave, followed by the same procedure for the x -axis. In order to load the atoms into the lowest band of the lattice as adiabatic as possible the intensities of the lasers are slowly increased (decreased) using exponential ramps with time constants of 10 ms (25 ms) and durations of 20 ms (50 ms), respectively.

5.5.2 The new setup

The fact that the optical lattice is generated by the same laser beams which are previously used for the FORT entails some crucial drawbacks apart from implying a complicated ramping sequence for the laser intensities (as detailed in the previous paragraph). During the ramping of the beams the sag changes several times such that Bloch oscillations [137] may be induced. These occur because the atoms experience a potential gradient in the lattice as soon as they are not in their equilibrium position anymore.

In view of the objective to realise strongly correlated quantum phases the old setup had a further disadvantage. Many interesting quantum states such as the fermionic Mott insulator or the antiferromagnetic state appear at a lattice filling factor of around one half [83, 138]. This in turn requires a Fermi gas with a low density to be loaded into the optical lattice. In the former setup the rather tight beam waists resulted in a strong harmonic confinement where this was hard to achieve.

For these reasons, the setup to create the optical potentials was modified in the second half of 2005 and a solid-state Nd:YAG (Neodymium-doped Yttrium Aluminium Garnet) laser was integrated to create an optical lattice independent of the FORT. An overview of the parameters of the current optical potentials is given in Table 5.2 at the end of this section. Great care was taken to make the beams mechanically stable and to achieve small M^2 values. We use polarisation maintaining single-mode fibre optics whose facets on the output side are angle-cut such that no standing wave can build up between the facets and any other optical element in the optical path. This eliminates the need of optical isolators which could affect the beam quality. All optical elements including the

high-stability fibre couplers[†] are mounted on massive posts to minimise mechanical drifts.

Cooling in the new dipole trap

The waists of both beams were increased to approximately $50\text{ }\mu\text{m}$ and $150\text{ }\mu\text{m}$ in the vertical (z) and horizontal (x, y) directions, respectively, in order to create a large volume trap such that lower densities in a degenerate Fermi gas can be achieved. The beams have elliptical Gaussian profiles with tighter waists in the vertical direction to facilitate holding the atoms against gravity. Optimisation of the cooling parameters in the new optical trap rewarded us with larger atom numbers at lower temperatures.

Initially, our intention was to transfer some ^{87}Rb atoms together with the ^{40}K to the FORT for sympathetic cooling with the spin mixture. Due to their larger sag the rubidium atoms experience a shallower potential and are evaporated out of the trap before the potassium atoms. After ramping up the dipole trap to a depth of $3.5\text{ }\mu\text{K}$ the rubidium is transferred to its absolute ground state $|F = 1, m_F = 1\rangle$ by a microwave pulse with constant frequency while sweeping the magnetic bias field in 5 ms from 13.4 G to 12.8 G, followed by the Landau-Zener transition of the potassium to the state $|F = 9/2, m_F = -9/2\rangle$. If the rubidium instead is in the $|F = 2, m_F = 2\rangle$ state, large losses are observed. After the preparation of the spin mixture $|F = 9/2, m_F = -9/2\rangle$ and $|F = 9/2, m_F = -7/2\rangle$ as described above, the magnetic bias field is tuned to a value of 203.3 G where the scattering length is approximately $-1000a_0$. It turns out that on this side of the Feshbach resonance atom loss due to three-body recombination processes is uncritical in contrast to the repulsive side [112, 139]. We lower the power of the trapping lasers exponentially in one second with a time constant of 0.5 s by a factor of three to four to obtain a Fermi gas of $(1-2)\times 10^5$ atoms at $(0.15-0.2)T/T_F$. Ultimately, the trap is slightly re-compressed, having frequencies of $\omega_{T,x} = \omega_{T,y} = 2\pi \cdot 35\text{ Hz}$ and $\omega_{T,z} = 2\pi \cdot 120\text{ Hz}$ in its final configuration.

With the optimised parameters for the preparation of a purely fermionic quantum gas, it turned out that nearly all bosonic rubidium atoms are evaporated from the magnetic trap, and none or very few are transferred into the optical trap. When preparing a Bose-Fermi mixture a modified sequence, which is described in chapter 8, is applied.

The new optical lattice

In the new configuration the lattice beams are independent of the trapping beams and derived from a Nd:YAG laser[‡] emitting light at a wavelength of 1064 nm with a line width of 1 kHz. The light is split into three beams (x -, y - and z -axis) which are frequency offset from each other by several tens of MHz by means of acousto-optical modulators and have mutually perpendicular linear polarisations to avoid cross-dimensional interference. Figure 5.4 sketches the optical setup for the dipole trap, the optical lattice and the imaging beams. Behind the glass cell the lattice beams are retro-reflected by dichroic mirrors to

[†]The fibre optics as well as the inclined fibre couplers were purchased from Schäfter+Kirchhoff GmbH, Hamburg, Germany.

[‡]Mephisto laser from Innolight, Hannover, Germany, with a power of 2 W.

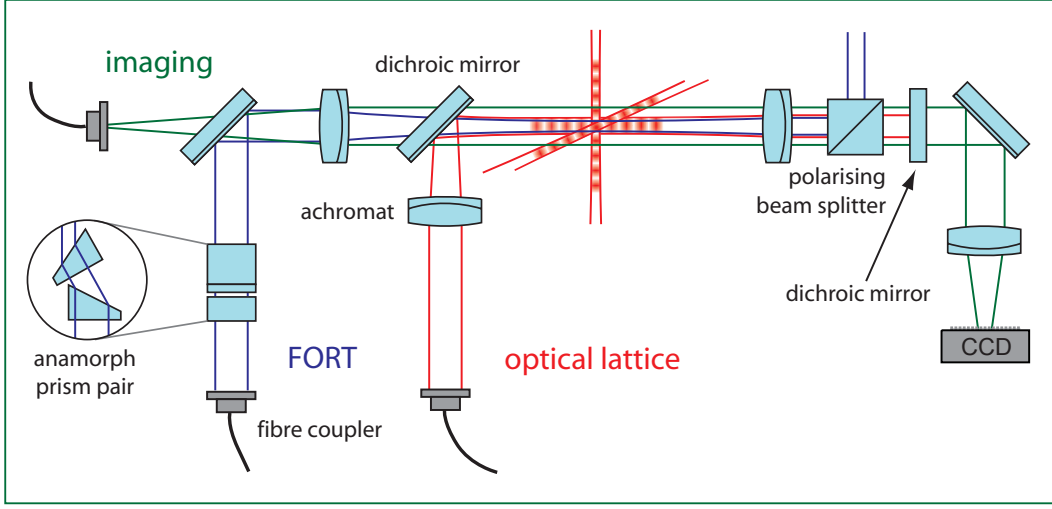


Figure 5.4: Optics setup for the laser beams of the optical lattice, the dipole trap and the imaging light in the horizontal x - and y -direction.

create the standing waves, whereas the FORT beams (in the horizontal plane) and the imaging light are supposed to pass without being reflected. However, the mirrors—not being perfectly dichroic—still reflect about 1% of the light at 826 nm, such that an additional weak standing wave builds up which noticeably disturbs the optical potential. We solved this problem by inserting a polarising beam splitter cube in front of the mirrors (x - and y -axis) to reflect off the light from the dipole trap. In principle, this arrangement allows us to tune the intensity of a super lattice by changing the polarisation angle of the 826 nm beams.

The three lattice beams have powers of 130 mW each and are focused to $1/e^2$ radii of $(160, 180, 160) \mu\text{m}$ along the (x, y, z) -directions centred at the position of the Fermi cloud in the optical trap. Their intensities are simultaneously ramped up in 100 ms following a smooth spline curve, while a magnetic bias field corresponding to a scattering length of about $50a_0$ is maintained to ensure thermodynamic adiabaticity. The radial confinement caused by the Gaussian shape of the beams is very weak, so that the external trapping potential of the FORT is only slightly increased in the horizontal x - and y -directions. In addition, the combination with the large volume dipole trap allows the realisation of systems with low fillings. Figure 5.5 shows plots of the combined potential created by the dipole trap and the 3D optical lattice.

To calibrate the power of the lattice beams we modulate the light intensity (amplitude modulation) and measure the parametric heating of a condensed bosonic cloud. Atoms are excited from the lowest to the third Bloch band (which has the same parity) if the modulation frequency matches the band separation [140]. From the measured resonance frequency we infer the potential depth of the lattice beams.

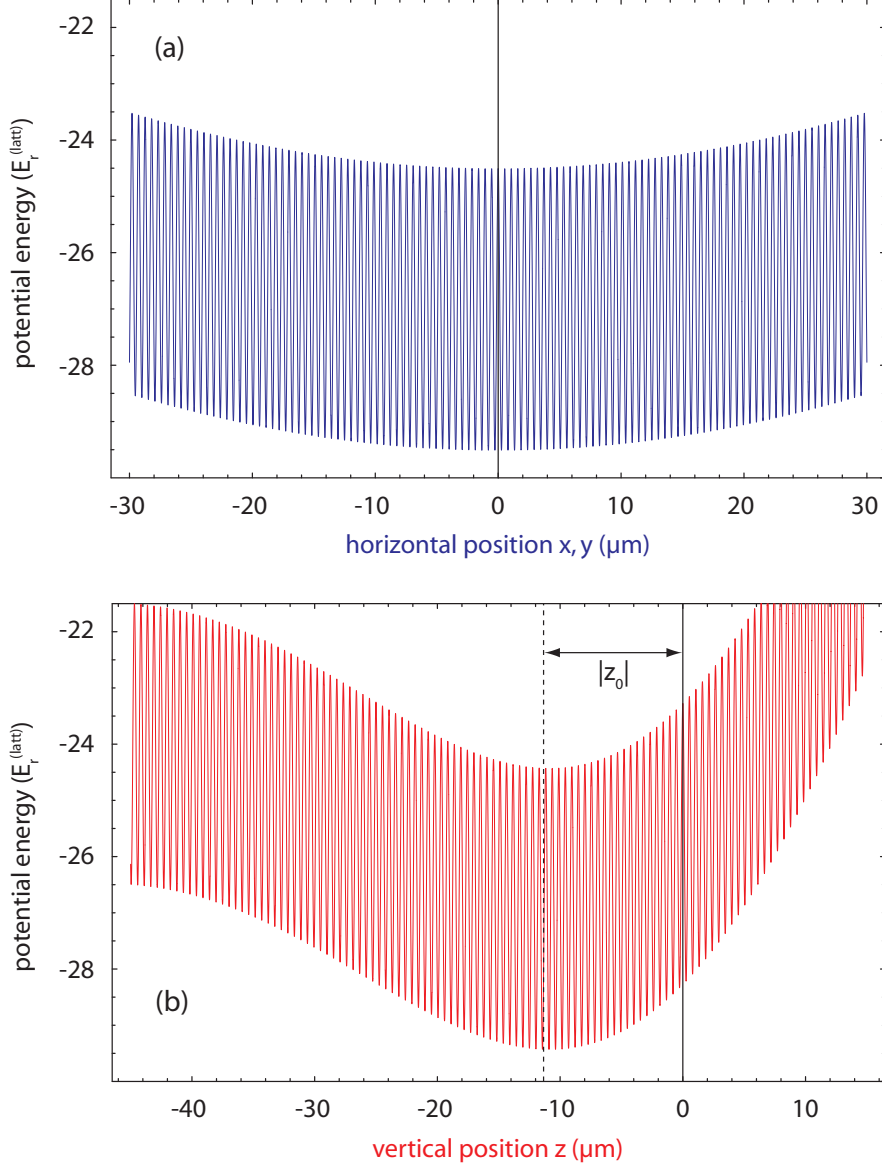


Figure 5.5: The combined potential of our crossed-beam optical dipole trap in the horizontal (x, y) plane, a three-dimensional optical lattice (x, y, z) and gravity for ^{40}K atoms (see section 3.1.3). (a) Potential in the horizontal direction ($y = 0$ and $z = z_0$) and (b) in the vertical direction ($x = y = 0$). Positions are given relative to the geometrical centre of the trap laser beams. The trap beams have a power of 35 mW each ($V_{T,x} = V_{T,y} = 4E_r$) resulting in a sag of $z_0 = -11.46 \mu\text{m}$. The lattice beams each have a depth of $V_{L,x} = V_{L,y} = V_{L,z} = 5E_r$. All other parameters are as given in Table 5.2.

<i>crossed-beam dipole trap (x, y)</i>	
wavelength	826 nm
horizontal waists w_h	150 μm
vertical waists w_v	50 μm
maximum beam power	120 mW
trap frequencies $\omega_{T,(x,y,z)}$ for ^{40}K (45 mW)	$2\pi \cdot (40, 40, 160)$ Hz
trap depth for ^{40}K (45 mW)	1.02 μK
<i>3D cubic optical lattice</i>	
wavelength λ	1064 nm
spectral line width	< 1 kHz
beam waists $w_L, (x, y, z)$	(160, 180, 180) μm
maximum power per beam	130 mW
maximum lattice depth for ^{40}K	7 E_r
external confinement ω_L for ^{40}K (5 E_r)	$2\pi \cdot 33$ Hz

Table 5.2: Summary of the parameters characterising the current optical potentials (see paragraph 3.1.3 for designations). The values given are approximate as most of them depend on the actual beam alignment.

6 s -wave interacting fermions and molecules in optical lattices

The exploration of quantum degenerate gases of fermionic atoms is driven by the ambition to get deeper insight into long-standing problems of quantum many-body physics, such as high temperature superconductivity. Not long ago, the cross-over regime between a strongly interacting two-component Fermi gas and a molecular Bose-Einstein condensate has been studied in harmonic traps [112, 95, 3, 141, 96]. These experiments mark a milestone towards the understanding of superfluidity of fermionic atoms. However, the analogy to an electron gas in a solid is limited since there the electrons experience a periodic lattice potential. The lattice structure is in fact a key ingredient for most models describing quantum many-body phenomena in materials. It has been suggested that strongly interacting fermionic atoms in optical lattices could be employed for studies of high- T_c -superconductivity [83], Mott insulating phases [69], Bose condensation of fermionic particle-hole pairs [142], or interacting spin systems [143].

In this chapter we report on our experiments with ideal and s -wave interacting fermions in different optical lattice configurations. This allows us to explore the physics in crystal structures as well as in low-dimensional systems.

6.1 Fermionic atoms in a three-dimensional optical lattice

Previous experiments in three-dimensional optical lattices employed bosonic atoms, and the analogy to solid state physics was limited. This section describes an experiment bridging the gap between current ultracold atom systems and fundamental concepts in condensed matter physics. A quantum degenerate Fermi gas is prepared in the crystal structure of a three dimensional optical lattice potential created by three crossed standing laser waves. The unique control over all relevant parameters in this system allows us to carry out experiments which are not feasible with solid-state systems. We directly image the Fermi surface of the atoms in the lattice by turning off the optical lattice adiabatically. Because of the confining potential, gradual filling of the lattice transforms the system from a normal state into a band insulator. The dynamics of the transition from a band insulator to a normal state is studied, and the time scale is measured to be an order of magnitude larger than the tunnelling time in the lattice. Using a Feshbach resonance, we increase the interaction between atoms in two different spin states and dynamically induce a coupling between the lowest energy bands.

Parts of this section are published in [25].

Previous experiments with far-detuned three dimensional optical lattices [144, 84, 145] were always carried out with bosonic atoms, and experiments with fermions were restricted to a single standing wave [146]. In the latter situation many atoms can reside in each standing wave minimum and the formation of a band insulator is prevented by the weak transverse confinement. The observed inhibition of transport [68] is due to localised states and therefore differs qualitatively from the band insulator which we create in the three dimensional optical lattice.

6.1.1 Experimental procedure

As described in section 5 we cool fermionic ^{40}K atoms in a magnetic trap sympathetically with ^{87}Rb atoms, on which microwave evaporation is performed. After reaching quantum degeneracy for both species with typically 6×10^5 potassium atoms at a temperature of $T/T_F = 0.32$ ($T_F = 260\text{ nK}$ is the Fermi-temperature of the non-interacting gas) all the rubidium atoms are removed from the trap. The potassium atoms are then transferred from the magnetic trap into a crossed beam optical dipole trap, as detailed in paragraph 5.5.1. In the optical trap we prepare a spin mixture with $(50 \pm 4)\%$ in each of the $|F = 9/2, m_F = -9/2\rangle$ and $|F = 9/2, m_F = -7/2\rangle$ spin states using a sequence of two radio frequency pulses. By lowering the depth of the optical trap on a time scale of 2 seconds we further evaporatively cool the potassium gas. This is done at a bias magnetic field of $B = 227\text{ G}$, which is well above the magnetic Feshbach resonance centred at $B_0 = 202.1\text{ G}$ [112] and the s-wave scattering length between the two fermionic spin states is $a = 118a_0$ (a_0 is the Bohr radius). At the end of the evaporation we reach temperatures between $T/T_F = 0.2$ and 0.25 with 5×10^4 to 2×10^5 particles, respectively.

The cloud is now loaded into the three-dimensional optical lattice (see paragraph 5.5.1) whose potential depth $V_{x,y,z}$ is proportional to the laser intensity and is conveniently expressed in terms of the recoil energy $E_r = \hbar^2 k^2 / (2m)$, with $k = 2\pi/\lambda$ and m being the atomic mass. The lattice depth was calibrated by modulating the laser intensity and studying the parametric heating. The calibration error is estimated to be $< 10\%$.

6.1.2 Observing Fermi surfaces

The potential created by the optical lattice results in a simple cubic crystal structure and the Gaussian intensity profiles of the lattice beams give rise to an additional confining potential which varies with the laser intensity. As a result, the sharp edges characterising the $T = 0$ distribution function for the quasi-momentum in the homogeneous case [65] are expected to be rounded off (see section 3.4). A quantitative picture for the inhomogeneous system can be obtained by considering the characteristic density (3.22) introduced in section 3.4. The density distribution scaled by ζ_α and the momentum distribution of the atoms in the lattice only depend on the characteristic density $\rho_c = Nd^3/\zeta_x\zeta_y\zeta_z$, where d is the lattice spacing [69]. For a three-dimensional lattice with $20 \times 20 \times 20$ sites we have numerically calculated the characteristic density for the onset of a band insulator to be $\rho_c \simeq 60$. For this value of ρ_c the occupation number at the centre of the trap is larger than 0.99. It has been pointed out that a fermionic band insulator in an optical lattice with confining potential constitutes a high fidelity quantum register [147].

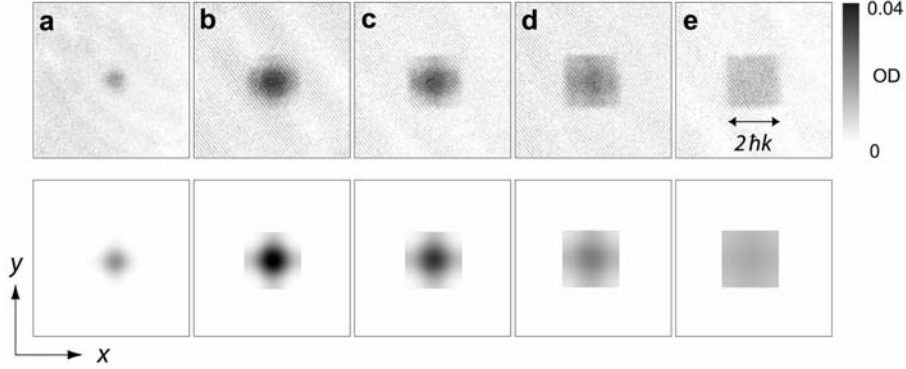


Figure 6.1: Observing the Fermi surface. Time of flight images obtained after adiabatically ramping down the optical lattice. The lower row shows the images obtained with a numerical simulation for the same parameters as in the experiment. The characteristic density increases from left to right. (a) 3500 atoms per spin state and a potential depth of the optical lattice of $5 E_r$. Images (b)-(e) were obtained with 15000 atoms per spin state. The potential depths of the optical lattices were $5 E_r$ (b), $6 E_r$ (c), $8 E_r$ (d) and $12 E_r$ (e). The images show the optical density (OD) integrated along the vertically oriented z -axis after 9 ms of ballistic expansion.

In the experiment we probe the population within the first Brillouin zones by ramping down the optical lattice slowly enough for the atoms to stay adiabatically in the lowest band whilst quasi-momentum is approximately conserved [126]. We lower the lattice potential to zero over a timescale of 1 ms. After 1 ms we switch off the homogeneous magnetic field and allow for total of 9 ms of ballistic expansion before we take an absorption image of the expanded atom cloud. The momentum distribution obtained from these time of flight images, shown in Fig. 6.1, reproduces the quasi-momentum distributions of the atoms inside the lattice. With increasing characteristic density the initially circular shape of the Fermi surface develops extensions pointing towards the Bragg planes and finally transforms into a square shape completely filling the first Brillouin zone deeply in the band insulator. We have observed population of higher bands if more atoms are filled into the lattice initially. In Fig. 6.2 the experimental data for momentum distributions along the line with quasi-momentum $\hbar q_y = 0$ are compared to the results of numerical simulations using the same characteristic densities.

When imaging the cloud along the x -direction we find a homogeneous filling of the band in the vertical (z -) direction, probably due to the change in the harmonic confinement while loading the lattice combined with the presence of gravity. This asymmetry between the horizontal x -, y -, and the vertical z -directions vanishes when the gas approaches the band insulating regime. We have examined the level of adiabaticity of our loading scheme into the optical lattice by transferring the atoms from the band insulator back into the crossed beam dipole trap. There we find a temperature of $0.35 T_F$ when the initial temperature prior to loading into the lattice was $0.2 T_F$.

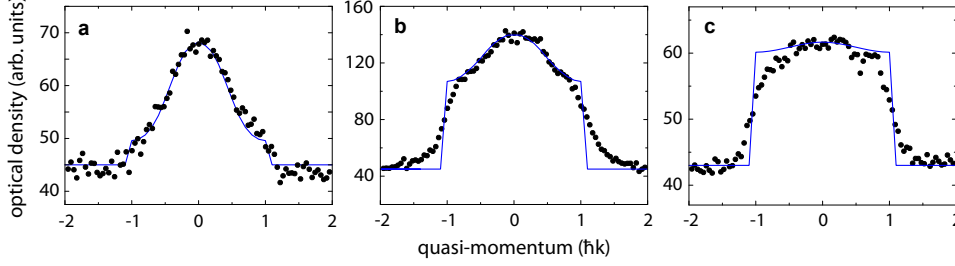


Figure 6.2: Analysis of the density distributions. The dots are cuts through the measured density distribution for quasi-momentum $q_y = 0$ after adiabatically ramping down the optical lattice. (a) Normal state with $\rho_c = 14.5$, (b) band insulator with $\rho_c = 137$, (c) band insulator with $\rho_c = 2500$. We have numerically calculated the momentum distribution function of fermions in the lowest band of a three-dimensional lattice with $20 \times 20 \times 20$ sites and characteristic lengths $\zeta_x/d = 3.2$, $\zeta_y/d = 2.6$, $\zeta_z/d = 2.5$ ((a) and (b)) and $\zeta_x/d = 1$, $\zeta_y/d = 0.8$, $\zeta_z/d = 0.8$ (c), assuming zero temperature (solid lines). Experimental data of (c) are averaged over 5 images. Imperfect adiabaticity during the switch-off of the optical lattice may cause the rounding-off of the experimental data at the edge of the Brillouin zone in (b) and (c). The calculated momentum distribution function is scaled to match the experimental data using identical scale factors for all graphs.

6.1.3 Redistribution dynamics

We have studied the dynamic response of the non-interacting Fermi gas to a change in the characteristic density from a value deep in the band insulating regime to a value below. In the latter regime the fermions are delocalised over several sites of the optical lattice and an interference pattern is observed when the atoms are abruptly released from the lattice. The width of the interference peaks is a measure of the length scale over which the atoms are delocalised in the lattice or, equivalently, their coherence length. We change the characteristic density in situ by varying the strength of the lattice laser beams. Starting from an initial characteristic density of $\rho_c = 16$ in an optical lattice with a potential depth of $5 E_r$ we create a band insulator with a characteristic density of $\rho_c = 2700$ at a potential depth of $15 E_r$. After holding the atoms for 5 ms we reduce the potential depth back to $5 E_r$, using an exponential ramp with duration and time constant t_r . This is followed by a rapid switch off of the lattice (see Fig. 6.3a). We measure the width of the central momentum peak in the time of flight images for different durations t_r and obtain the time scales $\tau_x = (2.7 \pm 0.4)$ ms and $\tau_y = (3.8 \pm 0.3)$ ms in the x - and y -direction, respectively, on which the coherence is restored. This corresponds to approximately ten times the timescale for tunnelling given by $\hbar/2zJ$ at a potential depth of $5 E_r$, where z is the coordination number of the lattice. This non-trivial dynamics appears to be significantly slower than the time scale measured for the transition of a Mott insulating state to a superfluid state using bosonic atoms in an optical lattice [84]. The comparatively slow dynamics of delocalisation of the fermions when approaching the normal state is most likely due to Pauli blocking which prevents tunnelling of atoms in

regions where the lowest band is full and the atoms are well localised.

6.1.4 Interaction induced coupling to higher Bloch bands

We have seen in section 3.5 that interacting fermionic atoms are in many cases well described by the Fermi-Hubbard model. However, for large enough interactions physics beyond this model becomes accessible. We investigate the interacting regime in the lattice starting from a non-interacting gas deep in a band insulator with $V_x = 12 E_r$ and $V_y = V_z = 18 E_r$ and corresponding trapping frequencies of $\omega_x = 2\pi \times 50$ kHz and $\omega_y = \omega_z = 2\pi \times 62$ kHz in the individual minima. A short radio-frequency pulse is applied to transfer all atoms from the $|F = 9/2, m_F = -7/2\rangle$ into the $|F = 9/2, m_F = -5/2\rangle$ state, with the atoms in the $|F = 9/2, m_F = -9/2\rangle$ remaining unaffected. We ramp the magnetic field with an inverse sweep rate of $12 \mu\text{s/G}$ to different final values around the Feshbach resonance (see Fig. 6.4a) located at $B = 224$ G [7]. The sweep across the Feshbach resonance goes from the side of repulsive interactions towards the side of attractive interactions. When using this direction of the sweep there is no adiabatic conversion to molecules. After turning off the optical lattice adiabatically and switching off the magnetic field we measure the momentum distribution. To see the effect of the interactions we determine the fraction of atoms transferred into higher bands. For final magnetic field values well above the Feshbach resonance we observe a significant increase in the number of atoms in higher bands along the weak axis of the lattice, demonstrating an interaction-induced coupling between the lowest bands [86, 148]. Since the s -wave interaction is changed on a time scale short compared to the tunnelling time between adjacent potential minima we may regard the band insulator as an array of harmonic potential wells. It has been shown that increasing the s -wave scattering length for two particles in a harmonic oscillator shifts the energy of the two-particle state upwards until the next oscillator level is reached [120] (see also section 4.4). In our case this leads to a population of higher energy bands. The fraction of atoms transferred is smaller than expected from the solution of an effective Hamiltonian [86]. It could be limited by the number of doubly occupied lattice sites and by the fast tunnelling in the higher bands. The number of doubly occupied sites could be measured by studying the formation of molecules in the lattice (see section 6.3). In addition, we observe a shift of the position of the Feshbach resonance from its value in free space to larger values of the magnetic field (see Fig. 6.4a), which has been predicted for tightly confined atoms in an optical lattice [149]. This mechanism for a confinement induced resonance is related to the phenomenon predicted for one-dimensional quantum gases [118] which we have experimentally observed and is described in the next section. For a quantitative description of this strongly interacting Fermi gas on a lattice a multi-band Hubbard model could be considered but these are even in the static case notoriously difficult or even impossible to solve with present methods [150].

6.1.5 Conclusions

In conclusion we have created a fermionic many-particle quantum system on a lattice. We have demonstrated the dynamic control over the parameters of the system such as

filling and interactions which is not feasible in solid state systems. For the non-interacting static regime we find good agreement between our measurements and a theoretical model. Both the dynamic measurements and the strongly interacting case pose challenges for the present theoretical understanding of many-particle fermionic systems on optical lattices.

As the Feshbach resonance is approached in our experiment, the population of higher bands excludes the existence of a band insulator. A key question is therefore the following: Does the system undergo a phase transition from the initial band insulating state to any other phase? Within a simple model Ho found that above a critical on-site interaction the ground state is a correlated Mott insulating phase exhibiting the spin dynamics of a spin-1 Heisenberg antiferromagnet [151]. The observation of this transition would give an even deeper insight into the physics of strongly interacting fermions in optical lattices, but is still hampered by the lowest achievable temperatures in current experiments.

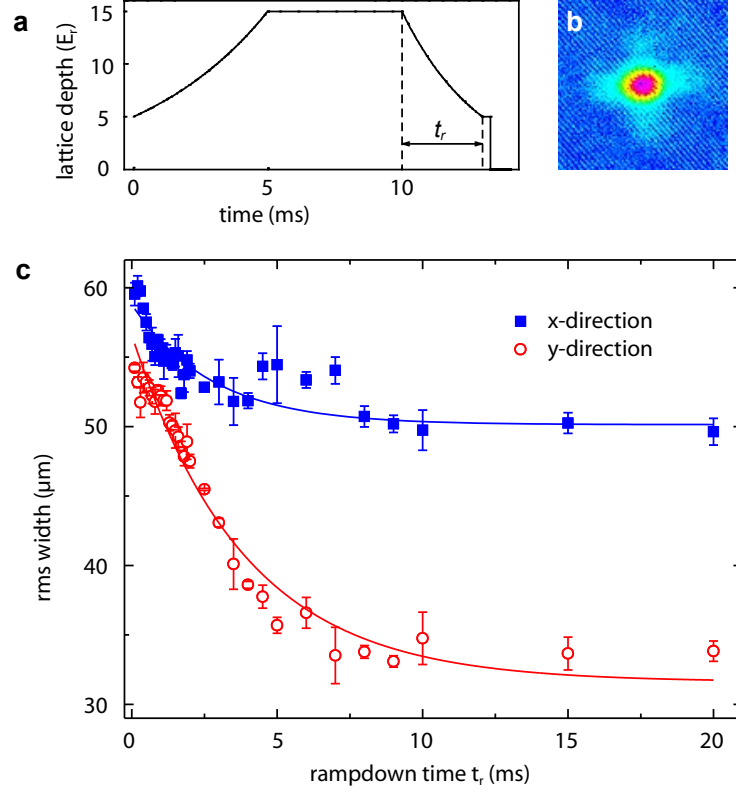


Figure 6.3: Restoring phase coherence. (a) Control sequence for the depth of the optical lattice. (b) Pseudo colour image of the momentum distribution after releasing the atoms from the initial optical lattice of $5 E_r$ and 7 ms ballistic expansion. It reveals the central momentum peak and the matter wave interference peaks at $\pm 2\hbar k$. The data are averaged over 5 repetitive measurements. (c) Width of the central momentum peak obtained from Gaussian fits to the atomic density distribution. The initial width is determined by the momentum spread of an atom localised in the vibrational ground state of a lattice well. The 10% difference in this size comes from slightly different magnifications of the imaging system in the two orthogonal directions. The difference in the asymptotic values of the width can most likely be attributed to the loading sequence of the lattice and to the asymmetry of the confining potentials due to the different beam waists. The error bars show the statistical error of 4 repetitive measurements.

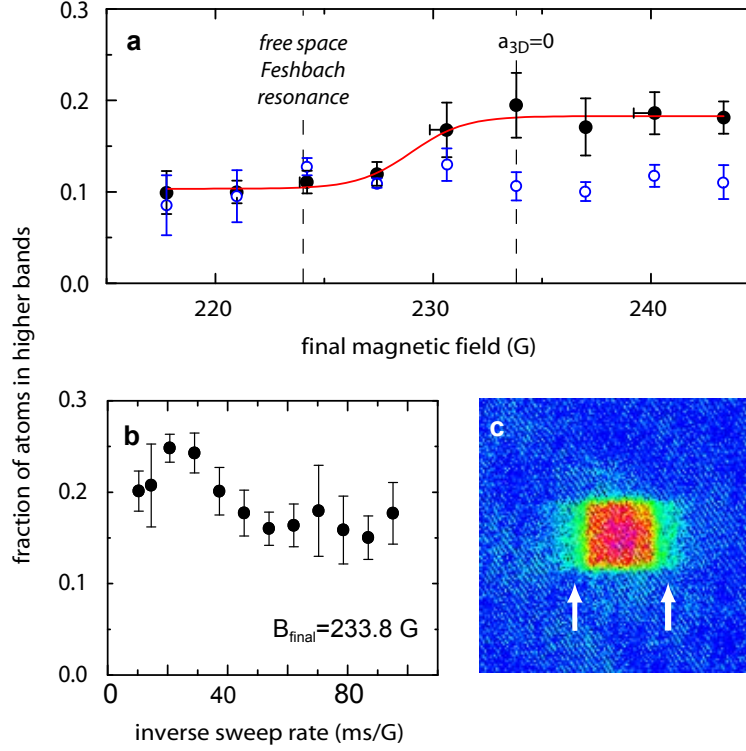


Figure 6.4: Interaction-induced transition between Bloch bands. (a) Transferring fermions into higher bands using a sweep across the Feshbach resonance (filled symbols). The inverse magnetic field sweep rate is $12 \mu\text{s}/\text{G}$. The line shows a sigmoidal fit to the data. The open symbols show a repetition of the experiment with the atoms prepared in the spin states $|F = 9/2, m_F = -9/2\rangle$ and $|F = 9/2, m_F = -7/2\rangle$ where the scattering length is not sensitive to the magnetic field. The magnetic field is calibrated by rf spectroscopy between Zeeman levels. Due to the rapid ramp the field lags behind its asymptotic value and the horizontal error bars represent this deviation. (b) Fraction of atoms in higher bands for a final magnetic field of 233 G for different magnetic field sweep rates. The vertical error bars show the statistical error of 4 repetitive measurements. (c) Momentum distribution for a final magnetic field of $B = 233$ G and a $12 \mu\text{s}/\text{G}$ sweep rate. Arrows indicate the atoms in the higher bands.

6.2 Confinement-induced molecules in one-dimensional Fermi gases

The study of two particles forming a bound state has a long history both in physics and chemistry because it constitutes the most elementary chemical reaction. In most situations, such as atoms in the gas phase or in a liquid, the two particles can be considered as being in free space and their collisions can be described by standard quantum mechanical scattering theory. For ultracold atoms undergoing s-wave interaction a bound molecular state is only supported when the scattering length between the atoms is positive whereas for negative scattering length the bound state is absent [153].

We have observed two-particle bound states of atoms confined in a one-dimensional matter waveguide. These bound states exist irrespective of the sign of scattering length, contrary to the situation in free space. Using radio-frequency spectroscopy we have measured the binding energy of these dimers as a function of the scattering length and confinement and find good agreement with theory. The strongly interacting one-dimensional Fermi gas which we create in a two-dimensional optical lattice represents a realisation of a tunable Luttinger liquid.

6.2.1 Bound states in quasi-1D systems

Weakly bound diatomic molecules in ultracold atomic gases can be produced using magnetic field induced Feshbach resonances [154, 7, 155, 156, 157, 158, 8, 159, 160]. The scattering length between the atoms and thus the binding energy of the molecules can be tuned by an external magnetic field. The fundamental property that a bound state exists only for positive scattering length was clearly revealed experimentally [7]. For negative scattering length pairing due to many-body effects has been observed in fermionic atoms [4, 161]. In this section we report on the observation of bound states of atoms with negative scattering length where the particles are subject to one-dimensional confinement. The reduced dimensionality strongly affects the two-particle physics provided that the scattering length and the size of the transverse ground state are similar [118, 162, 119, 163]. This contrasts with previous studies of interaction-induced phenomena in one-dimensional quantum systems where the reduced dimensionality affects only the many-body properties, such as spin-charge separation in cuprates [164], the Mott insulator transition for bosonic atoms in an optical lattice [145], and the fermionisation of a Bose gas [165, 166, 167].

Tight transverse confinement alters the scattering properties of two colliding atoms fundamentally and a bound state exists irrespective of the sign of the scattering length. This peculiar behaviour in a one-dimensional system arises from the additional radial confinement which raises the continuum energy to the zero point energy of the confining potential, e. g. the two-dimensional harmonic oscillator ground state energy $\hbar\omega_{\perp}$. The energy of a bound or quasi-bound state remains nearly unaffected by the external confinement as long as the effective range of the interaction is small compared to the extension of the confined ground state. Therefore, a quasi-bound state, which for negative

Parts of this section are published in [152].

scattering length a lies above the continuum in free space, is below the new continuum in the confined system.

The binding energy E_b of dimers in a one-dimensional gas is given by [119]

$$\frac{a}{a_\perp} = -\frac{\sqrt{2}}{\zeta(1/2, -E_b/2\hbar\omega_\perp)}, \quad (6.1)$$

where $a_\perp = \sqrt{\hbar/m\omega_\perp}$ is the extension of the transverse ground state (with m being the atomic mass) and ζ denotes the Hurwitz zeta function. For negative a and $|a| \ll a_\perp$ a weakly bound state with $E_b \approx -m\omega_\perp^2 a^2$ exists which has a very anisotropic shape [168]. In the limit $|a| \gg a_\perp$ the binding energy takes the universal form $E_b \approx -0.6 \hbar\omega_\perp$ and for positive a and $a \ll a_\perp$ the usual 3D expression for the binding energy $E_b = -\hbar^2/ma^2$ is recovered.

A trapped gas is kinematically one-dimensional if both the chemical potential and the temperature are smaller than the level spacing due to the transverse confinement. For a harmonically trapped Fermi gas the Fermi energy $E_F = N \cdot \hbar\omega_z$ must be smaller than the energy gap to the first excited state in the transverse direction $\hbar\omega_\perp$. N denotes the number of particles and ω_z is the trapping frequency along the weakly confining axis. In our experiment we employ a two-dimensional optical lattice in order to create 1D Fermi gases. For atoms trapped in the intensity maxima of the two perpendicular standing wave laser fields the radial confinement is only a fraction of the optical lattice period [126]. The much weaker axial trapping is a consequence of the gaussian intensity envelope of the lattice laser beams. The resulting aspect ratio $\omega_\perp/\omega_z = \pi w/\lambda$ is determined by the waist w and the wavelength λ of the beams. The two-dimensional optical lattice creates an array of several thousand 1D tubes. This array fulfills the 1D condition $N < \omega_\perp/\omega_z \approx 270$ in each tube while simultaneously providing a good signal-to-noise ratio in absorption images.

So far one-dimensional quantum gases have only been realised with bosons [169, 145, 165, 166, 167], and the scattering length in those experiments could not be tuned. Here we overcome this by using a magnetic field induced Feshbach resonance between two different spin states of the atoms, which allows us to access any value of the scattering length and study the predicted bound states in 1D.

6.2.2 Molecules and rf-spectroscopy

In the optical dipole trap we prepare a spin mixture with $(50 \pm 2)\%$ in each of the $|F = 9/2, m_F = -9/2\rangle$ and $|F = 9/2, m_F = -7/2\rangle$ spin states using a sequence of two radio-frequency pulses, as in the previous section. From now on we will refer to the atomic state only with its respective m_F number. By lowering the optical trap depth at a magnetic field of $B = 227$ G, which is well above the magnetic Feshbach resonance centred at $B_0 = 202.1$ G [112], we evaporatively cool the potassium cloud to a temperature of $T/T_F = 0.2$ with 1.5×10^5 particles.

The atoms are loaded into the optical lattice at a magnetic field of $B = 210$ G, where the s-wave scattering length between the two states vanishes. The magnetic field strength is calibrated by radio-frequency spectroscopy between different Zeeman levels of ^{40}K and

the uncertainty is below 0.1 G. The lattice depth was calibrated by intensity modulation and studying the parametric heating. The calibration error is estimated to be $< 10\%$.

We create molecules by ramping the magnetic field from the zero crossing of the scattering length at $B = 210$ G in 10 ms to its desired value close to the Feshbach resonance. Depending on the final value of this sweep the binding energy of the molecules varies according to eqn. (6.1). We measure the binding energy E_b of the dimers by radio-frequency spectroscopy [7]. A pulse with a frequency ν_{RF} and a duration of $40 \mu\text{s}$ dissociates the molecules and transfers atoms into the initially unpopulated $|-5/2\rangle$ state which does not exhibit a Feshbach resonance with the state $|-9/2\rangle$ at this magnetic field. We vary the detuning $\delta = \nu_{\text{RF}} - \nu_0$ from the resonance frequency ν_0 of the atomic $|-7/2\rangle \rightarrow |-5/2\rangle$ transition. The power and duration of the pulse is optimised to constitute a π -pulse on the free atom transition. The number of atoms in each spin state is detected using absorption imaging after ballistic expansion. For this we ramp down the lattice exponentially with a duration of 1 ms and time constant of 0.5 ms from the initial depth V_0 to $5 E_r$ to reduce the kinetic energy of the gas in the transverse directions and then quickly turn off the trapping potential. The magnetic offset field is switched off at the start of the expansion, so that no molecules can be formed in the short time that it passes the Feshbach resonance. We apply a magnetic field gradient during 3 ms of the total 7 ms of ballistic expansion to spatially separate the spin components.

6.2.3 Binding energy spectra

Figure 6.5 shows rf spectra for one-dimensional gases with a potential depth of the optical lattice of $V_0 = 25 E_r$, which corresponds to $\omega_{\perp} = 2\pi \times 69$ kHz. In Fig. 6.5a the magnetic field is detuned 0.57 G below the Feshbach resonance, i. e. $a > 0$. This spectrum exhibits two resonances: one corresponds to the $|-7/2\rangle \rightarrow |-5/2\rangle$ transition for free atoms at $\delta = 0$, the other at $\delta > 0$ corresponds to dissociated molecules. The constituent atoms of the dimers are observed in the $|-9/2\rangle$ and $|-5/2\rangle$ states. At this magnetic field, the molecules are not detected by our state-selective imaging procedure unless they are dissociated by an rf-pulse. This is due to the fact that they are transformed into deeply bound molecules during the switch-off of the magnetic field.

In Fig. 6.5b the magnetic field is chosen 0.95 G above the resonance, i. e. $a < 0$. Again, the appearance of a second peak in the $|-5/2\rangle$ atom number at $\delta > 0$ demonstrates the existence of bound state in our 1D geometry. These bound states are confinement induced since no molecules exist without confinement above the Feshbach resonance. They are only stabilised by the presence of the confining potential. Ramping down the lattice before detection dissociates the dimers and therefore all atoms should be detected in the image and the total particle number is expected to remain constant. This is reflected in our data, where the $|-7/2\rangle$ atom number decreases upon dissociation while the $|-5/2\rangle$ atom number increases. We attribute the slight increase of atoms in $|-9/2\rangle$ to reduced losses of the rf dissociated atom pairs during the 1 ms lattice turn off which follows the radio-frequency spectroscopy. The fragments in the $|-9/2\rangle$ and $|-5/2\rangle$ state do not experience the enhanced inelastic losses characteristic to the molecules, which are near the $|-9/2\rangle \leftrightarrow |-7/2\rangle$ Feshbach resonance.

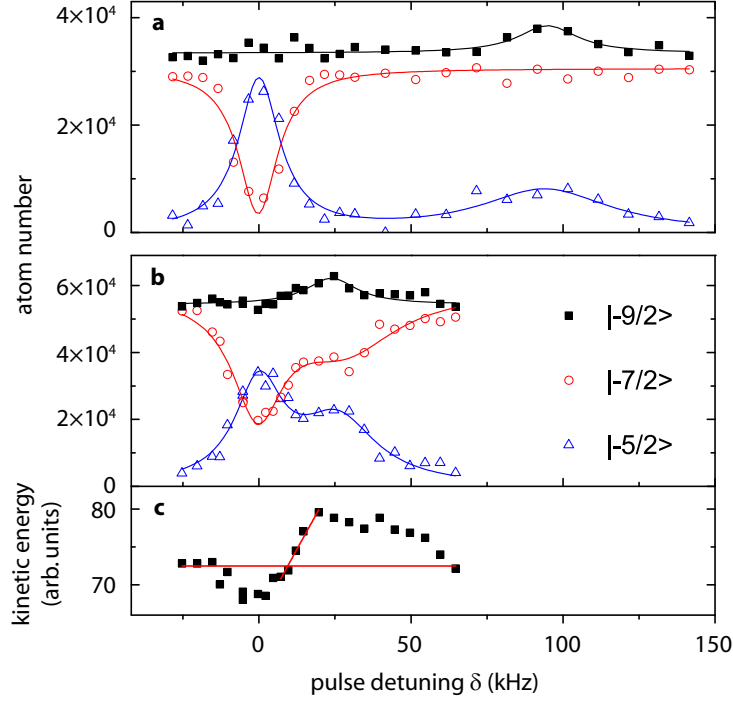


Figure 6.5: Radio-frequency (rf) spectroscopy of a one-dimensional gas at magnetic fields 201.5 G (a) and 203.1 G (b, c). The atom number in the respective spin states is plotted versus the detuning of the applied rf pulse in (a) and (b). The solid lines are single or double Lorentzian fits. (c) Kinetic energy of the $| -9/2 \rangle$ atom cloud along the 1D tube direction after 7 ms time-of-flight obtained from a fit to the atomic density distribution. The horizontal line marks the average energy for an off-resonant rf pulse, the other the increase at the molecule dissociation threshold.

The rf pulse not only breaks the pairs if the detuning δ exceeds the binding energy E_b , but also imparts the kinetic energy $\Delta E = 2\pi\hbar\delta - E_b$ to the fragments. In the 1D tubes only the kinetic energy along the tube axis increases as the motion in the other direction is frozen out for $\Delta E < \hbar\omega_\perp$. The kinetic energy shown in Fig. 6.5c is extracted from the momentum distribution obtained from time of flight images. We use this characteristic to determine the binding energy. With a linear fit we identify the threshold position at which the kinetic energy exceeds the energy of a cloud with off-resonant rf-pulse. The latter is determined by the Fermi statistics of the trapped atoms and the interaction of the $| -9/2 \rangle$ with the $| -7/2 \rangle$ atoms close to the Feshbach resonance. The decrease at $\delta \approx 0$ is due to the particle transfer into the $| -5/2 \rangle$ state and an accordingly weaker interaction energy. Owing to this complication we estimate the systematic error of our binding energy measurements in all data sets to be 10 kHz.

We have investigated the dependence of the binding energy of the 1D dimers on the

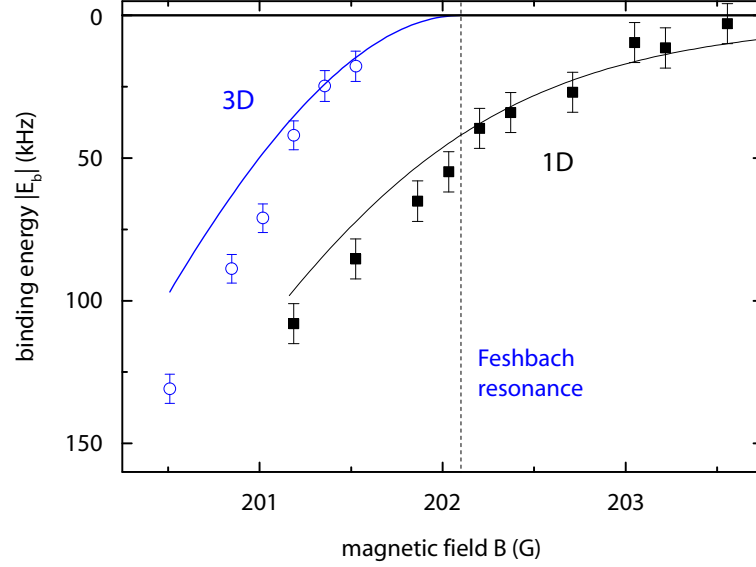


Figure 6.6: 1D and 3D molecules. Confinement induced molecules in the 1D geometry exist for arbitrary sign of the scattering length. The solid lines show the theoretical prediction of the binding energy with no free parameters (see text). In the 3D case we observed no bound states at magnetic fields above the Feshbach resonance (vertical dashed line). The error bars reflect the uncertainty in determining the position of the dissociation threshold.

magnetic field (Fig. 6.6) and we observed bound states for every examined magnetic field strength. The dimers at magnetic fields above the Feshbach resonance are induced by the confinement. The data is in good agreement with the theoretical expectation calculated from eqn. (6.1) (solid line) with no free parameters. For this calculation we compute the effective harmonic oscillator length a_{\perp} and the ground state energy $\hbar\omega_{\perp}$ by minimising the energy of a gaussian trial wave function in a single well of the lattice to account for the anharmonicity of the potential. To calculate the scattering length we use a width of the Feshbach resonance of $\Delta B = 7.8$ G [112] and the background scattering length $a_{bg} = 174 a_0$ [113].

For a comparison with the situation in free space we created molecules in a crossed beam optical dipole trap without optical lattice where confinement effects are not relevant. The binding energy in 3D is measured with the same rf spectroscopy technique as for the 1D gas and we find molecules only for scattering lengths $a > 0$. The binding energy is calculated according to [104] as

$$E_{b,3D} = \frac{\hbar^2}{m(a - \bar{a})^2} \quad \text{with} \quad \bar{a} = (mC_6/\hbar^2)^{1/4} \frac{\Gamma(3/4)}{2\sqrt{2}\Gamma(5/4)}$$

being the effective scattering length and $C_6 = 3897$ (in atomic units) [170]. The deviation of the theory from the measured data for more deeply bound molecules is probably due

to limitations of this single channel theory. A multi-channel calculation would determine the binding energy more accurately. In ref. [171] Dickerscheid et al. have compared our results with a two-channel theory and found excellent agreement.

Exactly on the Feshbach resonance where the scattering length diverges, the binding energy takes the universal form $E_b \approx -0.6\hbar\omega_\perp$ and is solely dependent on the external confinement. We have varied the potential depth of the optical lattice and thereby the transverse confinement and measured the binding energy. We find good agreement of our data with the theoretical prediction (see Fig. 6.7). For a very low depth of the optical lattice the measured data deviate from the 1D theory due to the fact that the gas is not one-dimensional anymore.

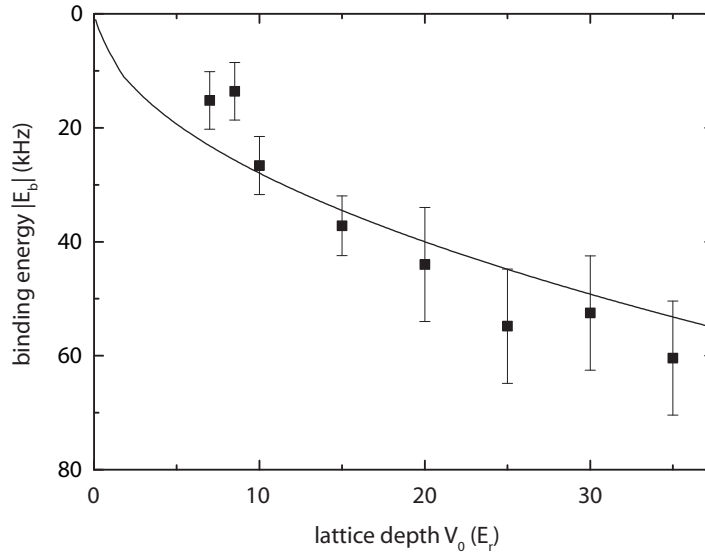


Figure 6.7: Changing the confinement. The spectra are taken very close to the Feshbach resonance at a magnetic field of $B = 202.0$ G. The binding energy is measured by rf spectroscopy. For $V_0 \geq 30 E_r$ no increase in kinetic energy could be detected and we used the rising edge in the $|-5/2\rangle$ atom number in the spectrum to determine the binding energy. The error bars reflect the uncertainty in determining the position of the dissociation threshold. The solid line shows the theoretically expected value $E_b = 0.6 \hbar \omega_\perp$.

In conclusion, we have realised an interacting 1D Fermi gas in a two-dimensional optical lattice. Using a Feshbach resonance we have created molecules and measured their binding energy. We find two-particle bound states for arbitrary sign of the scattering length, which in the case of negative scattering length are stabilised only by the tight transverse confinement. We find good agreement with theory describing the two-particle physics. The strongly interacting 1D Fermi gas realises an atomic Luttinger liquid and fascinating many-body phenomena are predicted in this system [51, 172, 173]. Especially intriguing appears the BCS-BEC crossover for which exactly solvable models exist in one dimension [168, 10].

6.3 Molecules of fermionic atoms in a three-dimensional optical lattice

In the vicinity of a Feshbach resonance the collisional interaction strength between two atoms is tunable over a wide range. For two fermionic atoms on one lattice site strong interactions change the properties of the system qualitatively and physics beyond the standard Hubbard model becomes accessible. In section 6.1 we have seen that crossing the Feshbach resonance in one direction leads to an interaction induced coupling between Bloch bands which has been described theoretically [86]. Crossing the resonance in the other direction converts fermionic atoms into bosonic molecules. These processes have no counterpart in standard condensed matter systems and demand novel approaches to understand the mixed world of fermions and bosons in optical lattices [175, 176, 177, 178]. Descriptions based on multi-band Hubbard models are extremely difficult to handle and therefore the low-tunnelling limit is often used as an approximation.

We create molecules from fermionic atoms in a three-dimensional optical lattice using a Feshbach resonance. In the limit of low tunnelling, the individual wells can be regarded as independent three-dimensional harmonic oscillators. The measured binding energies for varying scattering length agree excellently with the theoretical prediction for two interacting atoms in a harmonic oscillator. We demonstrate that the formation of molecules can be used to measure the occupancy of the lattice and perform thermometry.

6.3.1 Two interacting atoms in a harmonic oscillator well

The harmonic oscillator with two interacting atoms has been studied theoretically and the eigenenergies have been calculated in various approximations [175, 120, 123, 124, 73]. Its physics is governed by several length scales (see section 4.4). The shortest scale is the characteristic length of the van der Waals interaction potential between the atoms. The next larger length scale is given by the s -wave scattering length characterising low-energy atomic collisions. However, near the Feshbach resonance it may become much larger than the extension of the harmonic oscillator ground state. A precise understanding of the interactions in this elementary model is a prerequisite in order to comprehend the many-body physics occurring in optical lattice systems with resonantly enhanced interactions.

We study a spin mixture of fermionic atoms in an optical lattice and their conversion into molecules by means of a Feshbach resonance. The binding energy as a function of the s -wave scattering length between the particles is measured and compared with theoretical predictions. Moreover, we demonstrate that the molecule formation can serve as a measure of the temperature of the atoms in the lattice. The temperature is a key parameter for mapping out the phase diagram of many-body quantum states in the lattice. So far, temperature has not been measured in a lattice since standard methods – such as observing the rounding-off of the Fermi surface – turned out to be dominated by the inhomogeneity of the trapping potential rather than by temperature [73]. However, we find that the occupancy of the lattice depends strongly on the temperature [148, 179, 180]

Parts of this section are published in [174].

and the conversion of pairs of atoms into molecules is a sensitive probe, similar to the case of harmonically trapped fermions [181].

In a previous experiment, deeply bound molecules of bosonic atoms have been created in an optical lattice by photo-association and were detected by a loss of atoms [182, 183]. There the binding energy is only determined by the atomic properties and does not depend on the external potential, nor can the scattering properties between the molecules be adjusted. In low-dimensional systems molecules produced by a Feshbach resonance using fermionic atoms have been observed recently [159, 152].

6.3.2 Molecule production and detection

In the optical trap we prepare a mixture of the $|F = 9/2, m_F = -9/2\rangle$ and the $|F = 9/2, m_F = -7/2\rangle$ state with $(50 \pm 4)\%$ in each spin state (which in the following will be abbreviated by $|m_F\rangle$) and perform additional evaporative cooling at a magnetic field of $B = 227$ G. At the end of the evaporation we reach temperatures of $T/T_F = 0.25$ with up to 2×10^5 particles. The temperatures are determined from a fit to the density distribution of the non-interacting atomic cloud after ballistic expansion. The atoms are then transferred into the optical lattice formed by three orthogonal standing waves.

In the optical lattice we create a band insulator for each of the two fermionic spin states [25]. Subsequently, the molecules are formed by ramping the magnetic field from the zero crossing of the scattering length at $B = 210$ G in 10 ms to its final value close to the Feshbach resonance located at $B_0 = 202.1$ G [112]. From the parameters of our magnetic field ramp we estimate that the molecule formation is performed adiabatically. We measure the binding energy E_b of the dimers by radio-frequency spectroscopy [7, 4, 152]. A pulse with a frequency ν_{RF} and a duration of $40 \mu\text{s}$ dissociates the molecules and transfers atoms from the state $|-7/2\rangle$ into the initially unpopulated state $|-5/2\rangle$ which does not exhibit a Feshbach resonance with the state $|-9/2\rangle$ at this magnetic field. Therefore the fragments after dissociation are essentially non-interacting (see Fig. 6.8a). We vary the detuning $\delta = \nu_{\text{RF}} - \nu_0$ from the resonance frequency ν_0 of the atomic $|-7/2\rangle \rightarrow |-5/2\rangle$ transition. The power and duration of the pulse is chosen to constitute approximately a π -pulse on the free atom transition. The number of atoms in each spin state is determined using absorption imaging after ballistic expansion. For this we ramp down the lattice exponentially with a duration of 1 ms and time constant of 0.5 ms from the initial depth V_0 to $5 E_r$ to reduce the kinetic energy of the gas and then quickly turn off the trapping potential within a few μs . The magnetic offset field is switched off at the start of the expansion, so that no molecules can be formed in the short time that it passes the Feshbach resonance. We apply a magnetic field gradient during 3 ms of the total 7 ms of ballistic expansion to spatially separate the spin components.

6.3.3 Binding energy and molecular fraction

Figures 6.8(b) and 6.8(c) show rf spectra of atoms and molecules trapped in a three-dimensional lattice with a potential depth of $V_0 = 22 E_r$, which corresponds to a trapping frequency of $\omega = 2\pi \times 65$ kHz in the potential wells of the lattice. The spectrum in Fig. 6.8(b) is taken at a magnetic field of $B = 202.9$ G, corresponding to $a/a_{\text{ho}} = -1.3$.

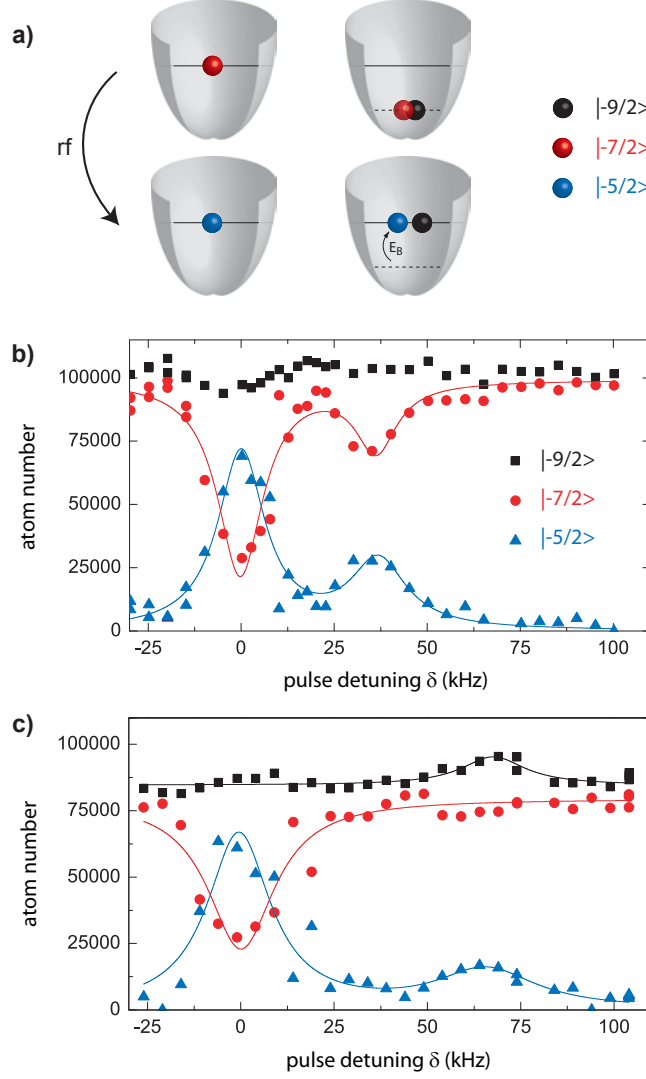


Figure 6.8: **a)** Illustration of the rf spectroscopy between two atoms (left side) and two bound states (right side) within a single well of the optical lattice. Two atoms in the initial states $|-7/2\rangle$ and $|-9/2\rangle$ are converted into a bound dimer by sweeping across a Feshbach resonance. Subsequently we drive an rf transition $|-7/2\rangle \rightarrow |-5/2\rangle$ to dissociate the molecule. **b)** rf spectrum taken at $B = 202.9$ G, i. e. for $a < 0$. **c)** rf spectrum taken at $B = 202.0$ G, i. e. for $a > 0$. All data are taken for a lattice depth of $22 E_r$. The lines are Lorentzian fits to the data.

We have calculated the ground state radius $a_{\text{ho}} = 64 \text{ nm}$ by minimising the energy of a Gaussian trial wave function inside a single well of our lattice potential. As compared to a Taylor expansion of the sinusoidal potential around the minimum this results in slightly more accurate values. The *s*-wave scattering length is denoted by a . For negative scattering length the molecules are only bound when they are strongly confined whereas no bound state would exist in the homogeneous case. The spectrum exhibits two resonances: the one at $\delta = 0$ corresponds to the atomic transition from the $|-7/2\rangle$ into the $|-5/2\rangle$ state. This transition takes place at all lattice sites which initially were only singly occupied and no molecule has been formed. The second resonance at $\delta > 0$ corresponds to the molecular dissociation and is shifted from the atomic resonance by the binding energy. Simultaneous with the increase in the $|-5/2\rangle$ atom number we observe a loss of atoms in the $|-7/2\rangle$ state, whereas the $|-9/2\rangle$ remains unaffected. This is expected since the rampdown of the lattice before detection dissociates all molecules and the $|-9/2\rangle$ atom number should be fully recovered. Residual fluctuations of the $|-9/2\rangle$ atom number are probably due to uncertainties in the atom number determination since we do not observe a specific pattern in our spectra.

With the magnetic field tuned to $B = 202.0 \text{ G}$ [see Fig. 6.8(c)], which corresponds to $a/a_{\text{ho}} = 16.8$, the spectrum changes qualitatively. For this value of the scattering length stable molecules exist even in free space but the molecules formed in the lattice are not detected by our state-selective imaging procedure unless they are dissociated by the rf-pulse. Therefore only rf dissociated atom pairs show up in the time-of-flight images, resulting in an increasing number of atoms in the $|-5/2\rangle$ and the $|-9/2\rangle$ state at the molecular resonance.

In contrast to earlier work, where molecules were dissociated into a continuum and the fragments were essentially free particles [7, 4, 152], the fragments in our configuration occupy an energy eigenstate of the confining potential. In such a bound-bound transition no extra kinetic energy is imparted onto the dissociated fragments since any excess excitation energy would have to match the band gap. We determine the binding energy from the separation of the atomic and the molecular peak. Moreover, since there is at most one molecule present per lattice site, collisional shifts [184, 185] are absent and we can estimate the error in the binding energy from the fit error which is less than 5 kHz.

We have investigated the dependence of the binding energy of the molecules on the scattering length (Fig. 6.9). The scattering length is derived from the magnetic field using the usual parametrisation (4.14) of the Feshbach resonance, with $a_{\text{bg}} = 174 a_0$ [113] and $\Delta B = 7.8 \text{ G}$ [112]. We compare our data with the theory for two particles trapped in a harmonic oscillator potential interacting via an energy-independent pseudo-potential [120] (see paragraph 4.4). We find the normalised binding energy $E_b/\hbar\omega$ to be independent of the strength of the lattice and all data points agree well with the theoretical prediction of eqn. (4.19) without adjustable parameters. It was shown in section 4.4 that a pseudo-potential approximation is valid, as long as a_{ho} is large compared to the characteristic length scale of the van der Waals potential between the two atoms $\beta_6 = (mC_6/\hbar^2)^{1/4}$ [123, 124], which for our experiments is $a_{\text{ho}}/\beta_6 > 10$. However, for $a \gg a_{\text{ho}}$ an energy-dependent pseudo-potential will model the system more accurately. We have calculated the effective range of the interaction to be $r_e = 98 a_0$ [89] and the

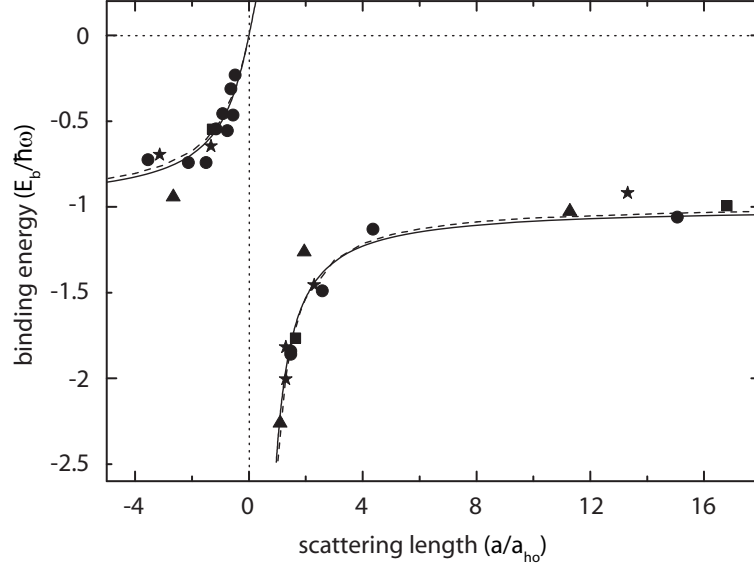


Figure 6.9: The measured binding energy of molecules in a three-dimensional optical lattice. The data are taken for several potential depths of the optical lattice of $6 E_r$ (triangles), $10 E_r$ (stars), $15 E_r$ (circles), and $22 E_r$ (squares). The solid line corresponds to the theory of ref. [120] with no free parameters, the dashed line uses an energy-dependent pseudo-potential according to ref. [123]. At the position of the Feshbach resonance ($a \rightarrow \pm\infty$) the binding energy takes the value $E_b = -\hbar\omega$.

eigenenergies using an energy-dependent pseudo-potential [123] (dashed line in Fig. 6.9). Both models agree to within a few percent, which is small compared to experimental uncertainties. Further theoretical improvements taking into account more details of the atom-atom interaction in a two-channel model have been suggested [124, 175] and could be tested with our data.

From a quantitative analysis of the spectra we obtain information about the occupancy of our lattice. We measure the ratio between the atomic and the molecular peak heights in the spectra of the $|-5/2\rangle$ atoms and determine the fraction of atoms that where bound in a molecule. Figure 6.10 shows the measured data for a lattice with a potential depth of $15 E_r$. The detected molecular fraction decreases for large values of $1/a$, i.e. for deeply bound molecules, because of the small overlap of the initial molecular and the final atomic wave function in the rf transition. The analytical wave function of the molecular state in relative coordinates is given by [120]

$$\psi_{l=0}(\mathbf{r}) = \frac{1}{2}\pi^{-3/2}Ae^{-\mathbf{r}^2/2a_{ho}^2}\Gamma(-\nu)U(-\nu, \frac{3}{2}, \mathbf{r}^2), \quad (6.2)$$

where $U(n, m, x)$ is the confluent hypergeometric function and $\nu = E_b/(2\hbar\omega) - 3/4$. We calculate the overlap integral of this function with the harmonic oscillator ground state

wave function $\psi_{\text{ho}}(\mathbf{r}) = (\pi a_{\text{ho}}^2)^{-3/4} \exp(-\mathbf{r}^2/2a_{\text{ho}}^2)$,

$$\left| \int d\mathbf{r} \psi_{\text{ho}}(\mathbf{r})^* \psi_{l=0}(\mathbf{r}) \right|^2, \quad (6.3)$$

which determines the relative strength of the molecular transition assuming that the centre-of-mass motion remains unaffected by the rf transition. We fit the overlap integral to our experimental data and obtain the fraction of molecules in the lattice to be $(43 \pm 5)\%$ (solid line in Fig. 6.10).

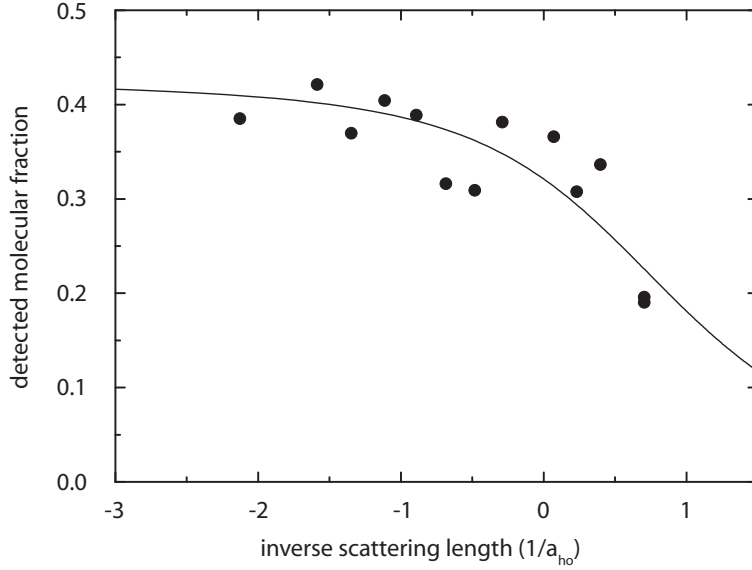


Figure 6.10: The fraction of molecules detected by rf-spectroscopy at a potential depth of $15 E_r$. For weakly bound molecules ($a_{\text{ho}}/a < -1$) the dissociation works well since the overlap between the molecular and the atomic wave function is large. For deeply bound molecules $a_{\text{ho}}/a > 0$ the detected molecular fraction is suppressed due to the vanishing overlap between the wave functions. The solid line shows the theoretical expectation for a constant molecular fraction of 43%.

We measure the lifetime of the molecules in the lattice to be on the same order of magnitude as of molecules in an optical dipole trap [112]. This is probably related to the tunnelling rate, which for our lattice parameters is on the order of 100 Hz and therefore the rate of three-body collisions is comparable to the optical trap. We expect that the lifetime of the molecules will significantly increase if the lattice depth becomes larger than $30 E_r$. Another possible mechanism which could lead to a loss of molecules is photo-association induced by the lattice laser beams.

6.3.4 Thermometry in the lattice

The temperature of the atoms in the lattice is of importance for many proposed experiments in which phase transitions of fermions in lattices are studied, and special cooling techniques to reach these temperatures have been devised [83, 186, 77, 138]. The molecular fraction in the lattice turns out to be an ideal quantity to determine the temperature.

Because the atoms are well localised in the sites of the deep lattice, molecules can only be formed when two particles reside at the same lattice site. The observed fraction of molecules is thus primarily determined by the filling of the lattice. To study the relation between the temperature and filling we have numerically calculated the density of states for non-interacting fermions in an optical lattice including the Gaussian confining potential due to the transverse envelope of the lattice lasers. In the low-tunnelling limit we find that the density of states approaches $\rho(E) \propto E^\nu$ with $\nu = 1/2$ independent of the lattice depth [179]. The fraction of doubly occupied lattice sites in a 50:50 spin mixture depends on ν and T/T_F . This makes the molecule fraction a quantity well suited for thermometry. Assuming that the occupation probability per spin state and lattice site i is $0 < n_i < 1$, the probability of finding two atoms with different spin state on a lattice site is n_i^2 . We identify the molecule fraction with the mean value of n_i^2 over the whole lattice. From a comparison with a numerical calculation [179] we can conclude that the temperature of the atoms in the optical lattice is at most $T/T_F = 0.45 \pm 0.03$. A similar result for our experimental parameters was computed in [148]. This value gives an upper limit to the temperature since it assumes adiabatic formation of molecules at all doubly occupied sites and a perfectly equal mixture of the spin states. During the ramp across the Feshbach resonance the density distribution might slightly change as compared to the initial non-interacting case, which limits the accuracy of the temperature determination.

More generally, the molecular fraction is determined by the fraction of doubly occupied states rather than doubly occupied sites:

$$n_2(T) = \frac{N_2(T)}{N} = \frac{\int_{-\infty}^{\infty} dE \rho(E) f_{\text{FD}}^2(E, T)}{\int_{-\infty}^{\infty} dE \rho(E) f_{\text{FD}}(E, T)} \quad (6.4)$$

In a shallow lattice, where the atoms are delocalised over several sites, two atoms occupying the same state can always form a molecule, assuming the formation to be adiabatic. For instance, at $T = 0$ one can always expect a 100% conversion of molecules, $n_2(0) = 1$, independent of the filling. As has been shown in the case of atoms in a harmonic trap [181], the conversion efficiency is solely determined by the phase space density of the gas.

In conclusion, we have studied molecules in a three-dimensional optical lattice. We have measured the binding energies and find good agreement with the fundamental theoretical model of two interacting particles in a harmonic potential well. Moreover, we have measured the filling of the lattice by determining the fraction of molecules formed. This allows for thermometry in the lattice, which has previously been inaccessible. The fraction of created molecules gives direct access to the number of doubly occupied lattice sites in a two-component Fermi gas. Therefore it could be employed to characterise a Mott insulating phase where the double occupancy should be strongly reduced.

7 p -wave interactions in low-dimensional Fermi gases

The atomic motion and the dimensionality of the trapping geometry can be controlled using optical lattices. Yet, it is the collisional interaction between atoms which provides the avenue towards the physical richness of the strongly correlated regime [83, 69, 85, 25]. In contrast to s -wave interactions studied in the previous chapters, p -wave collisions are anisotropic. This makes their study in an optical lattice particularly intriguing since scattering in specific directions can be suppressed by reducing the dimensionality.

7.1 p -wave scattering

The scattering of two atoms with angular momentum $l = 1$ shows interesting properties absent in s -wave collisions. Most importantly, it introduces an anisotropy in the asymptotic scattering states which shows up in their angular dependance given by the spherical harmonics $Y_{l,m}(\theta, \phi)$. The quantum number $m \in \{-1, 0, 1\}$ stands for the projection of the angular momentum l onto the quantisation axis. If considering scattering into specific directions it is helpful to use a different basis:

$$\begin{aligned} p_x &= Y_{1,0} \\ p_y &= \frac{1}{\sqrt{2}}(Y_{1,-1} - Y_{1,1}) \\ p_z &= -\frac{i}{\sqrt{2}}(Y_{1,-1} + Y_{1,1}). \end{aligned} \tag{7.1}$$

The angular dependance is illustrated in Fig. 7.3(a) which shows the surfaces parameterised by $(|p_i|^2, \theta, \phi)$ for $i = x, y, z$. From the definition (7.1) it is evident that the states p_y and p_z both contain $m = -1$ and $m = 1$ scattering while p_x is identical with the $m = 0$ state.

Another consequence of the finite angular momentum is that the atoms feel an effective potential including a centrifugal barrier [see eqn. (4.5)], as shown in Fig. 7.1. At ultralow temperatures the atoms do not have enough energy to overcome the barrier and p -wave scattering is suppressed. In ^{40}K the p -wave cross section is orders of magnitude smaller than the s -wave cross section at temperatures in the μK regime [188, 116] (in absence of any scattering resonance). Exploiting a p -wave Feshbach resonance [7, 189, 190]

Parts of this chapter are published in [187].

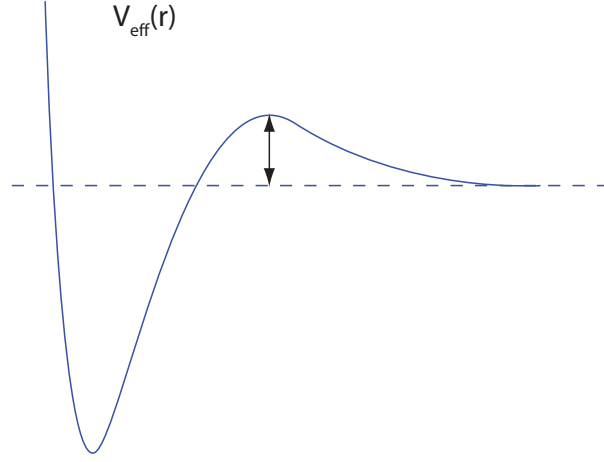


Figure 7.1: The effective interatomic potential for $l > 0$ includes a centrifugal barrier due to the angular momentum.

this suppression can be overcome. Similar to the effective range expansion (4.7) in the s -wave problem, the p -wave phase shift δ_1 can be expressed in a low- k approximation

$$\frac{\tan \delta_1}{k^3} = \frac{1}{-v^{-1} + ck^2}, \quad (7.2)$$

where the role of the scattering length is now played by the scattering volume v defined as

$$v(k) = -\lim_{k \rightarrow 0} \frac{\tan \delta_1(k)}{k^3}, \quad (7.3)$$

and c is the second coefficient in the expansion. These quantities can be used to parameterise the p -wave Feshbach resonance. Because the atoms have to tunnel through the centrifugal barrier to couple to the bound state, the position as well as the width of the very narrow resonance are energy dependent.

Due to magnetic dipole-dipole interactions between two atoms a p -wave Feshbach resonance is split in two resonances [116]. The Hamiltonian

$$H_{ss} = -\alpha^2 \frac{3(\mathbf{R} \cdot \mathbf{s}_1)(\mathbf{R} \cdot \mathbf{s}_2) - \mathbf{s}_1 \cdot \mathbf{s}_2}{R^3} \quad (7.4)$$

leads to an interplay between the atomic spins \mathbf{s}_1 and \mathbf{s}_2 and the partial waves (\mathbf{R} is the interatomic distance) and lifts the degeneracy between the states with $m = 0$ and $|m| = 1$. In a classical picture as illustrated in Fig. 7.2 this is easily understood: While the atoms orbit, the two spins in a) alternately change from an attractive head-to-tail to a repulsive side-by-side configuration, while in b) they always stay side-by-side. The $m = 0$ scattering state thus has a lower energy (if the quantisation axis is chosen along the spin) and its resonance occurs at lower magnetic fields.

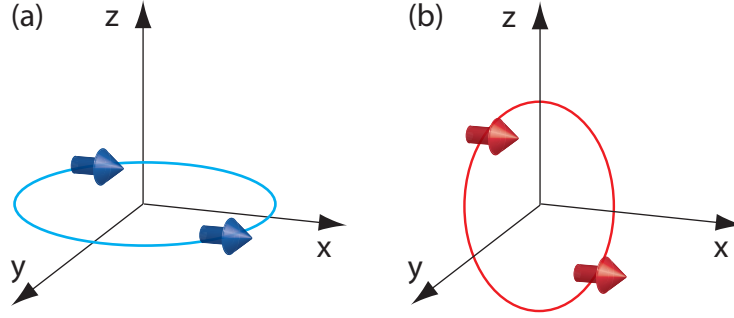


Figure 7.2: The magnetic dipole-dipole interaction depends on the angular momentum in the direction of the spin. It is in (a) perpendicular to the spin, $m = 0$, and in (b) parallel to the spin, $|m| = 1$ (quantisation axis along x).

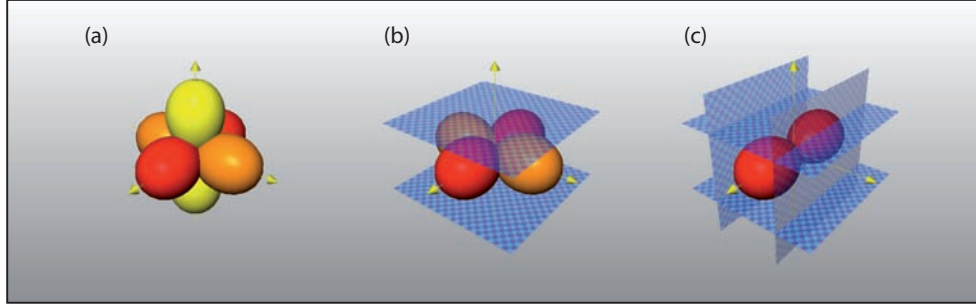


Figure 7.3: Illustration of the anisotropic scattering states p_x , p_y and p_z and their suppression by the lattice confinement. (a) Without confinement (no lattice), (b) in a 2D system (1D lattice) and (c) in 1D system (2D lattice). The radial coordinate corresponds to the absolute square of the scattering amplitude (see text).

7.2 Suppression of scattering by reducing the dimensionality

We investigate p -wave collisions in a spin-polarised Fermi gas in an optical lattice in the vicinity of a Feshbach resonance controlled by the magnetic field. We study the resonant behaviour of the atom losses as a function of the magnetic field and observe distinct features depending on the dimensionality and the symmetry of the system.

For a three-dimensional gas a double-peaked structure appears, as has previously been reported by Ticknor *et al.* [116]. This characteristic survives when the dimensionality is reduced to two dimensions (2D) but appears shifted in magnetic field. For one-dimensional (1D) geometries only a single shifted resonance peak is observed. All resonantly enhanced losses vanish when the spin-polarised gas is loaded into the lowest band of a three-dimensional optical lattice, in which each site can be regarded as a system of "zero dimensions".

These observations can be qualitatively explained by considering the symmetry of

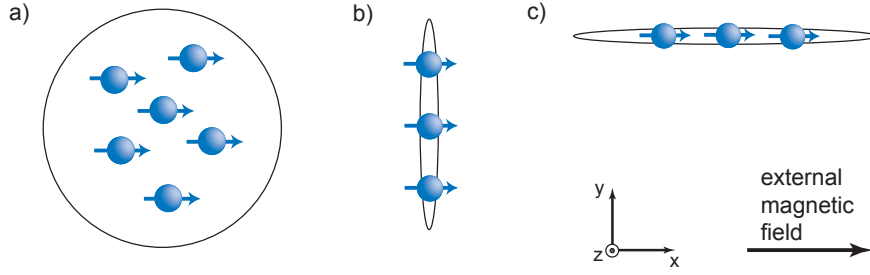


Figure 7.4: Spin-alignment dependent interactions in 1D and 2D. In the two-dimensional configuration of a) all projections of the angular momentum in the *p*-wave collision are allowed. b) and c) show a one-dimensional spin-polarised Fermi gas with the spins aligned orthogonal and parallel to the extension of the gas, respectively. In b) only the $|m| = 1$ projection of the *p*-wave contributes to the scattering, in c) only the $m = 0$ projection.

the collisions, as illustrated in Figs. 7.3 and 7.4. The external magnetic field orients the polarisation of the atoms and its direction x may be chosen as the quantisation axis. Alignment of the scattering state parallel to the quantisation axis corresponds to the spherical harmonic $p_x = Y_{1,0}$ and alignment in the plane perpendicular to the quantisation axis corresponds to superpositions p_y and p_z of the spherical harmonics $Y_{1,\pm 1}$. The dipole-dipole interaction between the electronic spins lifts the degeneracy between the $|m| = 1$ and the $m = 0$ collisional channels which leads to a splitting of the Feshbach resonance [116]. In the two- and three-dimensional configurations both collisional channels are present, giving rise to the observed doublet feature (see Fig. 7.7a and b). In one dimension, with the spin aligned orthogonal or parallel to the atomic motion, either the $|m| = 1$ (see Fig. 7.7c) or the $m = 0$ (see Fig. 7.7d) collisional channel is contributing, leading to a single peak. In "zero dimensions"—as realised in a three-dimensional optical lattice—*p*-wave collisions and the corresponding losses are absent (see Fig. 7.7e). In these low-dimensional systems the asymptotic scattering states are kinematically restricted. However the atomic collision process is still three-dimensional since the size of the ground state is large compared to the range of the interatomic potentials. Hence the strongly confined directions can contribute to the collision energy [191].

One- and two-dimensional fermionic quantum systems have been realised in semiconductor nanostructures [192, 193] and recently with non-interacting [146] and interacting [159, 152] atomic gases in optical lattices. As shown in section 6.2, in these systems the strong confinement modifies the scattering properties of the particles: It stabilises molecular states and shifts the position of Feshbach resonances. This has been predicted for one- [118, 119] and two-dimensional systems [194, 195] interacting via *s*-wave scattering. Similarly, for spin-polarised Fermions in one dimension a confinement induced shift of *p*-wave Feshbach resonances is predicted [196].

7.3 Preparation of a spin-polarised Fermi gas

In ^{40}K we have access to a p -wave Feshbach resonance located around 199 G for atoms in the $|F = 9/2, m_F = -7/2\rangle$ spin state. Since we work with spin-polarised atoms, s -wave interactions are completely suppressed.

After the usual cooling sequence in the magnetic trap we prepare the atoms in the $|F = 9/2, m_F = -7/2\rangle$ state in the optical trap at a magnetic bias field of 232.9 G using two radio frequency (rf) sweeps. To remove residual atoms in the $|F = 9/2, m_F = -9/2\rangle$ state we change the magnetic field in 100 ms to a value of 201.7 G, close to the s -wave Feshbach resonance between $|F = 9/2, m_F = -9/2\rangle$ and $|F = 9/2, m_F = -7/2\rangle$ [7, 152], where we encounter inelastic losses resulting in a pure spin-polarised Fermi gas. Subsequently we increase the magnetic field within 100 ms to 203.7 G. Then we evaporate atoms by lowering the optical trapping potential during 2.5 s to a final value of $7 E_r$ in each of the two beams, where $E_r = \hbar^2 k^2 / (2m_K)$ denotes the recoil energy, $k = 2\pi/\lambda$ the wave vector of the laser and m_K the atomic mass. The preparation of the gas is completed by rapidly (< 1 ms) decreasing the magnetic field to 194.4 G, which is below the p -wave Feshbach resonance. We have calibrated the magnetic field by rf spectroscopy between Zeeman levels with an accuracy better than 100 mG, and we estimate the reproducibility of our magnetic fields to be better than 50 mG.

Successful cooling of a spin-polarised Fermi gas is not evident as the gas is non-interacting away from the p -wave Feshbach resonance. To be sure, the hottest atoms escape from the dipole trap when the laser intensities are reduced, but due to the lacking collisions no thermalisation of the remaining particles can take place. To our astonishment, we nevertheless observe momentum distributions which indicate that our clouds are only marginally hotter than a two-component spin mixture with equal atom number (see previous chapter).

7.4 Three-dimensional gas

For comparison with the low-dimensional situations we first study the p -wave Feshbach resonance in the crossed-beam optical trap where motion in all three dimensions is possible. We sweep the magnetic field from its initial value of 194.4 G using a linear ramp within 1 ms to its final value in the vicinity of the Feshbach resonance. There the atoms are subject to inelastic losses [7]. After a hold time of 6.4 ms we switch off both the magnetic field and the optical trap and let the atomic cloud expand ballistically for 7 ms before we take an absorption image. From the image we extract the remaining number of atoms. In these data (see Fig. 7.7a) we observe the doublet structure of the p -wave Feshbach resonance.

The decay constant of the atom number close to the Feshbach resonance is on the order of 1 ms, which is comparable to the settling time of the magnetic field. Therefore we encounter a systematic shift on the order of +0.1 G due to the direction of the magnetic field ramp. We have actually observed the opposite systematic shift when reversing the direction of the final sweep.

7.5 Two-dimensional gas

In a next step, we additionally apply a single optical standing wave along the vertical z -axis. The standing wave with a potential depth V_z creates a stack of two-dimensional Fermi gases in the horizontal x - y -plane. The lattice laser intensity is increased using an exponential ramp with a time constant of 10 ms and a duration of 20 ms. The beam for the vertical optical lattice is derived from a diode laser at a wavelength of $\lambda = 826$ nm and is focused to a $1/e^2$ -radius of $70\text{ }\mu\text{m}$. The magnetic field is aligned along the horizontal x -axis, as depicted in Fig. 7.4a. In the two-dimensional Fermi gas we have studied the p -wave Feshbach resonance analogous to the method described above, only the release process of the atoms is slightly altered: within 1 ms before the simultaneous switch-off of the magnetic and the optical potentials, we lower the lattice intensity to $V_z = 5 E_r$ to reduce the kinetic energy. This results in a more isotropic expansion which allows to determine the atom number more precisely.

For the two-dimensional gas we observe a similar doublet structure of the Feshbach resonance but shifted towards higher magnetic field values with respect to the position without strong confinement (see Fig. 7.7b). Due to the angular momentum in a p -wave collision there is a centrifugal barrier in addition to the interatomic potential, which results in a pronounced energy dependence of the scattering. In the confined gas the collision energy is modified by the motional ground state energy and the larger Fermi energy of the gas due to the confinement. Moreover, a confinement induced shift of the resonance could be envisaged, similar to what has been studied for s -wave interactions in two dimensions [194, 195].

We experimentally find that the shift of the resonance feature depends on the strength of the optical lattice. In Fig. 7.5 we compare the measured shift with a model in which we set the collision energy of the particles to be the Fermi energy plus the ground state energy. We numerically calculate the Fermi energy for the non-interacting gas in the full three-dimensional configuration of the optical lattice and the harmonic confining potential. We use a tight-binding model for the direction of the lattice laser and a harmonic oscillator potential in the transverse directions. Using the parametrisation of the Feshbach resonance according to [116], we obtain the shifted position of the resonance for a given lattice depth. For the $|m| = 1$ branch of the resonance we find good agreement of our data with the theory whereas for the $m = 0$ branch the observed shift is larger than predicted by our model. There may be an additional confinement induced shift of the p -wave resonance which depends on the m -quantum numbers in the collision process [196], however no quantitative theory is available. The observed increasing width of the Feshbach resonance is also due to a larger collision energy [116].

7.6 One-dimensional gas

Reducing the dimensionality further, we study the effect of the alignment of the electronic spins on the p -wave interaction in a one-dimensional quantum gas. Therefore all spins are lined up either orthogonal (see Fig. 7.4b) or parallel (Fig. 7.4c) to the orientation of the gas. We prepare the one-dimensional Fermi gases by superimposing a second standing

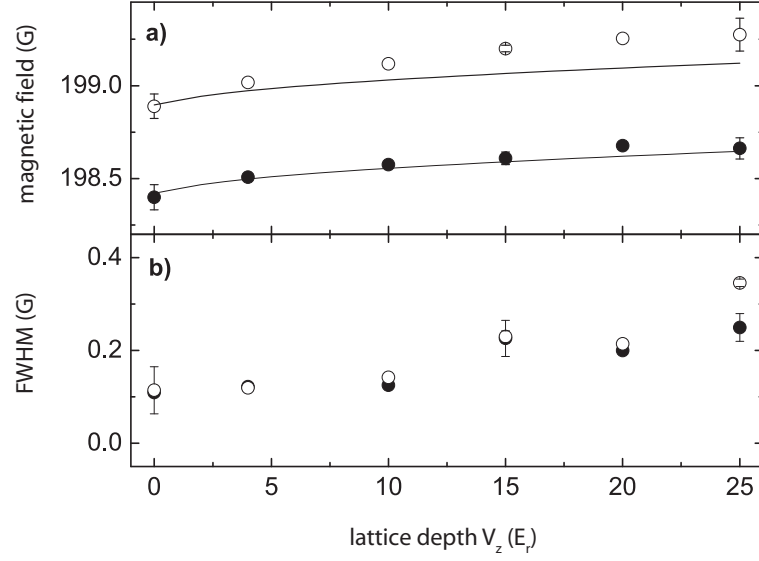


Figure 7.5: a) Shift of the Feshbach resonance position when tuning the gas from three to two dimensions. Open symbols indicate the position of the $m = 0$ branch, solid symbols the $|m| = 1$ branch of the resonance. The error bars denote the statistical error of 3 measurements. The solid lines show a calculation of the expected positions (see text). b) Evolution of the full width at half maximum (FWHM) of the loss feature.

wave laser field onto the two-dimensional quantum gases [152]. Either the x - or the y -direction of the optical dipole trap is slowly turned off and replaced by an optical lattice along the same direction and having the same beam geometry.

We now consider the orthogonal configuration where only collisions with $|m| = 1$ are possible, and correspondingly we observe only this branch of the Feshbach resonance (see Fig. 7.7c). To study the suppression of the $m = 0$ branch quantitatively we create a two-dimensional optical lattice along the x - and the z -direction with $V_z = 25 E_r$ and adjustable V_x . We have measured the peak loss on the $m = 0$ and the $|m| = 1$ resonance position, respectively. In Fig. 7.6a we plot the ratio of the peak loss versus the tunnelling matrix element along the x -direction, i. e. between the tubes of the optical lattice. For no tunnelling the one-dimensional gases are well isolated and losses on the $m = 0$ branch are completely suppressed. For larger tunnelling rates hopping of atoms between the tubes is possible and the system is not kinematically one-dimensional anymore but in a crossover regime. Therefore collisions in the $m = 0$ branch become possible which give rise to losses. The measurement directly verifies suppressed tunnelling between neighbouring lattice tubes and proves that the gases in the individual lattice tubes are kinematically one-dimensional. Orienting the one-dimensional quantum gases parallel to the magnetic field axis, we observe the $m = 0$ branch of the Feshbach resonance only (see Fig. 7.7d). Note that the width and the position of crossover regime is determined by the time scale

of the physical processes under investigation: in this experiment we are one-dimensional with respect to atomic collision time scales but not necessarily for slower dynamical processes such as collective oscillations [169].

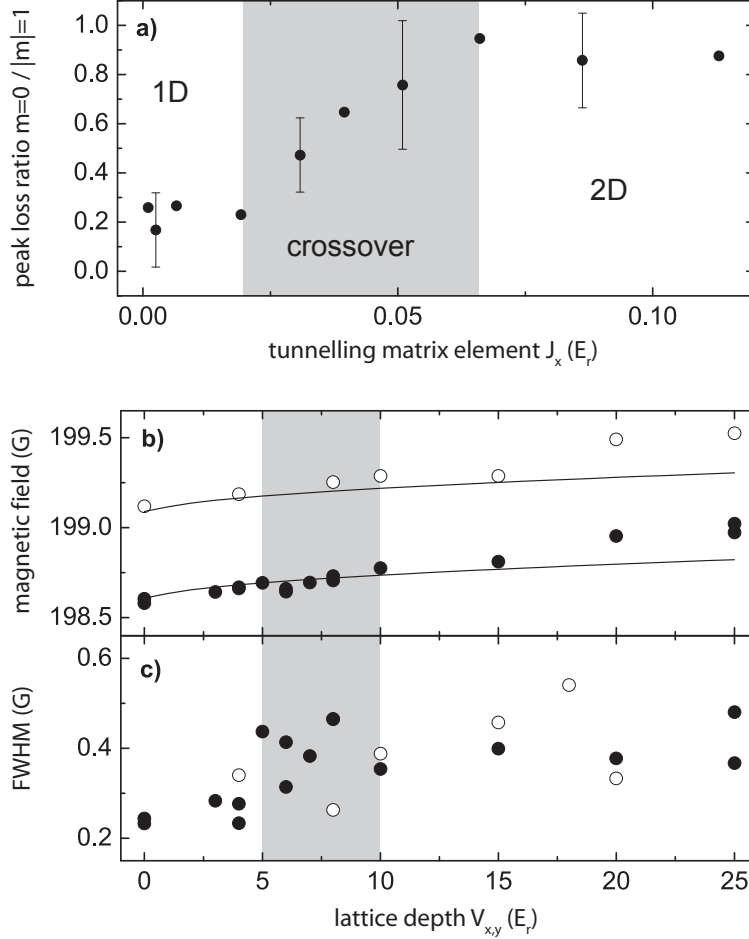


Figure 7.6: a) Suppression of collisional losses in the $m = 0$ partial wave versus the tunnelling matrix element between the one-dimensional quantum gases. The bars reflect the errors determined from the fit to the loss peaks of two measurements. The grey box indicates the crossover region from a 2D to a 1D quantum gas as inferred from the inhibition of transverse collisions. b) Shift of the position of the Feshbach resonance when tuning the gas from 2D to 1D. Open symbols indicate the position of the $m = 0$ branch in the y - z -lattice (see Fig. 7.4c) and the solid symbols the $|m| = 1$ branch of the resonance in the x - z -lattice (see Fig. 7.4b). The solid lines show a calculation of the expected positions (see text). c) Width of the Feshbach resonance loss feature.

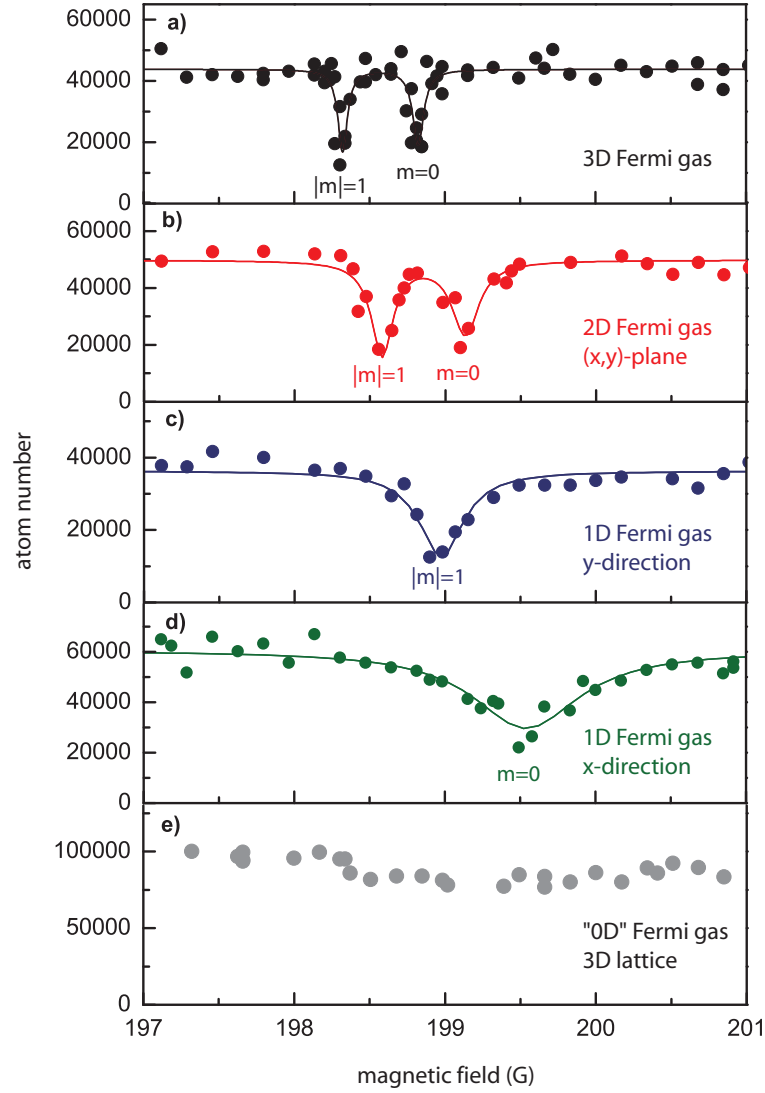


Figure 7.7: Loss measurements of the p -wave Feshbach resonance. a) Atoms are held in a crossed-beam optical dipole trap. b) Two-dimensional Fermi gas ($V_z = 25 E_r$). c) One-dimensional Fermi gas with the motion confined orthogonal to the direction of the magnetic field ($V_z = V_x = 25 E_r$). d) One-dimensional Fermi gas with the motion confined parallel to the direction of the magnetic field ($V_z = V_y = 25 E_r$). e) Fermi gas in a three-dimensional optical lattice ($V_x = V_y = V_z = 25 E_r$). The solid lines are Lorentzian fits to the data from which we extract the position and the width of the resonance.

For the one-dimensional Fermi gases we observe a further shift of the resonance position and a broadening of the loss feature as compared to the higher-dimensional config-

urations. A confinement induced shift of the p -wave resonance in one dimension for the $m = 0$ branch has been predicted in addition to the increased ground state and Fermi energy [196]. We apply the calculation technique as described above to obtain the Fermi energy of the gas and use the same parametrisation of the Feshbach resonance. For the $m = 0$ branch we additionally include the theory of ref. [196] for all lattice depths. This introduces a small error in the 2D and crossover regime. We note, however, that the confinement induced shift is small as compared to the shift due to the increased collision energy. A comparison between the resulting shift and the experimental data is shown in Fig. 7.6b. The increasing width of the loss feature is expected because the width of the Feshbach resonance also depends on the energy of the particles involved in the collision process [116].

By using three orthogonal standing waves, we prepare a band-insulating state in a 3D optical lattice [25] where the atoms are localised in the potential wells with at most one atom per lattice site. In this "zero-dimensional" situation all p -wave scattering is completely inhibited (see Fig. 7.7e) and no loss features are observed.

In conclusion, we have studied spin-polarised interacting Fermi gases in low dimensions using a p -wave Feshbach resonance. We demonstrate that in reduced dimensions the direction of spin-alignment significantly influences the scattering properties of the particles. Moreover, we find a confinement induced shift of the resonance position and observe good agreement with a theoretical model. Strongly interacting low-dimensional Fermi gases offer a wealth of fascinating many-body phenomena [197].

8 Bose-Fermi mixtures in a three-dimensional optical lattice

Quantum fluids and quantum gases are remarkable objects which reveal macroscopic quantum phenomena, such as superfluidity and Bose-Einstein condensation. These fundamental concepts have profoundly influenced our understanding of quantum many-body physics. The distinct behaviour observed for purely bosonic or purely fermionic systems sheds light on the role played by quantum statistics. New insights can be attained by mixing bosonic and fermionic species. One of the most prominent examples is a mixture of bosonic ^4He and fermionic ^3He . There it has been observed that with increasing admixture of ^3He the critical temperature of the transition between the superfluid and the normal fluid phase is lowered and below the tricritical point phase separation is encountered [199].

8.1 Bose-Fermi mixtures in atomic quantum gases

In trapped atomic gases mixing of bosonic and fermionic species has led to the observation of interaction induced losses or collapse phenomena [24, 200] and collisionally induced transport in one-dimensional lattices [72]. In this work we report on the creation of a novel quantum system consisting of a mixture of bosonic and fermionic quantum gases trapped in the periodic potential of a three-dimensional optical lattice. The optical lattice allows us to change the character of the system by tuning the depth of the periodic potential. This leads to a change of the effective mass and varies the role played by atom-atom interactions. The fascinating physics of purely bosonic [13, 84] and purely fermionic [83, 25] quantum gases in optical lattices becomes even richer when both species are mixed. The additional interaction between the bosonic and the fermionic atoms interconnects two systems of fundamentally different quantum statistics. A wealth of theoretical work has been devoted to Bose-Fermi mixtures in optical lattices and new quantum phases have been predicted at zero temperature [201, 17, 202, 203]. Moreover, the coupling between a fermion and a phonon excitation in the Bose condensate mimics the physics of polarons [204]. At finite temperature phase transitions to a supersolid state and phase separation are anticipated [15].

In our experiment, we prepare fermionic ^{40}K atoms together with a cloud of Bose-Einstein condensed ^{87}Rb atoms. The qualitative behaviour when changing the mixing ratio between bosons and fermions is depicted in Fig. 8.1. The momentum distribution

Parts of this chapter are published in [198].

of the pure bosonic sample shows a high contrast interference pattern reflecting the long-range phase coherence of the system. Adding fermionic particles results in the loss of phase coherence of the Bose gas, i. e. a diminishing visibility of the interference pattern and a reduction of the coherence length.

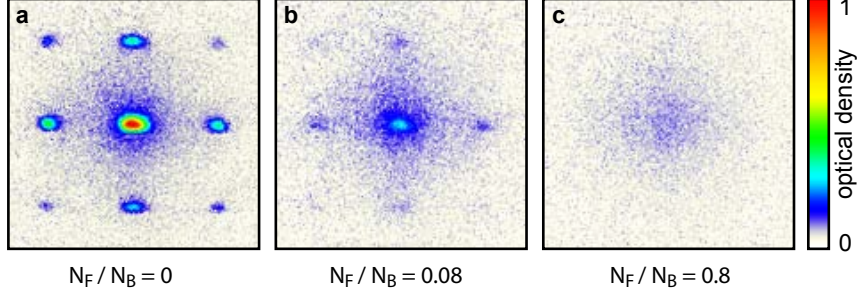


Figure 8.1: Interference pattern of bosonic atoms released from a three-dimensional optical lattice for varying admixture of N_F fermionic atoms at a value $U_{BB}/zJ_B = 5$. The bosonic atom numbers are $N_B = 1.2 \times 10^5$ (a and b) and $N_B = 8 \times 10^4$ (c) and the image size is $660 \mu\text{m} \times 660 \mu\text{m}$.

8.2 Preparing and characterising the mixture in the lattice

The fermionic ^{40}K and the bosonic ^{87}Rb atoms are cooled in the magnetic trap, as for the experiments with pure fermionic gases and described in chapter 5. The potassium atoms are in the hyperfine ground state $|F = 9/2, m_F = 9/2\rangle$ and the rubidium atoms in the hyperfine ground state $|F = 2, m_F = 2\rangle$. After reaching quantum degeneracy for both species we transfer both clouds into the crossed beam optical dipole trap operating at a wavelength of 826 nm (see paragraph 5.5.2). In the optical trap we perform evaporative cooling by lowering the power in each of the laser beams to $\simeq 35$ mW. After recompression, the optical dipole trap has the final trapping frequencies $(\omega_x, \omega_y, \omega_z) = 2\pi \times (30, 35, 118)$ Hz for the rubidium atoms. We estimate the condensate fraction to be 90% and use this value to obtain the temperature of both clouds. The Fermi temperature T_F in the optical dipole trap is set by the number of potassium atoms and the trapping frequencies, and we obtain $T/T_F \simeq 0.3$, which is in agreement with a direct temperature measurement of the fermionic cloud. For the mixing fractions investigated in this experiment the extension of the Fermi cloud was larger than the Thomas-Fermi radius of the BEC.

The three-dimensional optical lattice is generated by three mutually orthogonal laser standing waves at a wavelength of $\lambda = 1064$ nm and a mutual frequency difference of several 10 MHz. Each of the standing wave fields is focused onto the position of the quantum degenerate gases and the $1/e^2$ radii of the circular beams along the (x, y, z) -directions are $(160, 180, 160) \mu\text{m}$. To load the atoms into the optical lattice we increase the intensity of the lattice laser beams using a smooth spline ramp with a duration of 100 ms. This ensures adiabatic loading of the optical lattice with populations of bosons

and fermions in the lowest Bloch band only. We have checked the reversibility of the loading process into the optical lattice by reversing the loading ramp and subsequently let the particles equilibrate during 100 ms in the optical dipole trap without evaporation. We measure that for both the pure Bose gas and the Bose-Fermi mixture the condensate fraction decreases by $\simeq 1.4\%$ per E_r of lattice depth, where $E_r = \hbar^2/2m_{\text{Rb}}\lambda^2$ denotes the recoil energy and m_{Rb} the mass of the rubidium atoms.

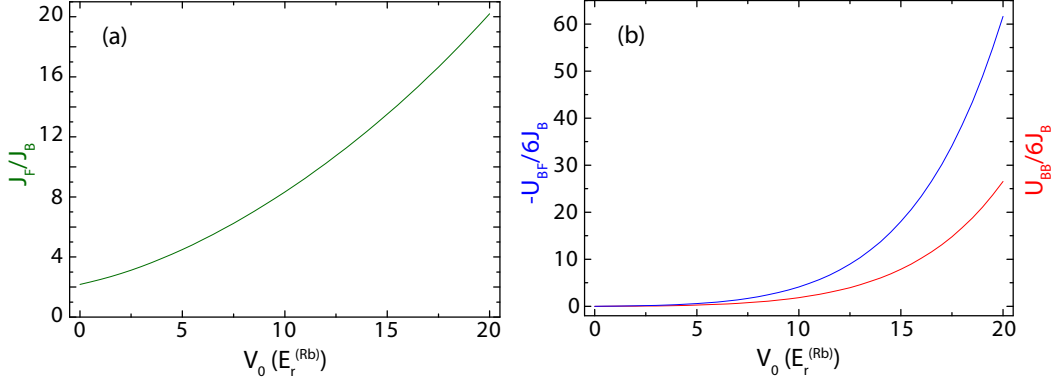


Figure 8.2: Tunnelling and interaction parameters for the Bose-Fermi mixture ^{87}Rb and ^{40}K . (a) Ratio of the tunnelling matrix elements for the bosons and the fermions. (b) Boson-boson and fermion-boson on-site interaction normalised to the tunnelling matrix element of ^{87}Rb .

The physics of the Bose-Fermi mixture in an optical lattice is described by the Bose-Fermi Hubbard model [205]. A derivation similar to the Fermi-Hubbard model (3.32) leads to the Hamiltonian:

$$\hat{H}_{\text{BF}} = -\frac{1}{2} \sum_i \left(J_B \hat{a}_{i+1}^\dagger \hat{a}_i + J_F \hat{b}_{i+1}^\dagger \hat{b}_i \right) + h.c. \quad (8.1a)$$

$$+ \frac{U_{\text{BB}}}{2} \sum_i \hat{n}_{Bi} (\hat{n}_{Bi} - 1) + U_{\text{BF}} \sum_i \hat{n}_{Bi} \hat{n}_{Fi} \quad (8.1b)$$

$$+ \sum_i (V_{Bi} \hat{n}_{Bi} + V_{Fi} \hat{n}_{Fi}). \quad (8.1c)$$

Solving this model is a difficult theoretical task, however, its parameters are well known in the experiment. The first term (8.1a) of the Hamiltonian contains the tunnelling matrix elements J_B and J_F , respectively (see section 3.5). Due to their smaller mass, the fermionic potassium atoms experience a shallower lattice potential ($V_0/E_r \propto m$) than the bosonic rubidium atoms. Since the tunnelling only depends on V_0/E_r , they are much more mobile (see Fig. 8.2(a)). The interaction part in the second line (8.1b) is specified by the on-site interaction strengths U_{BB} between two bosons and U_{BF} between a boson and a fermion. Knowing the Wannier functions $w^F(\mathbf{r})$ and $w^B(\mathbf{r})$ from the band structure allows to calculate U_{BF} by computing the integral

$$U_{\text{BF}} = \frac{2\pi\hbar^2 a_{\text{BF}}}{m_{\text{red}}} \int d\mathbf{r} |w^F(\mathbf{r})|^2 |w^B(\mathbf{r})|^2, \quad (8.2)$$

where $m_{\text{red}} = (m_K m_{\text{Rb}})/(m_K + m_{\text{Rb}})$ is the reduced mass of the two species. Using the most recent experimental value of the K–Rb s -wave (triplet) scattering length for atoms in the absolute ground state, $a_{\text{BF}} = -215 \pm 10a_0$ [206], and $a_{\text{BB}} = 100a_0$ [207] we obtain $U_{\text{BF}}/U_{\text{BB}} \approx -2$ in the parameter range of our experiment (Fig. 8.2(b)). Finally, the external trapping potential is described by the last term (8.1c) of the Hamiltonian.

8.3 Measuring the phase coherence of the superfluid

We have studied the phase coherence of the bosonic atoms in the optical lattice for various admixtures of fermionic particles. We switch off the optical lattice quickly and allow for 25 ms of ballistic expansion before taking an absorption image of the atomic cloud. From the absorption image we measure the visibility of the interference pattern, which is analogous to eqn. (3.27) given by:

$$n(\mathbf{r}) = \left(\frac{m}{\hbar t}\right)^3 \left|\tilde{w}\left(\frac{m\mathbf{r}}{\hbar t}\right)\right|^2 S\left(\mathbf{k} = \frac{m\mathbf{r}}{\hbar t}\right) \quad (8.3a)$$

$$S(\mathbf{k}) = \sum_{i,j} e^{i\mathbf{k} \cdot (\mathbf{r}_i - \mathbf{r}_j)} \langle \hat{a}_i^\dagger \hat{a}_j \rangle \quad (8.3b)$$

This formula is valid if the interactions have a negligible effect during the expansion of the atoms [208]. We determine the maximum n_{max} and the minimum n_{min} of the density of the atoms at a momentum $|\mathbf{q}| = 2\hbar k$ with $k = 2\pi/\lambda$ (see inset in Fig. 8.1a) [209]. From this we calculate the visibility $\mathcal{V} = (n_{\text{max}} - n_{\text{min}})/(n_{\text{max}} + n_{\text{min}}) = (S_{\text{max}} - S_{\text{min}})/(S_{\text{max}} + S_{\text{min}})$.

The phase coherence of the bosons in the lattice is not only described by the visibility of the interference pattern but also by the coherence length of the sample [145, 210]. In a superfluid state the coherence length is comparable to the size of the system. It is related to the inverse of the width of the zero-momentum peak plus a small contribution from the repulsive interaction between the bosonic atoms.

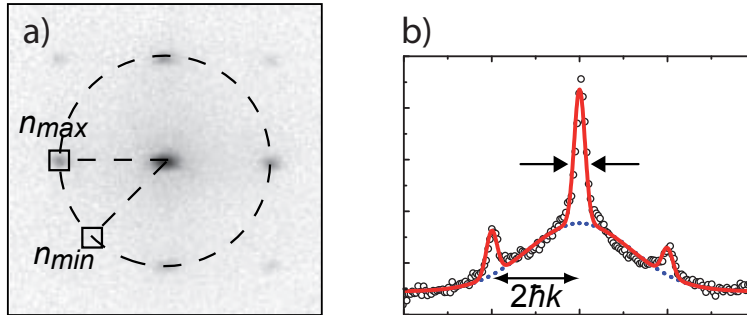


Figure 8.3: Two different quantities to extract information about the bosonic coherence: a) visibility of the interference pattern, and b) width of the central interference peak.

8.4 Adding fermions to the condensate

In the case of a purely bosonic gas the ground state for different lattice depths is well known [13, 80]. For shallow three-dimensional lattices, the kinetic energy dominates over the interaction energy and the bosons are superfluid, showing long-range phase coherence. As the lattice depth is increased beyond a certain value of U/J ($= 6.5.8$ in 3D) it becomes energetically favourable for the atoms to localise on the lattice sites, thereby avoiding to pay the interaction energy U when hopping to an already occupied neighbouring site. In this Mott insulating phase all the sites have the same integer occupation number, and the absence of number fluctuations destroys the phase coherence. The quantum phase transition from the superfluid to the Mott insulating state has been observed in a famous experiment in a three-dimensional system [84] and also in one dimension [145].

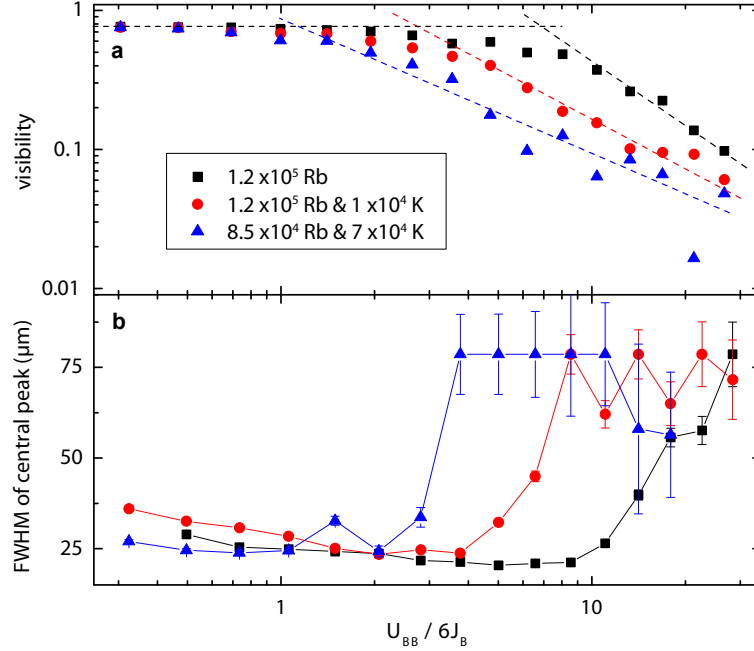


Figure 8.4: a) Visibility of the Bose-Fermi mixture in the optical lattice for various mixing ratios between bosons and fermions. The intersection between the dashed lines defines the characteristic value $(U_{BB}/zJ_B)_c$. The inset shows the principle of the measurement (see text). b) Measurement of the width of the central momentum peak which reflects the inverse of the coherence length of the gas. The inset shows how the peak width is extracted from the column sum of the optical density. The dashed line indicates the upper constraint of the width imposed by the fitting routine and the error bars reflect the fit uncertainty.

In this experiment we obtain for a pure bosonic cloud results similar to previous measurements [145, 209, 211]. In our data (see Fig. 8.1a), the visibility \mathcal{V} starts to drop

off at a characteristic value $(U_{\text{BB}}/zJ_B)_c \approx 6.5$. For larger values of U_{BB}/zJ_B the decrease in visibility is approximated by $\mathcal{V} \propto (U_{\text{BB}}/zJ_B)^\nu$ with $\nu = -1.41(9)$, which is consistent with our earlier measurement in a different lattice setup giving $\nu = -1.36(5)$ [145] but different from the exponent $\nu = -0.98(7)$ obtained in ref. [209]. For a mixture of bosonic and fermionic atoms the results change; see also [200]. Whereas in the superfluid regime for very low values of U_{BB}/zJ_B the visibility is similar to the pure bosonic case, the presence of the fermions decreases the characteristic value $(U_{\text{BB}}/zJ_B)_c$ beyond which the visibility drops off significantly. Nevertheless, the visibility still shows a power-law dependence on U_{BB}/zJ_B with an exponent in the range of $-1 < \nu < -1.5$.

To quantify the shift of the visibility data towards smaller values of U_{BB}/zJ_B we have fitted the power-law decay for large values of U_{BB}/zJ_B and extrapolated the slope to the visibility for the superfluid situation (dashed lines in Fig. 8.1a). The intersection defines the characteristic value $(U_{\text{BB}}/zJ_B)_c$ which depends on the mixing ratio between fermions and bosons N_F/N_B as shown in Fig. 8.5. From this graph it is evident that even very small admixtures of fermionic atoms change the coherence properties of the bosonic cloud significantly.

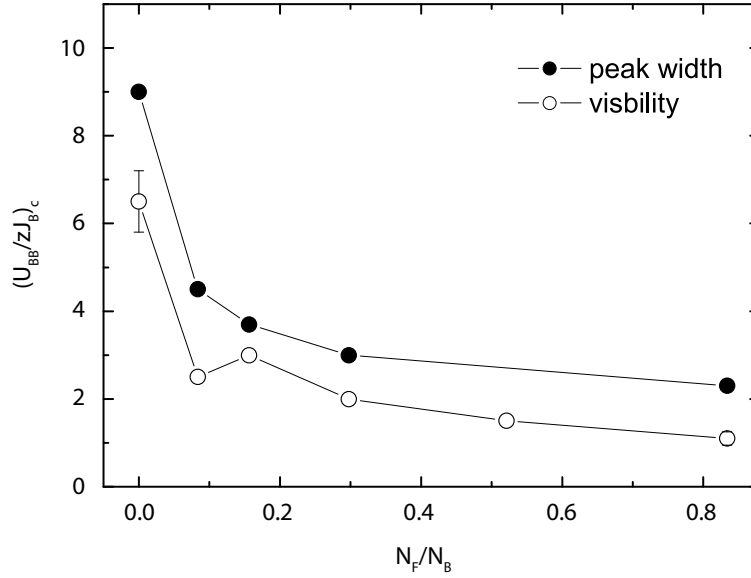


Figure 8.5: Decrease of the coherence of the Bose gas in the lattice vs. the admixture of fermions.

Measuring the central peak width we find for the pure bosonic case we find that it starts to increase at a value of $(U_{\text{BB}}/zJ_B)_c \approx 9$ (see Fig. 8.1b). For the case of a Bose-Fermi mixture the value of $(U_{\text{BB}}/zJ_B)_c$ beyond which the peak width increases is dramatically altered: for an increasing admixture of fermionic atoms to the bosonic sample, its value decreases and it behaves very similar to the corresponding value $(U_{\text{BB}}/zJ_B)_c$ for the visibility (see Fig. 8.5).

8.5 Fermion-driven condensate depletion

Our interpretation of the simultaneous decrease of both the coherence length and the visibility with increasing admixture of fermions is that the superfluid phase is left. While for the pure bosonic case this indicates a Mott insulator transition [145, 209], for the mixture the analysis is more delicate due to the different interactions and the different quantum statistics of the two species. The full understanding of the observed effects including strong interactions and finite temperature is challenging. We will consider two limiting situations, namely a strongly interacting Bose-Fermi mixture at $T = 0$ in which polarons and composite fermions are formed, and a non-interacting mixture at finite temperature. In both explanations we encounter a destruction of the superfluid with increasing fermionic admixture which qualitatively reflects our results.

At zero temperature several quantum phases of the system are predicted [15, 204, 17, 202], depending on the sign and the strength of the Bose-Fermi interaction. At low depth of the optical lattice the interaction of the Bose-Einstein condensate with the Fermi gas leads to the depletion of the condensate and to the formation of polarons where a fermion couples to a phonon excitation of the condensate [204]. The coupling strength of the fermions to the phonon modes depends on U_{BF} and the ratio U_{BB}/J_B . If the coupling becomes very strong the system is unstable to phase separation ($U_{BF} > 0$) or to collapse ($U_{BF} < 0$). In the stable regime, the polarons can form a p -wave superfluid or induce a charge density wave, as has been analysed in one spatial dimension [204]. The enhanced bosonic density around a fermionic impurity increases the effective mass of the fermion and might enhance the tendency of the bosons to localise. For our parameters, the phonon velocity is comparable to the Fermi velocity, a regime that is usually inaccessible in solids. On the other hand, the interaction of the Bose gas with the second species leads to an effectively attractive interaction between the bosons which would favour a Mott insulator transition at a larger depth of the optical lattice [204]. At a larger depth of the optical lattice other effects come also into play. Composite fermions consisting of one fermion and n_B bosons form when the binding energy of the composite fermion exceeds the gain in kinetic energy that the particles would encounter by delocalising. An effective Hamiltonian for these (spinless) composite fermions with renormalised tunnelling and nearest neighbour interaction has been derived and their quantum phases have been investigated theoretically [201, 17]. In this situation, the Bose-Einstein condensate can be completely depleted by the interactions between bosons and fermions.

For the finite temperature model of the non-interacting gas we consider the entropy of the cloud of bosons and fermions, which is $S = \alpha N_F T/T_F + \beta N_B (T/T_c)^3$. $T_F = \hbar\bar{\omega}_F(6N_F)^{1/3}$ denotes the Fermi temperature for N_F fermions in a trap with frequency $\bar{\omega}_F$ and $T_c = \hbar\bar{\omega}_B(N_B/\zeta(3))^{1/3}$ the critical temperature for Bose-Einstein condensation with α and β being numerical constants. When increasing the depth of the optical lattice adiabatically, the temperatures of the two species remain equal to each other due to collisions, while T_c and T_F evolve very differently. This is due to the fact that the tunnelling rates for the fermions are up to an order of magnitude larger than for the bosons for our lattice parameters. Since the effective masses $m_{B,F}^* \propto 1/J_{B,F}$ [see eqn. (3.21)] enter into the degeneracy temperatures, T_c decreases much faster than T_F . At constant

entropy, this results in adiabatic heating of the bosonic cloud (T/T_c increases) and a reduction of the condensate fraction [212]. Simultaneously the fermionic cloud is cooled adiabatically (T/T_F decreases), similar to the situation considered without a lattice in [213]. For the non-interacting mixture with our parameters one expects a reduction of T/T_F by a factor of approximately 2 at a lattice depth of $20 E_r$. From a very recent theoretical treatment [214] it has been found that below a certain initial temperature the lattice ramp-up gives rise to an adiabatic cooling (T decreases), whereas above this threshold temperature adiabatic heating takes place. The absolute temperature of the mixture is always higher than for the pure bosonic case.

8.6 Change of the bosonic site occupation

In the experiment we have further studied the occupation of the optical lattice by measuring three-body recombination. Lattice sites with a higher occupation than two atoms are subject to inelastic losses where a deeply bound molecule is formed and ejected from the lattice together with an energetic atom. Independent of their occupation all lattice sites are furthermore subject to loss processes such as off-resonant light scattering, background gas collisions, or photo-association due to the trapping laser light. The attractive interaction between the bosons and the fermions changes the occupation of bosons on the sites of the optical lattice. For the given ratio of the on-site interaction strength of $U_{BF}/U_{BB} \simeq -2$ it is energetically favourable to have up to five bosons per site if a fermion is present.

The experimental sequence to study the three-body decay starts from an initially superfluid Bose gas at a potential depth of $10 E_r$. We use a ramp time of 30 ms to increase the potential depth of the lattice from zero to $10 E_r$ during which we do not observe a loss of atoms. Subsequently, we freeze the atom number distribution by quickly changing the lattice depth to a large value of $18 E_r$ where the tunnelling time of the bosons is $\tau_B = \hbar/zJ_B = 23$ ms. We monitor the total atom number as a function of the hold time in the deep optical lattice (see Fig. 8.6) and observe two distinct time scales of the decay of the atoms. The fast initial time scale is due to three-body losses from multiply occupied lattice sites. The slower decay is due to single-particle loss processes.

To extract quantitative information from the loss curves we fit the data with the following model. We assume that any singly or doubly occupied site decays with a single particle loss rate Γ_1 . Multiply occupied sites decay with a rate determined by the three-body loss constant $K_3^B = 1.8 \times 10^{-29} \text{ cm}^6/\text{s}$ [215] and the three-body density $[n(\mathbf{r})]^3$ at the lattice site. Since we start from a superfluid the number distribution at the lattice sites can be approximated by a coherent state with a third order correlation function being equal to unity [216]. We calculate the three-body loss rate assuming gaussian ground state wave functions at each lattice site to be $\Gamma_3 = 0.24 \times n_B^3 \text{ s}^{-1}$, where n_B is the number of bosons on the site. By fitting the data with this model we extract the occupation of the lattice. We obtain $n_{1,2} = 67(3)\%$ of the sites with single or double occupation, $n_3 = 23(9)\%$ sites with triple occupation and $n_4 = 10(8)\%$ of lattice sites with occupation four. A mean field calculation neglecting tunnelling yields the theoretical values $\bar{n}_{1,2} = 58\%$, $\bar{n}_3 = 33\%$, and $\bar{n}_4 = 17\%$ which gives reasonable agreement given the

simplicity of the model. The slow decay rate is determined to be $0.35(7) \text{ s}^{-1}$.

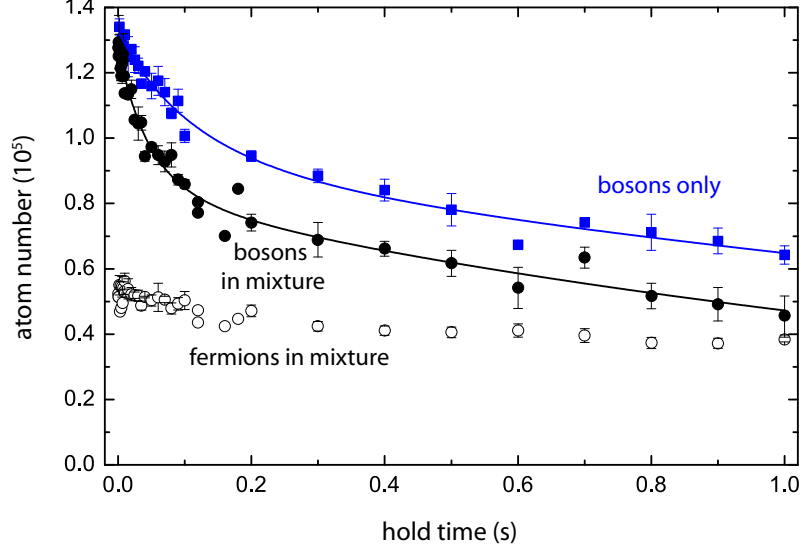


Figure 8.6: Decay of a pure bosonic gas (squares) and a Bose-Fermi mixture (circles) in the optical lattice. The fast initial decay of the bosons is much more pronounced in the mixture, reflecting the higher density due to Bose-Fermi attraction. For the fermions hardly any loss is observed. The error bars indicate statistical errors from three repetitive measurements.

Upon adding fermions to the system we find a much faster initial decay due to three-body loss for the rubidium atoms. The single particle loss constant is, however, the same. In contrast, for the fermionic atoms we do not observe a particle loss of a comparable order of magnitude. This suggests that the observed loss is only due to three-body recombination between three rubidium atoms. Recent results have suggested that the three-body loss constant K_3^{BF} for K-Rb-Rb collisions is an order of magnitude larger than for Rb-Rb-Rb collisions [200]. This is not consistent with our data since we do not observe the corresponding fast loss of potassium atoms, similar to previous results [217].

8.7 Conclusions

In conclusion, we have investigated a Bose-Fermi mixture in a three-dimensional optical lattice. We have observed that the presence of fermions changes the coherence properties of the Bose gas and substantially enhances the three-body loss of bosonic atoms. Bose-Fermi mixtures in an optical lattice promise to be an extremely rich quantum system [201, 17, 202, 204, 15]. A number of Feshbach resonances between ^{87}Rb and ^{40}K [218, 219] exists which will give access to various quantum many-body regimes predicted in the literature as well as to the creation of ultracold heteronuclear molecules.

9 Conclusions and outlook

In recent years cold atoms in optical lattices have emerged as an important domain in the research of dilute quantum gases. In this thesis I have presented the first experiments with interacting fermionic ^{40}K atoms and Bose-Fermi mixtures of ^{40}K and ^{87}Rb in optical lattices. These systems bridge the gap between cold atomic physics and solid state physics and open the way towards the exploration of intriguing quantum phases in lattices.

In the following the experimental results described in the previous chapters are summarised and future perspectives are pointed out.

9.1 Controlling the interactions of fermions in a lattice

In a three-dimensional optical lattice we prepared the two most elementary states of ideal fermions in a periodic potential, a metallic and a band-insulating state, and dynamically induced a transition between them. Imaging the Fermi surface provides direct access to the quasi-momentum distribution in either state. In order to investigate the specific scattering properties of atoms confined in an optical lattice we exploited a Feshbach resonance to adjust the scattering length. Crossing the resonance adiabatically from one side, we created weakly bound molecules in 1D systems and in deep cubic lattices. The measured energy spectra demonstrate the strong influence of the lattice confinement on the atomic scattering. Crossing the Feshbach resonance from the other side, atoms are transferred to higher bands, which reveals the limits of single-band Hubbard models.

Furthermore, the combination of low-dimensional geometries and anisotropic scattering gives rise to new phenomena not previously encountered for s -wave interactions. We realised p -wave interacting Fermi gases in low dimensions for the first time, making use of a p -wave Feshbach resonance for spin-aligned atoms. The anisotropy of the scattering allowed us to suppress the asymptotic wave functions extending in the transverse directions of the confinement. In one dimension, strongly attracting spin-aligned fermions can be mapped to non-interacting bosons. Such a fermionic Tonks should display a bosonic density distribution which has yet escaped experimental observation. Other intriguing perspectives include the exploration of the BCS-BEC crossover in 1D [10] and the observation of exotic p -wave superfluid phases [220].

Our experiments demonstrate the amazing versatility of cold fermionic atoms in optical lattices and their use as a model system for quantum many-body physics. The high degree of control over the parameters permits us to test and simulate interesting Hamiltonians and to discover new phenomena.

9.2 Quantum simulation with fermions

Experiments with two-component spin mixtures in optical lattices are to a great extent motivated by the possibility of simulating the Fermi-Hubbard model, on which a substantial part of modern condensed matter physics is based. One can, for instance, study *s*-wave superfluidity and the BCS-BEC crossover for attractive interactions in a lattice [83, 9]. The domain of repulsive on-site interaction (positive U -Hubbard model) is especially exciting since it embodies the physics of high-temperature superconductors [221]. For fillings close to one half corresponding to $n = 1$ atom per site, an antiferromagnetic phase (AFM) forms below the critical Néel temperature T_N , as illustrated in Fig. 9.1. At temperatures not much above T_N , the fermions tend to localise in the lattice sites for sufficiently large U/J and build a Mott insulating state (MI). A *d*-wave superfluid phase (*d*-SF) is expected for very low temperatures and fillings slightly below one half. Interestingly, in the limit of large U/J , where the tunnelling term can be treated perturbatively, the Hubbard model maps to the Heisenberg model with a spin coupling of $J_{\text{AF}} = 4J^2/U$ [138]. This energy scale gives an estimate for the Néel temperature T_N , which is of the order of $0.1 T_F$. Achieving such low temperatures poses a new challenge for experiments,

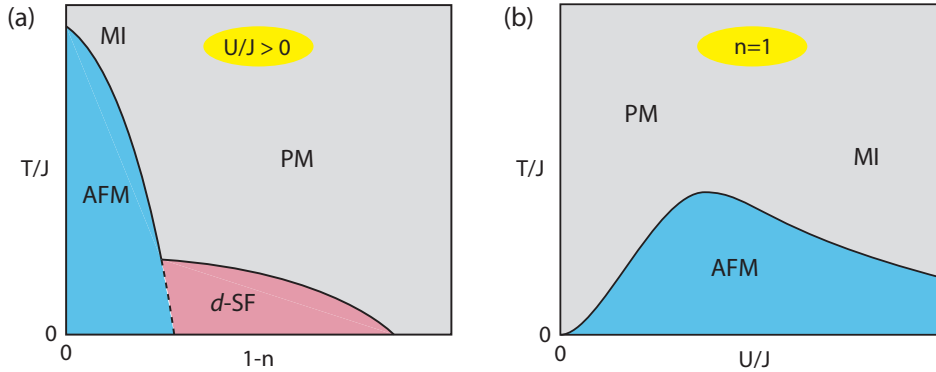


Figure 9.1: Schematic phase diagrams of the repulsive Fermi-Hubbard model: Critical temperatures in units of the tunnelling J , in (a) versus the filling n and in (b) versus the interaction U/J for half filling ($n = 1$). Around half filling an antiferromagnetic phase (AFM) appears at low temperature, while for lower fillings a *d*-wave superfluid phase is expected. Above the Néel temperature the system is Mott insulating (MI) for sufficiently large U/J . (PM) denotes the unordered paramagnetic phase.

and proposals for new cooling mechanisms as in refs [138, 222] are very desirable. In this respect the realisation of a fermionic Mott insulator seems definitely within closer reach for current experiments than the spin-ordered phases.

A concrete example of quantum simulation is our investigation of the transport properties of an interacting Fermi gas within the negative- U Fermi-Hubbard model. These experiments were carried out during the writing of this thesis and are detailed in the preprint of ref. [223]. In short, we prepare an attractively interacting gas and displace

the minimum of the external trapping potential to observe the relaxation of the cloud towards the new equilibrium position in the lattice. For attractive interactions we have amazingly good control over the atomic motion in the lattice by tuning the scattering between different negative values. For large values of U/J we find that the cloud relaxes very slowly as a consequence of the low tunnelling rate of weakly bound local pairs [224, 225]. The presence of these pairs also leads to an increase of the local density in the lattice wells, which we observe in a larger fraction of Feshbach molecules formed after a magnetic field sweep.

It is conceivable to explore a phase transition to a Mott insulating state with a similar experiment for repulsive interactions. Furthermore, measuring the fraction of doubly occupied lattice sites in a Mott insulator by molecule formation should reveal the interaction-induced localisation of atoms in different lattice sites. For magnetic field sweeps faster than the tunnelling time between adjacent sites, one expects the fraction of formed molecules to vanish. In the meantime we have integrated a more powerful lattice laser in our setup which achieves potentials deep enough to freeze the site occupation and thereby facilitates non-adiabatic molecule formation. A Mott insulating phase is further characterised by an energy gap in the excitation spectrum, which may be measured spectroscopically by modulating the lattice potential [226].

9.3 Tuning the interaction between fermions and bosons

By loading bosonic and fermionic atoms simultaneously into a 3D optical lattice we realised a Bose-Fermi mixture. We observed that the presence of fermions changes the coherence properties of the Bose gas and substantially enhances the three-body loss of bosonic atoms.

Future prospects for Bose-Fermi mixtures in optical lattices are promising, especially when the interspecies interaction is tuneable via a Feshbach resonance [219]. Similar to phonons in a solid, the bosonic atoms can mediate an effective attractive interaction between the fermions, and enable superfluid pairing [16]. Moreover, the existence of a supersolid phase has been predicted, where superfluid (off-diagonal long-range) order and crystalline (diagonal long-range) order are both present [15]. While the first one is associated with phase order in the Bose condensate, the latter is imprinted on the bosonic density by the interaction with the fermions which form a density wave.

Another exciting perspective is the creation of hetero-nuclear K-Rb molecules. In the vibrational ground state these molecules have a permanent electric dipole moment of the order of 1 Debye, resulting in a long-range dipole-dipole interaction. This would give access to new phenomenology and allow the manipulation via electric fields for quantum computing applications [227]. Ideally, in a 3D optical lattice each site is populated with one boson and one fermion so that isolated Feshbach molecules can be created via a magnetic field sweep [228]. In contrast to the situation in a weakly confining trap, in the lattice molecule-molecule collisions are suppressed. Moreover, a favourable Frank-Condon factor should facilitate transferring the weakly-bound molecules to their vibrational ground state via a two-photon Raman transition [229].

The experiments presented in this thesis have initiated the exploration of interacting

9 CONCLUSIONS AND OUTLOOK

fermions and Bose-Fermi mixtures in optical lattices. The almost boundless possibilities of controlling experimental parameters promise thrilling physics to be discovered in the future.

10 Appendix

10.1 Singlet and triplet character of the scattering length

In this section I show with a specific example how the s -wave scattering length for two atoms in certain hyperfine states can be estimated from the knowledge of the singlet and triplet scattering lengths, a_S and a_T , for the considered isotopes.

We are interested in the $F = 9/2$ hyperfine ground state of the ^{40}K isotope with total nuclear spin $I = 4$ and electronic angular momentum $J = S = 1/2$. We consider two independent atoms in the lowest magnetic sub-levels of the hyperfine ground state, $|9/2, -9/2\rangle$ and $|9/2, -7/2\rangle$, respectively, where the states are denoted as $|F, m_F\rangle$ with m_F being the projection of the total spin F onto the quantisation axis. What is the electronic spin configuration of the two-body state? The atoms are in superpositions of states with electron spin up $|\uparrow\rangle$ ($m_S = 1/2$) and down $|\downarrow\rangle$ ($m_S = -1/2$). To determine the singlet and triplet character of the electronic spin we do the Clebsch-Gordan decomposition into states $|m_I, m_S\rangle$ with definite projections m_I and m_S of the nuclear and the electronic spin, respectively,

$$|9/2, -9/2\rangle = |-4, \downarrow\rangle \quad (10.1a)$$

$$|9/2, -7/2\rangle = \frac{1}{3}|-4, \uparrow\rangle + \frac{\sqrt{8}}{3}|-3, \downarrow\rangle. \quad (10.1b)$$

For the two-particle state of the atom pair we can now write

$$\begin{aligned} |9/2, -9/2\rangle \otimes |9/2, -7/2\rangle &= |-4, \downarrow\rangle \otimes \left(\frac{1}{3}|-4, \uparrow\rangle + \frac{\sqrt{8}}{3}|-3, \downarrow\rangle \right) \\ &= \frac{1}{3}|-4, \downarrow\rangle|-4, \uparrow\rangle + \frac{\sqrt{8}}{3}|-4, \downarrow\rangle|-3, \downarrow\rangle \\ &= \frac{1}{6}(|-4, \downarrow\rangle|-4, \uparrow\rangle - |-4, \uparrow\rangle|-4, \downarrow\rangle) \end{aligned} \quad (10.2a)$$

$$+ \frac{1}{6}(|-4, \downarrow\rangle|-4, \uparrow\rangle + |-4, \uparrow\rangle|-4, \downarrow\rangle) + \frac{\sqrt{8}}{3}|-4, \downarrow\rangle|-3, \downarrow\rangle. \quad (10.2b)$$

In the last expression the term (10.2a) is a singlet state whereas the terms (10.2b) correspond to triplet states. The squares of their amplitudes give the probabilities P_S and P_T for the pair to be in the singlet or the triplet state, respectively:

$$P_S = 1/18 \quad (10.3a)$$

$$P_T = 17/18. \quad (10.3b)$$

The pair $|9/2, -9/2\rangle$ and $|9/2, -7/2\rangle$ has thus an almost pure triplet character. The same is then true for the scattering length which in the elastic approximation [230] is given by

$$a \simeq P_S a_S + P_T a_T. \quad (10.4)$$

10.2 Atomic properties

10.2.1 Fermionic potassium ^{40}K

natural abundance	0.0117(1) %	[231]
atomic mass m	39.9639985 u	[231]
vapour pressure at 50°C	3.8×10^{-7} mbar	[231]
nuclear spin I	4	[231]
nuclear g_I factor	0.000176490(34) *	[232]
g_J factor ($4^2S_{1/2}$)	2.00229421(24)	[232]
wavelength of D_2 line	766.7017 nm	[233]
wavelength of D_1 line	770.1098 nm	[233]
natural line width of D_2 transition Γ	$2\pi \cdot 6.09$ MHz	[234]
ground state hyperfine splitting	$2\pi \cdot 1285.7$ MHz	[232]
van der Waals coefficient C_6	$3927 \pm 50 a_0^6 \alpha^2 m_e c^2$	[114, 116, 235]
range of van der Waals potential β_6	130 a_0	[114]
singlet scattering length a_S	104.0 a_0	[116]
triplet scattering length a_T	174 a_0	[116]
background scattering length a_{bg}	174 a_0	[116]
effective range r_e	98 a_0	[89]

10.2.2 Bosonic rubidium ^{87}Rb

natural abundance	27.83(2)	%	[231]
atomic mass m	86.90918053	u	[231]
vapour pressure at 20°C	3.1×10^{-7}	mbar	[231]
nuclear spin I	3/2		[231]
nuclear g_I factor	-0.0009951414(10)	*	[232]
g_J factor ($5^2S_{1/2}$)	2.00233113(20)		[232]
wavelength of D_2 line (vacuum)	780.241209686(13)	nm	[237]
wavelength of D_1 line (vacuum)	794.9788509(8)	nm	[237]
natural line width of D_2 transition Γ	$2\pi \cdot 5.746(8)$	MHz	[234]
ground state hyperfine splitting	$2\pi \cdot 6834.6823$	MHz	[232]
background scattering length a_{bg}	100	a_0	[207]

^{40}K – ^{87}Rb interspecies background scattering length ($B = 0$): $(-185 \pm 7) a_0$ [219, 206].

*The nuclear gyromagnetic ratio is defined through the nuclear magnetic moment $\mu_{\text{nuc}} = -g_I \mu_B \mathbf{I}$, where μ_B is the Bohr magneton.

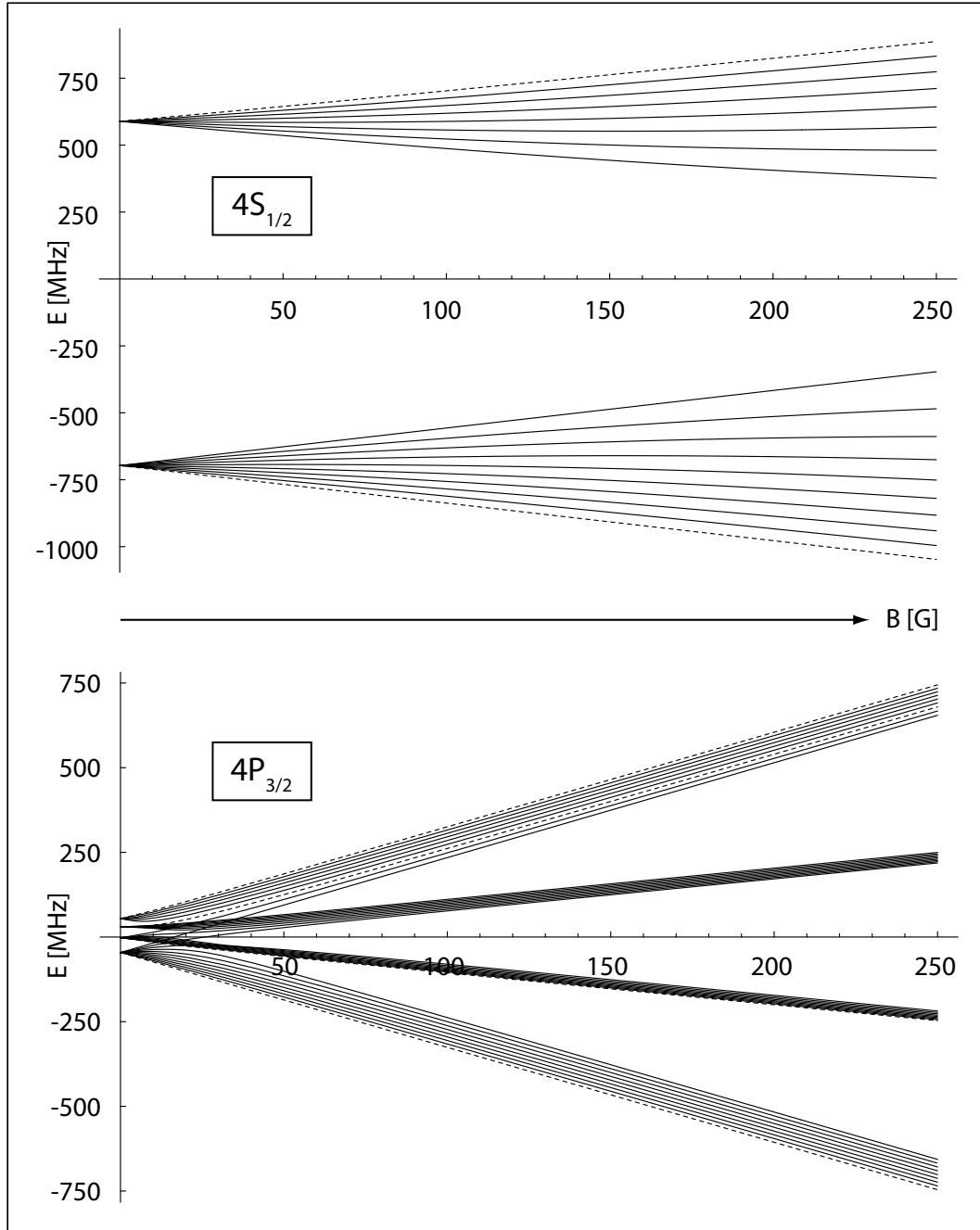


Figure 10.1: Magnetic sub-levels of the ground state $4S_{1/2}$ and the excited state $4P_{3/2}$ fine structure manifold in ^{40}K . The zero of energy is defined as the energy of the fine structure levels in absence of hyperfine interactions at $B = 0$. For each hyperfine manifold F the magnetic sub-level with $m_F = -F$ is plotted as a dashed line. The energies were calculated by exact diagonalisation [236].

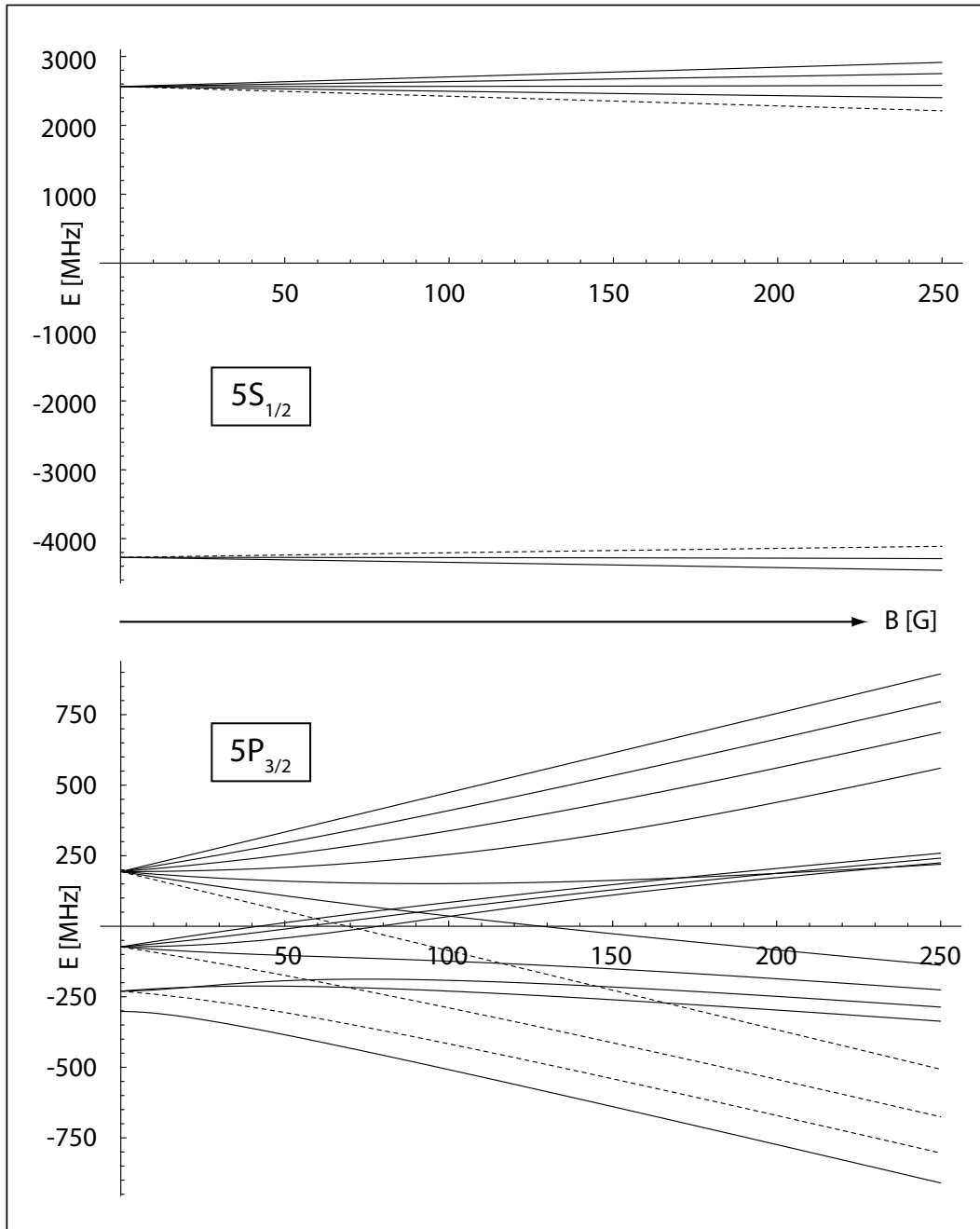


Figure 10.2: Magnetic sub-levels of the ground state $5S_{1/2}$ and the excited state $5P_{3/2}$ fine structure manifold in ^{87}Rb , analogous to Fig. 10.1

10.3 Publications

The following table lists articles that were published within the frame of my PhD work:

Paper	Title	Published	Citation
1	Fermionic Atoms in a Three Dimensional Optical Lattice: Observing Fermi Surfaces, Dynamics, and Interactions	2005	[25]
2	Confinement Induced Molecules in a 1D Fermi Gas	2005	[152]
3	Molecules of Fermionic Atoms in an Optical Lattice	2006	[174]
4	Strongly interacting atoms and molecules in a 3D optical lattice	2006	[179]
5	p -Wave Interactions in Low-Dimensional Fermionic Gases	2005	[187]
6	Bose-Fermi Mixtures in a Three-Dimensional Optical Lattice	2006	[198]
7	Realization of a Magnetically Guided Atomic Beam in the Collisional Regime	2004	[238]

Bibliography

- [1] J. G. Bednorz and K. A. Müller, *Possible high T_c superconductivity in the Ba-La-Cu-O system*, Zeitschrift für Physik B Condensed Matter **64**, 189 (1986).
- [2] C. A. Regal, M. Greiner, and D. S. Jin, *Observation of Resonance Condensation of Fermionic Atom Pairs*, Phys. Rev. Lett. **92**, 040403 (2004).
- [3] M. W. Zwierlein, C. A. Stan, C. H. Schunck, S. M. F. Raupach, A. J. Kerman, and W. Ketterle, *Condensation of Pairs of Fermionic Atoms near a Feshbach Resonance*, Phys. Rev. Lett. **92**, 120403 (2004).
- [4] C. Chin, M. Bartenstein, A. Altmeyer, S. Riedl, S. Jochim, J. H. Denschlag, and R. Grimm, *Observation of the Pairing Gap in a Strongly Interacting Fermi Gas*, Science **305**, 1128 (2004).
- [5] M. W. Zwierlein, J. R. Abo-Shaeer, A. Schirotzek, C. H. Schunck, and W. Ketterle, *Vortices and superfluidity in a strongly interacting Fermi gas*, Nature **435**, 1047 (2005).
- [6] G. Modugno, E. de Mirandes, F. Ferlando, H. Ott, G. Roati, and M. Inguscio, *Atomic Fermi gases in optical lattices*, in *AIP Conf. Proc.*, vol. 770, 197–208, AIP, Rio de Janeiro (Brazil) (2005).
- [7] C. A. Regal, C. Ticknor, J. L. Bohn, and D. S. Jin, *Creation of ultracold molecules from a Fermi gas of atoms*, Nature **424**, 47 (2003).
- [8] J. Cubizolles, T. Bourdel, S. J. J. M. F. Kokkelmans, G. V. Shlyapnikov, and C. Salomon, *Production of Long-Lived Ultracold Li_2 Molecules from a Fermi Gas*, Phys. Rev. Lett. **91**, 240401 (2003).
- [9] A. Koetsier, D. B. M. Dickerscheid, and H. T. C. Stoof, *BEC-BCS crossover in an optical lattice*, Phys. Rev. A **74**, 033621 (2006).
- [10] J. N. Fuchs, A. Recati, and W. Zwerger, *Exactly Solvable Model of the BCS-BEC Crossover*, Phys. Rev. Lett. **93**, 090408 (2004).
- [11] M. Girardeau, H. Nguyen, and M. Olshanii, *Effective interactions, Fermi-Bose duality, and ground states of ultracold atomic vapors in tight de Broglie waveguides*, Opt. Comm. **243**, 3 (2004).

BIBLIOGRAPHY

- [12] M. Iskin and C. A. R. S. de Melo, *Superfluidity of p-wave and s-wave atomic Fermi gases in optical lattices*, Phys. Rev. B **72**, 224513 (2005).
- [13] D. Jaksch, C. Bruder, J. I. Cirac, C. W. Gardiner, and P. Zoller, *Cold Bosonic Atoms in Optical Lattices*, Phys. Rev. Lett. **81**, 3108 (1998).
- [14] D. J. Scalapino, *The case for $d_{x^2 - y^2}$ pairing in the cuprate superconductors*, Physics Reports **250**, 329 (1995).
- [15] H. P. Büchler and G. Blatter, *Supersolid versus Phase Separation in Atomic Bose-Fermi Mixtures*, Phys. Rev. Lett. **91**, 130404 (2003).
- [16] F. Illuminati and A. Albus, *High-Temperature Atomic Superfluidity in Lattice Bose-Fermi Mixtures*, Phys. Rev. Lett. **93**, 090406 (2004).
- [17] M. Lewenstein, L. Santos, M. A. Baranov, and H. Fehrmann, *Atomic Bose-Fermi Mixtures in an Optical Lattice*, Phys. Rev. Lett. **92**, 050401 (2004).
- [18] W. Pauli, *The Connection Between Spin and Statistics*, Phys. Rev. **58**, 716 (1940).
- [19] A. J. Leggett, *Quantum Liquids (Bose Condensation and Cooper Pairing in Condensed-Matter Systems)*, Oxford University Press (2006).
- [20] M. E. Peskin and D. V. Schroeder, *An Introduction to Quantum Field Theory*, Westview Press (1995).
- [21] M. H. Anderson, J. R. Ensher, M. R. Matthews, C. E. Wieman, and E. A. Cornell, *Observation of Bose-Einstein Condensation in a Dilute Atomic Vapor*, Science **269**, 198 (1995).
- [22] K. B. Davis, M. O. Mewes, M. R. Andrews, N. J. van Druten, D. S. Durfee, D. M. Kurn, and W. Ketterle, *Bose-Einstein Condensation in a Gas of Sodium Atoms*, Phys. Rev. Lett. **75**, 3969 (1995).
- [23] B. DeMarco and D. S. Jin, *Onset of Fermi Degeneracy in a Trapped Atomic Gas*, Science **285**, 1703 (1999).
- [24] G. Modugno, G. Roati, F. Riboli, F. Ferlaino, R. J. Brecha, and M. Inguscio, *Collapse of a Degenerate Fermi Gas*, Science **297**, 2240 (2002).
- [25] M. Köhl, H. Moritz, T. Stöferle, K. Günter, and T. Esslinger, *Fermionic Atoms in a Three Dimensional Optical Lattice: Observing Fermi Surfaces, Dynamics, and Interactions*, Phys. Rev. Lett. **94**, 080403 (2005).
- [26] C. Ospelkaus, S. Ospelkaus, K. Sengstock, and K. Bongs, *Interaction-Driven Dynamics of ^{40}K - ^{87}Rb Fermion-Boson Gas Mixtures in the Large-Particle-Number Limit*, Phys. Rev. Lett. **96**, 020401 (2006).

-
- [27] S. Aubin, S. Myrskog, M. H. T. Extavour, L. J. LeBlanc, D. McKay, A. Stummer, and J. H. Thywissen, *Rapid sympathetic cooling to Fermi degeneracy on a chip*, Nat Phys **2**, 384 (2006).
 - [28] T. Rom, T. Best, D. van Oosten, U. Schneider, S. Folling, B. Paredes, and I. Bloch, *Free fermion antibunching in a degenerate atomic Fermi gas released from an optical lattice*, Nature **444**, 733 (2006).
 - [29] A. G. Truscott, K. E. Strecker, W. I. McAlexander, G. B. Partridge, and R. G. Hulet, *Observation of Fermi Pressure in a Gas of Trapped Atoms*, Science **291**, 2570 (2001).
 - [30] F. Schreck, L. Khaykovich, K. L. Corwin, G. Ferrari, T. Bourdel, J. Cubizolles, and C. Salomon, *Quasipure Bose-Einstein Condensate Immersed in a Fermi Sea*, Phys. Rev. Lett. **87**, 080403 (2001).
 - [31] S. R. Granade, M. E. Gehm, K. M. O'Hara, and J. E. Thomas, *All-Optical Production of a Degenerate Fermi Gas*, Phys. Rev. Lett. **88**, 120405 (2002).
 - [32] Z. Hadzibabic, C. A. Stan, K. Dieckmann, S. Gupta, M. W. Zwierlein, A. Görlitz, and W. Ketterle, *Two-Species Mixture of Quantum Degenerate Bose and Fermi Gases*, Phys. Rev. Lett. **88**, 160401 (2002).
 - [33] S. Jochim, M. Bartenstein, G. Hendl, J. H. Denschlag, R. Grimm, A. Mosk, and M. Weidemüller, *Magnetic Field Control of Elastic Scattering in a Cold Gas of Fermionic Lithium Atoms*, Phys. Rev. Lett. **89**, 273202 (2002).
 - [34] C. Silber, S. Gunther, C. Marzok, B. Deh, P. W. Courteille, and C. Zimmermann, *Quantum-Degenerate Mixture of Fermionic Lithium and Bosonic Rubidium Gases*, Phys. Rev. Lett. **95**, 170408 (2005).
 - [35] J. M. McNamara, T. Jelte, A. S. Tychkov, W. Hogervorst, and W. Vassen, *Degenerate Bose-Fermi Mixture of Metastable Atoms*, Phys. Rev. Lett. **97**, 080404 (2006).
 - [36] T. Fukuhara, Y. Takasu, M. Kumakura, and Y. Takahashi, *Degenerate Fermi Gases of Ytterbium*, Phys. Rev. Lett. **98**, 030401 (2007).
 - [37] F. Dalfovo, S. Giorgini, L. P. Pitaevskii, and S. Stringari, *Theory of Bose-Einstein condensation in trapped gases* (1999).
 - [38] A. J. Leggett, *Bose-Einstein condensation in the alkali gases: Some fundamental concepts* (2001).
 - [39] L. Pitaevskii and S. Stringari, *Bose-Einstein Condensation*, International Series of Monographs on Physics, Oxford University Press (2003).
 - [40] K. Huang, *Statistical Mechanics*, John Wiley and Sons, second edn. (1987).

BIBLIOGRAPHY

- [41] Y. Castin and R. Dum, *Bose-Einstein Condensates in Time Dependent Traps*, Phys. Rev. Lett. **77**, 5315 (1996).
- [42] M. R. Andrews, C. G. Townsend, H.-J. Miesner, D. S. Durfee, D. M. Kurn, and W. Ketterle, *Observation of Interference Between Two Bose Condensates*, Science **275**, 637 (1997).
- [43] O. Penrose and L. Onsager, *Bose-Einstein Condensation and Liquid Helium*, Phys. Rev. **104**, 576 (1956).
- [44] D. A. Butts and D. S. Rokhsar, *Trapped Fermi gases*, Phys. Rev. A **55**, 4346 (1997).
- [45] Y. Castin, *Basic theory tools for degenerate Fermi gases* (2006).
- [46] G. M. Bruun and K. Burnett, *Interacting Fermi gas in a harmonic trap*, Phys. Rev. A **58**, 2427 (1998).
- [47] L. D. Landau and E. M. Lifshitz, *Statistical Physics Part 2*, vol. 9 of *Course of Theoretical Physics*, Pergamon Press, 3rd edition edn. (1980).
- [48] *Fermi liquids and Luttinger liquids* (1998), in ‘Field Theories for Low-Dimensional Condensed Matter Systems’. G. Morandi et al. Eds. Springer (2000).
- [49] J. M. Luttinger, *An Exactly Soluble Model of a Many-Fermion System*, J. Math. Phys. **4**, 1154 (1963).
- [50] F. D. M. Haldane, ‘*Luttinger liquid theory*’ of one-dimensional quantum fluids. I. *Properties of the Luttinger model and their extension to the general 1D interacting spinless Fermi gas*, J. Phys. C **14**, 2585 (1981).
- [51] A. Recati, P. O. Fedichev, W. Zwerger, and P. Zoller, *Fermi one-dimensional quantum gas: Luttinger liquid approach and spin-charge separation*, J. Opt. B **5**, S55 (2003).
- [52] E. A. Donley, N. R. Claussen, S. L. Cornish, J. L. Roberts, E. A. Cornell, and C. E. Wieman, *Dynamics of collapsing and exploding Bose-Einstein condensates*, Nature **412**, 295 (2001).
- [53] M. Greiner, C. A. Regal, and D. S. Jin, *Emergence of a molecular Bose-Einstein condensate from a Fermi gas*, Nature **426**, 537 (2003).
- [54] V. S. Letokhov, *Narrowing of the Doppler Width in a Standing Wave*, Soviet Journal of Experimental and Theoretical Physics Letters **7**, 272 (1968).
- [55] R. H. Dicke, *The Effect of Collisions upon the Doppler Width of Spectral Lines*, Phys. Rev. **89**, 472 (1953).
- [56] C. S. Adams and E. Riis, *Laser cooling and trapping of neutral atoms*, Progress in Quantum Electronics **21**, 1 (1997).

-
- [57] I. Bloch, *Ultracold quantum gases in optical lattices* (2005).
 - [58] H. Moritz, *One-dimensional Atomic Gases*, Ph.D. thesis, ETH Zurich (2006).
 - [59] S. Chu, J. E. Bjorkholm, A. Ashkin, and A. Cable, *Experimental Observation of Optically Trapped Atoms*, Phys. Rev. Lett. **57**, 314 (1986).
 - [60] M. D. Barrett, J. A. Sauer, and M. S. Chapman, *All-Optical Formation of an Atomic Bose-Einstein Condensate*, Phys. Rev. Lett. **87**, 010404 (2001).
 - [61] J. Dalibard and C. Cohen-Tannoudji, *Dressed-atom approach to atomic motion in laser light the dipole force revisited*, J. Opt. Soc. Am. B **2**, 1707 (1985).
 - [62] C. Cohen-Tannoudji, J. Dupont-Roc, and G. Grynberg, *Processus d'interaction entre photons et atomes*, EDP Sciences (2000).
 - [63] R. Grimm and M. Weidemüller, *Optical dipole traps for neutral atoms* (1999).
 - [64] M. Greiner, *Ultracold quantum gases in three-dimensional optical lattice potentials*, Ph.D. thesis, LMU (2003).
 - [65] N. W. Ashcroft and N. D. Mermin, *Solid State Physics*, Saunders College Publishing, Philadelphia, PA (1976).
 - [66] M. Wilkens, E. Schumacher, and P. Meystre, *Band theory of a common model of atom optics*, Phys. Rev. A **44**, 3130 (1991).
 - [67] R. Piil and K. Molmer, *Tunnelling couplings in discrete lattices, single particle band structure and eigenstates of interacting atom pairs*, arXiv:cond-mat/0703573v1 (2007).
 - [68] L. Pezze, L. Pitaevskii, A. Smerzi, S. Stringari, G. Modugno, E. de Mirandes, F. Ferlaino, H. Ott, G. Roati, and M. Inguscio, *Insulating Behavior of a Trapped Ideal Fermi Gas*, Phys. Rev. Lett. **93**, 120401 (2004).
 - [69] M. Rigol, A. Muramatsu, G. G. Batrouni, and R. T. Scalettar, *Local Quantum Criticality in Confined Fermions on Optical Lattices*, Phys. Rev. Lett. **91**, 130403 (2003).
 - [70] X.-J. Liu, P. D. Drummond, and H. Hu, *Signature of Mott-Insulator Transition with Ultracold Fermions in a One-Dimensional Optical Lattice*, Phys. Rev. Lett. **94**, 136406 (2005).
 - [71] H. Heiselberg, *Phases of bosons or fermions in confined optical lattices*, Phys. Rev. A **74**, 033608 (2006).
 - [72] H. Ott, E. de Mirandes, F. Ferlaino, G. Roati, V. Turck, G. Modugno, and M. Inguscio, *Radio Frequency Selective Addressing of Localized Atoms in a Periodic Potential*, Phys. Rev. Lett. **93**, 120407 (2004).

BIBLIOGRAPHY

- [73] M. Rigol and A. Muramatsu, *Quantum Monte Carlo study of confined fermions in one-dimensional optical lattices*, Phys. Rev. A **69**, 053612 (2004).
- [74] V. Ruuska and P. Törmä, *Quantum transport of non-interacting Fermi gas in an optical lattice combined with harmonic trapping*, New Journal of Physics **6**, 59 (2004).
- [75] M. Köhl, *Thermometry of fermionic atoms in an optical lattice*, Phys. Rev. A **73**, 031601 (2006).
- [76] P. B. Blakie, A. Bezett, and P. Buonsante, *Degenerate Fermi gas in a combined harmonic-lattice potential*, Phys. Rev. A **75**, 063609 (2007).
- [77] P. B. Blakie and A. Bezett, *Adiabatic cooling of fermions in an optical lattice*, Phys. Rev. A **71**, 033616 (2005).
- [78] A. Kastberg, W. D. Phillips, S. L. Rolston, R. J. C. Spreeuw, and P. S. Jessen, *Adiabatic Cooling of Cesium to 700 nK in an Optical Lattice*, Phys. Rev. Lett. **74**, 1542 (1995).
- [79] M. Greiner, I. Bloch, O. Mandel, T. W. Hänsch, and T. Esslinger, *Exploring Phase Coherence in a 2D Lattice of Bose-Einstein Condensates*, Phys. Rev. Lett. **87**, 160405 (2001).
- [80] W. Zwerger, *Mott-Hubbard transition of cold atoms in optical lattices*, J. Opt. B **5**, S9 (2003).
- [81] F. Gerbier, A. Widera, S. Fölling, O. Mandel, T. Gericke, and I. Bloch, *Phase Coherence of an Atomic Mott Insulator*, Phys. Rev. Lett. **95**, 050404 (2005).
- [82] J. Hubbard, *Electron Correlations in Narrow Energy Bands*, Proc. R. Soc. A **276**, 238 (1963).
- [83] W. Hofstetter, J. I. Cirac, P. Zoller, E. Demler, and M. D. Lukin, *High-Temperature Superfluidity of Fermionic Atoms in Optical Lattices*, Phys. Rev. Lett. **89**, 220407 (2002).
- [84] M. Greiner, O. Mandel, T. Esslinger, T. W. Hansch, and I. Bloch, *Quantum phase transition from a superfluid to a Mott insulator in a gas of ultracold atoms*, Nature **415**, 39 (2002).
- [85] D. Jaksch and P. Zoller, *The cold atom Hubbard toolbox* (2005).
- [86] R. B. Diener and T.-L. Ho, *Fermions in Optical Lattices Swept across Feshbach Resonances*, Phys. Rev. Lett. **96**, 010402 (2006).
- [87] *Condensed Matter Physics With Light And Atoms: Strongly Correlated Cold Fermions in Optical Lattices.*, Varenna Summer School Enrico Fermi (2007).

-
- [88] J. J. Sakurai, *Modern Quantum Mechanics Revised Edition*, Addison-Wesley Publishing Company (1994).
 - [89] B. Gao, *Quantum-defect theory of atomic collisions and molecular vibration spectra*, Phys. Rev. A **58**, 4222 (1998).
 - [90] R. B. Diener and T.-L. Ho, *The Condition for Universality at Resonance and Direct Measurement of Pair Wavefunctions Using rf Spectroscopy*, arXiv:cond-mat/0405174v2 (2004).
 - [91] H. Wang, A. N. Nikolov, J. R. Ensher, P. L. Gould, E. E. Eyler, W. C. Stwalley, J. P. Burke, J. L. Bohn, C. H. Greene, E. Tiesinga, C. J. Williams, and P. S. Julienne, *Ground-state scattering lengths for potassium isotopes determined by double-resonance photoassociative spectroscopy of ultracold ^{39}K* , Phys. Rev. A **62**, 052704 (2000).
 - [92] *Collisional dynamics of ultra-cold atomic gases* (1998).
 - [93] *Bose-Einstein condensates in atomic gases: simple theoretical results* (2000), in 'Coherent atomic matter waves', Lecture Notes of Les Houches Summer School, p.1-136, edited by R. Kaiser, C. Westbrook, and F. David, EDP Sciences and Springer-Verlag (2001).
 - [94] S. Inouye, M. R. Andrews, J. Stenger, H.-J. Miesner, D. M. Stamper-Kurn, and W. Ketterle, *Observation of Feshbach resonances in a Bose-Einstein condensate*, Nature **392**, 151 (1998).
 - [95] M. Bartenstein, A. Altmeyer, S. Riedl, S. Jochim, C. Chin, J. H. Denschlag, and R. Grimm, *Crossover from a Molecular Bose-Einstein Condensate to a Degenerate Fermi Gas*, Phys. Rev. Lett. **92**, 120401 (2004).
 - [96] T. Bourdel, L. Khaykovich, J. Cubizolles, J. Zhang, F. Chevy, M. Teichmann, L. Tarruell, S. J. J. M. F. Kokkelmans, and C. Salomon, *Experimental Study of the BEC-BCS Crossover Region in Lithium 6*, Phys. Rev. Lett. **93**, 050401 (2004).
 - [97] M. M. Parish, B. Mihaila, B. D. Simons, and P. B. Littlewood, *Fermion-Mediated BCS-BEC Crossover in Ultracold ^{40}K Gases*, Phys. Rev. Lett. **94**, 240402 (2005).
 - [98] G. M. Falco and H. T. C. Stoof, *Dressed molecules in resonantly interacting ultracold atomic Fermi gases*, Phys. Rev. A **75**, 023612 (2007).
 - [99] C. Chin, *A simple model of Feshbach molecules*, arXiv:cond-mat/0506313v2 5 (2005).
 - [100] A. J. Moerdijk, B. J. Verhaar, and A. Axelsson, *Resonances in ultracold collisions of ^6Li , ^7Li , and ^{23}Na* , Phys. Rev. A **51**, 4852 (1995).
 - [101] J. Cubizolles, *Fermions et bosons dégénérés au voisinage d'une résonance de Feshbach : Production de molécules et solitons d'ondes de matière*, Ph.D. thesis, LKB, ENS (2004).

BIBLIOGRAPHY

- [102] M. H. Szymanska, K. Goral, T. Köhler, and K. Burnett, *Conventional character of the BCS-BEC crossover in ultracold gases of ^{40}K* , Phys. Rev. A **72**, 013610 (2005).
- [103] T. Köhler, K. Goral, and P. S. Julienne, *Production of cold molecules via magnetically tunable Feshbach resonances* (2006).
- [104] G. F. Gribakin and V. V. Flambaum, *Calculation of the scattering length in atomic collisions using the semiclassical approximation*, Phys. Rev. A **48**, 546 (1993).
- [105] B. Gao, *Binding energy and scattering length for diatomic systems*, J. Phys. B **37**, 4273 (2004).
- [106] D. S. Petrov, C. Salomon, and G. V. Shlyapnikov, *Weakly Bound Dimers of Fermionic Atoms*, Phys. Rev. Lett. **93**, 090404 (2004).
- [107] S. Jochim, M. Bartenstein, A. Altmeyer, G. Hendl, S. Riedl, C. Chin, J. Hecker Denschlag, and R. Grimm, *Bose-Einstein Condensation of Molecules*, Science **302**, 2101 (2003).
- [108] M. W. Zwierlein, C. A. Stan, C. H. Schunck, S. M. F. Raupach, S. Gupta, Z. Hadzibabic, and W. Ketterle, *Observation of Bose-Einstein Condensation of Molecules*, Phys. Rev. Lett. **91**, 250401 (2003).
- [109] G. Bruun, Y. Castin, R. Dum, and K. Burnett, *BCS theory for trapped ultracold fermions*, Eur. Phys. J. D **7**, 433 (1999).
- [110] M. Holland, S. J. J. M. F. Kokkelmans, M. L. Chiofalo, and R. Walser, *Resonance Superfluidity in a Quantum Degenerate Fermi Gas*, Phys. Rev. Lett. **87**, 120406 (2001).
- [111] T.-L. Ho, *Universal Thermodynamics of Degenerate Quantum Gases in the Unitarity Limit*, Phys. Rev. Lett. **92**, 090402 (2004).
- [112] C. A. Regal, M. Greiner, and D. S. Jin, *Lifetime of Molecule-Atom Mixtures near a Feshbach Resonance in K* , Phys. Rev. Lett. **92**, 083201 (2004).
- [113] C. A. Regal and D. S. Jin, *Measurement of Positive and Negative Scattering Lengths in a Fermi Gas of Atoms*, Phys. Rev. Lett. **90**, 230404 (2003).
- [114] C. A. Regal, C. Ticknor, J. L. Bohn, and D. S. Jin, *Tuning p -Wave Interactions in an Ultracold Fermi Gas of Atoms*, Phys. Rev. Lett. **90**, 053201 (2003).
- [115] J. L. Bohn, J. P. Burke, C. H. Greene, H. Wang, P. L. Gould, and W. C. Stwalley, *Collisional properties of ultracold potassium: Consequences for degenerate Bose and Fermi gases*, Phys. Rev. A **59**, 3660 (1999).
- [116] C. Ticknor, C. A. Regal, D. S. Jin, and J. L. Bohn, *Multiplet structure of Feshbach resonances in nonzero partial waves*, Phys. Rev. A **69**, 042712 (2004).

-
- [117] D. Petrov, D. Gangardt, and G. Shlyapnikov, *Low-dimensional trapped gases*, J. Phys. IV France **116**, 5 (2004).
 - [118] M. Olshanii, *Atomic Scattering in the Presence of an External Confinement and a Gas of Impenetrable Bosons*, Phys. Rev. Lett. **81**, 938 (1998).
 - [119] T. Bergeman, M. G. Moore, and M. Olshanii, *Atom-Atom Scattering under Cylindrical Harmonic Confinement: Numerical and Analytic Studies of the Confinement Induced Resonance*, Phys. Rev. Lett. **91**, 163201 (2003).
 - [120] T. Busch, B.-G. Englert, K. Rzazewski, and M. Wilkens, *Two Cold Atoms in a Harmonic Trap*, Found. Phys. **28**, 549 (1998).
 - [121] M. Wouters and G. Orso, *Two-body problem in periodic potentials*, Phys. Rev. A **73**, 012707 (2006).
 - [122] E. Tiesinga, C. J. Williams, F. H. Mies, and P. S. Julienne, *Interacting atoms under strong quantum confinement*, Phys. Rev. A **61**, 063416 (2000).
 - [123] D. Blume and C. H. Greene, *Fermi pseudopotential approximation: Two particles under external confinement*, Phys. Rev. A **65**, 043613 (2002).
 - [124] E. L. Bolda, E. Tiesinga, and P. S. Julienne, *Effective-scattering-length model of ultracold atomic collisions and Feshbach resonances in tight harmonic traps*, Phys. Rev. A **66**, 013403 (2002).
 - [125] T. Stöferle, *Exploring Atomic Quantum Gases in Optical Lattices*, Ph.D. thesis, ETH Zurich (2005).
 - [126] M. Greiner, I. Bloch, T. W. Hänsch, and T. Esslinger, *Magnetic transport of trapped cold atoms over a large distance*, Phys. Rev. A **63**, 031401 (2001).
 - [127] G. Modugno, C. Benko, P. Hannaford, G. Roati, and M. Inguscio, *Sub-Doppler laser cooling of fermionic ^{40}K atoms*, Phys. Rev. A **60**, R3373 (1999).
 - [128] G. C. Bjorklund, M. D. Levenson, W. Lenth, and C. Ortiz, *Frequency modulation (FM) spectroscopy*, Appl. Phys. B **32**, 145 (1983).
 - [129] B. DeMarco, H. Rohner, and D. S. Jin, *An enriched ^{40}K source for fermionic atom studies*, Rev. Sci. Instrum. **70**, 1967 (1999).
 - [130] E. L. Raab, M. Prentiss, A. Cable, S. Chu, and D. E. Pritchard, *Trapping of Neutral Sodium Atoms with Radiation Pressure*, Phys. Rev. Lett. **59**, 2631 (1987).
 - [131] J. Dalibard and C. Cohen-Tannoudji, *Laser cooling below the Doppler limit by polarization gradients: simple theoretical models*, J. Opt. Soc. Am. B **6**, 2023 (1989).
 - [132] W. W. Ketterle, D. Durfee, and D. Stamper-Kurn, *Making, probing and understanding Bose-Einstein condensates* (1999).

BIBLIOGRAPHY

- [133] G. Roati, F. Riboli, G. Modugno, and M. Inguscio, *Fermi-Bose Quantum Degenerate ^{40}K - ^{87}Rb Mixture with Attractive Interaction*, Phys. Rev. Lett. **89**, 150403 (2002).
- [134] T. Esslinger, I. Bloch, and T. W. Hänsch, *Bose-Einstein condensation in a quadrupole-Ioffe-configuration trap*, Phys. Rev. A **58**, R2664 (1998).
- [135] C. V. Sukumar and D. M. Brink, *Spin-flip transitions in a magnetic trap*, Phys. Rev. A **56**, 2451 (1997).
- [136] K. M. O'Hara, M. E. Gehm, S. R. Granade, and J. E. Thomas, *Scaling laws for evaporative cooling in time-dependent optical traps*, Phys. Rev. A **64**, 051403 (2001).
- [137] M. Ben Dahan, E. Peik, J. Reichel, Y. Castin, and C. Salomon, *Bloch Oscillations of Atoms in an Optical Potential*, Phys. Rev. Lett. **76**, 4508 (1996).
- [138] F. Werner, O. Parcollet, A. Georges, and S. R. Hassan, *Interaction-Induced Adiabatic Cooling and Antiferromagnetism of Cold Fermions in Optical Lattices*, Phys. Rev. Lett. **95**, 056401 (2005).
- [139] P. O. Fedichev, M. W. Reynolds, and G. V. Shlyapnikov, *Three-Body Recombination of Ultracold Atoms to a Weakly Bound s Level*, Phys. Rev. Lett. **77**, 2921 (1996).
- [140] J. H. Denschlag, J. E. Simsarian, H. Häffner, C. McKenzie, A. Browaeys, D. Cho, K. Helmerson, S. L. Rolston, and W. D. Phillips, *A Bose-Einstein condensate in an optical lattice*, J. Phys. B **35**, 3095 (2002).
- [141] J. Kinast, S. L. Hemmer, M. E. Gehm, A. Turlapov, and J. E. Thomas, *Evidence for Superfluidity in a Resonantly Interacting Fermi Gas*, Phys. Rev. Lett. **92**, 150402 (2004).
- [142] C. Lee, *Bose-Einstein Condensation of Particle-Hole Pairs in Ultracold Fermionic Atoms Trapped within Optical Lattices*, Phys. Rev. Lett. **93**, 120406 (2004).
- [143] L. Santos, M. A. Baranov, J. I. Cirac, H.-U. Everts, H. Fehrmann, and M. Lewenstein, *Atomic Quantum Gases in Kagomé Lattices*, Phys. Rev. Lett. **93**, 030601 (2004).
- [144] M. T. DePue, C. McCormick, S. L. Winoto, S. Oliver, and D. S. Weiss, *Unity Occupation of Sites in a 3D Optical Lattice*, Phys. Rev. Lett. **82**, 2262 (1999).
- [145] T. Stöferle, H. Moritz, C. Schori, M. Köhl, and T. Esslinger, *Transition from a Strongly Interacting 1D Superfluid to a Mott Insulator*, Phys. Rev. Lett. **92**, 130403 (2004).
- [146] G. Modugno, F. Ferlaino, R. Heidemann, G. Roati, and M. Inguscio, *Production of a Fermi gas of atoms in an optical lattice*, Phys. Rev. A **68**, 011601 (2003).

-
- [147] L. Viverit, C. Menotti, T. Calarco, and A. Smerzi, *Efficient and Robust Initialization of a Qubit Register with Fermionic Atoms*, Phys. Rev. Lett. **93**, 110401 (2004).
 - [148] H. G. Katzgraber, A. Esposito, and M. Troyer, *Ramping fermions in optical lattices across a Feshbach resonance*, Phys. Rev. A **74**, 043602 (2006).
 - [149] P. O. Fedichev, M. J. Bijlsma, and P. Zoller, *Extended Molecules and Geometric Scattering Resonances in Optical Lattices*, Phys. Rev. Lett. **92**, 080401 (2004).
 - [150] M. Troyer and U.-J. Wiese, *Computational Complexity and Fundamental Limitations to Fermionic Quantum Monte Carlo Simulations*, Phys. Rev. Lett. **94**, 170201 (2005).
 - [151] A. F. Ho, *Fermions in optical lattices near a Feshbach resonance: From band insulator to Mott insulator*, Phys. Rev. A **73**, 061601 (2006).
 - [152] H. Moritz, T. Stöferle, K. Günter, M. Köhl, and T. Esslinger, *Confinement Induced Molecules in a 1D Fermi Gas*, Phys. Rev. Lett. **94**, 210401 (2005).
 - [153] E. Wigner, *Über die Streuung von Neutronen an Protonen*, Zeitschrift für Physik A Hadrons and Nuclei **83**, 253 (1933).
 - [154] E. A. Donley, N. R. Claussen, S. T. Thompson, and C. E. Wieman, *Atom-molecule coherence in a Bose-Einstein condensate*, Nature **417**, 529 (2002).
 - [155] C. Chin, A. J. Kerman, V. Vuletic, and S. Chu, *Sensitive Detection of Cold Cesium Molecules Formed on Feshbach Resonances*, Phys. Rev. Lett. **90**, 033201 (2003).
 - [156] J. Herbig, T. Kraemer, M. Mark, T. Weber, C. Chin, H.-C. Nagerl, and R. Grimm, *Preparation of a Pure Molecular Quantum Gas*, Science **301**, 1510 (2003).
 - [157] K. E. Strecker, G. B. Partridge, and R. G. Hulet, *Conversion of an Atomic Fermi Gas to a Long-Lived Molecular Bose Gas*, Phys. Rev. Lett. **91**, 080406 (2003).
 - [158] K. Xu, T. Mukaiyama, J. R. Abo-Shaeer, J. K. Chin, D. E. Miller, and W. Ketterle, *Formation of Quantum-Degenerate Sodium Molecules*, Phys. Rev. Lett. **91**, 210402 (2003).
 - [159] S. Jochim, M. Bartenstein, A. Altmeyer, G. Hendl, C. Chin, J. H. Denschlag, and R. Grimm, *Pure Gas of Optically Trapped Molecules Created from Fermionic Atoms*, Phys. Rev. Lett. **91**, 240402 (2003).
 - [160] S. Dürr, T. Volz, A. Marte, and G. Rempe, *Observation of Molecules Produced from a Bose-Einstein Condensate*, Phys. Rev. Lett. **92**, 020406 (2004).
 - [161] M. Greiner, C. A. Regal, J. T. Stewart, and D. S. Jin, *Probing Pair-Correlated Fermionic Atoms through Correlations in Atom Shot Noise*, Phys. Rev. Lett. **94**, 110401 (2005).

- [162] D. S. Petrov and G. V. Shlyapnikov, *Interatomic collisions in a tightly confined Bose gas*, Phys. Rev. A **64**, 012706 (2001).
- [163] C. Mora, R. Egger, A. O. Gogolin, and A. Komnik, *Atom-Dimer Scattering for Confined Ultracold Fermion Gases*, Phys. Rev. Lett. **93**, 170403 (2004).
- [164] C. Kim, A. Y. Matsuura, Z.-X. Shen, N. Motoyama, H. Eisaki, S. Uchida, T. Tohyama, and S. Maekawa, *Observation of Spin-Charge Separation in One-Dimensional SrCuO₂*, Phys. Rev. Lett. **77**, 4054 (1996).
- [165] B. L. Tolra, K. M. O'Hara, J. H. Huckans, W. D. Phillips, S. L. Rolston, and J. V. Porto, *Observation of Reduced Three-Body Recombination in a Correlated 1D Degenerate Bose Gas*, Phys. Rev. Lett. **92**, 190401 (2004).
- [166] B. Paredes, A. Widera, V. Murg, O. Mandel, S. Folling, I. Cirac, G. V. Shlyapnikov, T. W. Hansch, and I. Bloch, *Tonks-Girardeau gas of ultracold atoms in an optical lattice*, Nature **429**, 277 (2004).
- [167] T. Kinoshita, T. Wenger, and D. S. Weiss, *Observation of a One-Dimensional Tonks-Girardeau Gas*, Science **305**, 1125 (2004).
- [168] I. V. Tokatly, *Dilute Fermi Gas in Quasi-One-Dimensional Traps: From Weakly Interacting Fermions via Hard Core Bosons to a Weakly Interacting Bose Gas*, Phys. Rev. Lett. **93**, 090405 (2004).
- [169] H. Moritz, T. Stöferle, M. Köhl, and T. Esslinger, *Exciting Collective Oscillations in a Trapped 1D Gas*, Phys. Rev. Lett. **91**, 250402 (2003).
- [170] A. Derevianko, W. R. Johnson, M. S. Safronova, and J. F. Babb, *High-Precision Calculations of Dispersion Coefficients, Static Dipole Polarizabilities, and Atom-Wall Interaction Constants for Alkali-Metal Atoms*, Phys. Rev. Lett. **82**, 3589 (1999).
- [171] D. B. M. Dickerscheid and H. T. C. Stoof, *Feshbach molecules in a one-dimensional Fermi gas*, Phys. Rev. A **72**, 053625 (2005).
- [172] G. E. Astrakharchik, D. Blume, S. Giorgini, and L. P. Pitaevskii, *Interacting Fermions in Highly Elongated Harmonic Traps*, Phys. Rev. Lett. **93**, 050402 (2004).
- [173] T. Giamarchi, *Quantum Physics in One Dimension*, Oxford University, New York, 2004 (2004).
- [174] T. Stöferle, H. Moritz, K. Günter, M. Köhl, and T. Esslinger, *Molecules of Fermionic Atoms in an Optical Lattice*, Phys. Rev. Lett. **96**, 030401 (2006).
- [175] D. B. M. Dickerscheid, U. A. Khawaja, D. van Oosten, and H. T. C. Stoof, *Feshbach resonances in an optical lattice*, Phys. Rev. A **71**, 043604 (2005).
- [176] L. D. Carr and M. J. Holland, *Quantum phase transitions in the Fermi-Bose Hubbard model*, Phys. Rev. A **72**, 031604 (2005).

-
- [177] F. Zhou, *Mott states under the influence of fermion-boson conversion*, Phys. Rev. B **72**, 220501 (2005).
 - [178] L.-M. Duan, *Effective Hamiltonian for Fermions in an Optical Lattice across a Feshbach Resonance*, Phys. Rev. Lett. **95**, 243202 (2005).
 - [179] M. Köhl, K. Günter, T. Stöferle, H. Moritz, and T. Esslinger, *Strongly interacting atoms and molecules in a 3D optical lattice*, Journal of Physics B: Atomic, Molecular and Optical Physics **39**, S47 (2006).
 - [180] G. Pupillo, C. J. Williams, and N. V. Prokof'ev, *Effects of finite temperature on the Mott-insulator state*, Phys. Rev. A **73**, 013408 (2006).
 - [181] E. Hodby, S. T. Thompson, C. A. Regal, M. Greiner, A. C. Wilson, D. S. Jin, E. A. Cornell, and C. E. Wieman, *Production Efficiency of Ultracold Feshbach Molecules in Bosonic and Fermionic Systems*, Phys. Rev. Lett. **94**, 120402 (2005).
 - [182] T. Rom, T. Best, O. Mandel, A. Widera, M. Greiner, T. W. Hansch, and I. Bloch, *State Selective Production of Molecules in Optical Lattices*, Phys. Rev. Lett. **93**, 073002 (2004).
 - [183] C. Ryu, X. Du, E. Yesilada, A. M. Dudarev, S. Wan, Q. Niu, and D. J. Heinzen, *Raman-induced oscillation between an atomic and a molecular quantum gas*, arXiv:cond-mat/0508201v1 (2005).
 - [184] D. M. Harber, H. J. Lewandowski, J. M. McGuirk, and E. A. Cornell, *Effect of cold collisions on spin coherence and resonance shifts in a magnetically trapped ultracold gas*, Phys. Rev. A **66**, 053616 (2002).
 - [185] S. Gupta, Z. Hadzibabic, M. W. Zwierlein, C. A. Stan, K. Dieckmann, C. H. Schunck, E. G. M. van Kempen, B. J. Verhaar, and W. Ketterle, *Radio-Frequency Spectroscopy of Ultracold Fermions*, Science **300**, 1723 (2003).
 - [186] P. Rabl, A. J. Daley, P. O. Fedichev, J. I. Cirac, and P. Zoller, *Defect-Suppressed Atomic Crystals in an Optical Lattice*, Phys. Rev. Lett. **91**, 110403 (2003).
 - [187] K. Günter, T. Stöferle, H. Moritz, M. Köhl, and T. Esslinger, *p-Wave Interactions in Low-Dimensional Fermionic Gases*, Phys. Rev. Lett. **95**, 230401 (2005).
 - [188] B. DeMarco, J. L. Bohn, J. P. Burke, M. Holland, and D. S. Jin, *Measurement of p-Wave Threshold Law Using Evaporatively Cooled Fermionic Atoms*, Phys. Rev. Lett. **82**, 4208 (1999).
 - [189] J. Zhang, E. G. M. van Kempen, T. Bourdel, L. Khaykovich, J. Cubizolles, F. Chevy, M. Teichmann, L. Tarruell, S. J. J. M. F. Kokkelmans, and C. Salomon, *p-wave Feshbach resonances of ultracold ^6Li* , Phys. Rev. A **70**, 030702 (2004).
 - [190] C. H. Schunck, M. W. Zwierlein, C. A. Stan, S. M. F. Raupach, W. Ketterle, A. Simoni, E. Tiesinga, C. J. Williams, and P. S. Julienne, *Feshbach resonances in fermionic ^6Li* , Phys. Rev. A **71**, 045601 (2005).

BIBLIOGRAPHY

- [191] J. I. Kim, J. Schmiedmayer, and P. Schmelcher, *Quantum scattering in quasi-one-dimensional cylindrical confinement*, Phys. Rev. A **72**, 042711 (2005).
- [192] A. C. Warren, D. A. Antoniadis, and H. I. Smith, *Quasi One-Dimensional Conduction in Multiple, Parallel Inversion Lines*, Phys. Rev. Lett. **56**, 1858 (1986).
- [193] A. B. Fowler, F. F. Fang, W. E. Howard, and P. J. Stiles, *Magneto-Oscillatory Conductance in Silicon Surfaces*, Phys. Rev. Lett. **16**, 901 (1966).
- [194] D. S. Petrov, M. Holzmann, and G. V. Shlyapnikov, *Bose-Einstein Condensation in Quasi-2D Trapped Gases*, Phys. Rev. Lett. **84**, 2551 (2000).
- [195] M. Wouters, J. Tempere, and J. T. Devreese, *Feshbach resonances in a quasi-two-dimensional atomic gas*, Phys. Rev. A **68**, 053603 (2003).
- [196] B. E. Granger and D. Blume, *Tuning the Interactions of Spin-Polarized Fermions Using Quasi-One-Dimensional Confinement*, Phys. Rev. Lett. **92**, 133202 (2004).
- [197] T.-L. Ho and R. B. Diener, *Fermion Superfluids of Nonzero Orbital Angular Momentum near Resonance*, Phys. Rev. Lett. **94**, 090402 (2005).
- [198] K. Günter, T. Stöferle, H. Moritz, M. Köhl, and T. Esslinger, *Bose-Fermi Mixtures in a Three-Dimensional Optical Lattice*, Phys. Rev. Lett. **96**, 180402 (2006).
- [199] E. H. Graf, D. M. Lee, and J. D. Reppy, *Phase Separation and the Superfluid Transition in Liquid He^3 - He^4 Mixtures*, Phys. Rev. Lett. **19**, 417 (1967).
- [200] S. Ospelkaus, C. Ospelkaus, O. Wille, M. Succo, P. Ernst, K. Sengstock, and K. Bongs, *Localization of Bosonic Atoms by Fermionic Impurities in a Three-Dimensional Optical Lattice*, Phys. Rev. Lett. **96**, 180403 (2006).
- [201] A. B. Kuklov and B. V. Svistunov, *Counterflow Superfluidity of Two-Species Ultracold Atoms in a Commensurate Optical Lattice*, Phys. Rev. Lett. **90**, 100401 (2003).
- [202] M. Cramer, J. Eisert, and F. Illuminati, *Inhomogeneous Atomic Bose-Fermi Mixtures in Cubic Lattices*, Phys. Rev. Lett. **93**, 190405 (2004).
- [203] L. Pollet, M. Troyer, K. Van Houcke, and S. M. A. Rombouts, *Phase Diagram of Bose-Fermi Mixtures in One-Dimensional Optical Lattices*, Phys. Rev. Lett. **96**, 190402 (2006).
- [204] L. Mathey, D.-W. Wang, W. Hofstetter, M. D. Lukin, and E. Demler, *Luttinger Liquid of Polarons in One-Dimensional Boson-Fermion Mixtures*, Phys. Rev. Lett. **93**, 120404 (2004).
- [205] A. Albus, F. Illuminati, and J. Eisert, *Mixtures of bosonic and fermionic atoms in optical lattices*, Phys. Rev. A **68**, 023606 (2003).

-
- [206] F. Ferlaino, C. D’Errico, G. Roati, M. Zaccanti, M. Inguscio, G. Modugno, and A. Simoni, *Erratum: Feshbach spectroscopy of a K-Rb atomic mixture [Phys. Rev. A **73**, 040702 (2006)]*, Phys. Rev. A **74**, 039903 (2006).
 - [207] M. Theis, G. Thalhammer, K. Winkler, M. Hellwig, G. Ruff, R. Grimm, and J. H. Denschlag, *Tuning the Scattering Length with an Optically Induced Feshbach Resonance*, Phys. Rev. Lett. **93**, 123001 (2004).
 - [208] F. Gerbier, S. Fölling, A. Widera, and I. Bloch, *Visibility of a Bose-condensed gas released from an optical lattice at finite temperatures*, arXiv:cond-mat/0701420v1 (2007).
 - [209] F. Gerbier, A. Widera, S. Fölling, O. Mandel, T. Gericke, and I. Bloch, *Interference pattern and visibility of a Mott insulator*, Phys. Rev. A **72**, 053606 (2005).
 - [210] C. Kollath, U. Schollwock, J. von Delft, and W. Zwerger, *Spatial correlations of trapped one-dimensional bosons in an optical lattice*, Phys. Rev. A **69**, 031601 (2004).
 - [211] K. Xu, Y. Liu, D. E. Miller, J. K. Chin, W. Setiawan, and W. Ketterle, *Observation of Strong Quantum Depletion in a Gaseous Bose-Einstein Condensate*, Phys. Rev. Lett. **96**, 180405 (2006).
 - [212] L. Pollet, C. Kollath, U. Schollwoeck, and M. Troyer, *Mixture of bosonic and spin-polarized fermionic atoms in an optical lattice*, arXiv:cond-mat/0609604v1 (2007).
 - [213] C. Presilla and R. Onofrio, *Cooling Dynamics of Ultracold Two-Species Fermi-Bose Mixtures*, Phys. Rev. Lett. **90**, 030404 (2003).
 - [214] M. Cramer, S. Ospelkaus, C. Ospelkaus, K. Bongs, K. Sengstock, and J. Eisert, *Do mixtures of bosonic and fermionic atoms adiabatically heat up in optical lattices?*, arXiv:0707.3633 (2007).
 - [215] J. Söding, D. Guéry-Odelin, P. Desbiolles, F. Chevy, H. Inamori, and J. Dalibard, *Three-body decay of a rubidium Bose-Einstein condensate*, Appl. Phys. B **69**, 257 (1999).
 - [216] E. A. Burt, R. W. Ghrist, C. J. Myatt, M. J. Holland, E. A. Cornell, and C. E. Wieman, *Coherence, Correlations, and Collisions: What One Learns about Bose-Einstein Condensates from Their Decay*, Phys. Rev. Lett. **79**, 337 (1997).
 - [217] J. Goldwin, S. Inouye, M. L. Olsen, B. Newman, B. D. DePaola, and D. S. Jin, *Measurement of the interaction strength in a Bose-Fermi mixture with ^{87}Rb and ^{40}K* , Phys. Rev. A **70**, 021601 (2004).
 - [218] S. Inouye, J. Goldwin, M. L. Olsen, C. Ticknor, J. L. Bohn, and D. S. Jin, *Observation of Heteronuclear Feshbach Resonances in a Mixture of Bosons and Fermions*, Phys. Rev. Lett. **93**, 183201 (2004).

BIBLIOGRAPHY

- [219] F. Ferlaino, C. D’Errico, G. Roati, M. Zaccanti, M. Inguscio, G. Modugno, and A. Simoni, *Feshbach spectroscopy of a K-Rb atomic mixture*, Phys. Rev. A **73**, 040702 (2006).
- [220] M. Iskin and C. A. R. Sá de Melo, *Evolution from BCS to BEC Superfluidity in p-Wave Fermi Gases*, Phys. Rev. Lett. **96**, 040402 (2006).
- [221] R. Staudt, M. Dzierzawa, and A. Muramatsu, *Phase diagram of the three-dimensional Hubbard model at half filling*, The European Physical Journal B - Condensed Matter and Complex Systems **17**, 411 (2000).
- [222] A. Griessner, A. J. Daley, S. R. Clark, D. Jaksch, and P. Zoller, *Dark-State Cooling of Atoms by Superfluid Immersion*, Phys. Rev. Lett. **97**, 220403 (2006).
- [223] N. Strohmaier, Y. Takasu, K. Günter, R. Jördens, M. Köhl, H. Moritz, and T. Esslinger, *Interaction-controlled transport of an ultracold Fermi gas*, arXiv:0707.3140 (2007).
- [224] R. R. dos Santos, *Spin gap and superconductivity in the three-dimensional attractive Hubbard model*, Phys. Rev. B **50**, 635 (1994).
- [225] M. Keller, W. Metzner, and U. Schollwöck, *Dynamical Mean-Field Theory for Pairing and Spin Gap in the Attractive Hubbard Model*, Phys. Rev. Lett. **86**, 4612 (2001).
- [226] C. Kollath, A. Iucci, I. P. McCulloch, and T. Giamarchi, *Modulation spectroscopy with ultracold fermions in an optical lattice*, Phys. Rev. A **74**, 041604 (2006).
- [227] A. Micheli, G. K. Brennen, and P. Zoller, *A toolbox for lattice-spin models with polar molecules*, Nat Phys **2**, 341 (2006).
- [228] C. Ospelkaus, S. Ospelkaus, L. Humbert, P. Ernst, K. Sengstock, and K. Bongs, *Ultracold Heteronuclear Molecules in a 3D Optical Lattice*, Phys. Rev. Lett. **97**, 120402 (2006).
- [229] W. C. Stwalley, *Efficient conversion of ultracold Feshbach-resonance-related polar molecules into ultracold ground state ($X^1\Sigma^+ v=0, J=0$) molecules*, The European Physical Journal D - Atomic, Molecular, Optical and Plasma Physics **31**, 221 (2004).
- [230] R. Côté, A. Dalgarno, H. Wang, and W. C. Stwalley, *Potassium scattering lengths and prospects for Bose-Einstein condensation and sympathetic cooling*, Phys. Rev. A **57**, R4118 (1998).
- [231] D. R. Lide (ed.), *Handbook of Chemistry and Physics*, CRC Press, 87th edn. (2006-2007).
- [232] E. Arimondo, M. Inguscio, and P. Violino, *Experimental determinations of the hyperfine structure in the alkali atoms* (1977).

-
- [233] R. S. Williamson III, *Magneto-optical trapping of potassium isotopes*, Ph.D. thesis, University of Wisconsin-Madison (1997).
- [234] J. Goldwin, S. B. Papp, B. DeMarco, and D. S. Jin, *Two-species magneto-optical trap with ^{40}K and ^{87}Rb* , Phys. Rev. A **65**, 021402 (2002).
- [235] A. Derevianko, J. F. Babb, and A. Dalgarno, *High-precision calculations of van der Waals coefficients for heteronuclear alkali-metal dimers*, Phys. Rev. A **63**, 052704 (2001).
- [236] K. J. Günter, *Design and implementation of a Zeeman slower for ^{87}Rb* (2004).
- [237] D. A. Steck, *Rubidium 87 D Line Data* (2003).
- [238] T. Lahaye, J. M. Vogels, K. J. Günter, Z. Wang, J. Dalibard, and D. Guéry-Odelin, *Realization of a Magnetically Guided Atomic Beam in the Collisional Regime*, Phys. Rev. Lett. **93**, 093003 (2004).

Acknowledgements

My PhD studies in the Quantum Optics Group at ETH Zurich have been a very valuable and pleasant period. Several persons have contributed in different respects to the completion of this work. I would like to take the opportunity here to thank them:

Tilman Esslinger gave me the possibility to work in his group under excellent circumstances. With his cheerfulness and enthusiasm he created a relaxed and yet professional working atmosphere. I appreciated his physical intuition and his smart ideas in many fruitful discussions as much as his ability to manipulate the spin of table tennis balls, which he proved in our daily after-lunch matches.

Michael Köhl supervised our research projects with an exceptional commitment and expertise from the beginning on. I enjoyed this formidable collaboration, from which I could learn a lot.

Henning Moritz and Thilo Stöferle were my predecessors and fellow PhD students who introduced me into the “lattice experiment”. We had a great time together, sharing many working hours in the lab. Henning’s intuitive way of thinking about physical problems and Thilo’s excellent technical skills were important ingredients in the success of our experiments.

Niels Strohmaier and Robert Jördens are the new PhD students in the lattice team. They have quickly managed to contribute not only to the experiment but also to a friendly atmosphere in our office. They are now “taking the wheel”, and I have no doubt that they will do a fantastic job.

Yosuke Takasu and Christian Schori worked as postdocs on the experiment during the first and the last year of my PhD, respectively. I appreciated their experience and their readiness to answer any question I had.

Stephan Ritter and Toni Öttl were already working at the “cavity experiment” when I joined the group. They have been very kind and helpful colleagues. In the meantime Tobias Donner, Thomas Bourdel and Ferdinand Brennecke have joined their experiment, and later Bruno Zimmermann and Torben Müller arrived to build up the “Lithium experiment”. Collaborating with all of them was a lot of fun and the numerous discussions with them were enriching.

Alexander Frank facilitated solving many issues in our setup with his unhesitant electronic support, building supplies and control units, rf devices and sound modules. I would also like to thank Veronica Bürgisser for the handling of administrative and organisational tasks and for many nice conversations.

I am indebted to all the theorists with whom we had stimulating and fruitful dis-

cussions, in particular to Ehud Altman, Gianni Blatter, Thierry Giamarchi, Antoine Georges, Corinna Kollath, Walter Hofstetter, Sebastian Huber, Lode Pollet, Päivi Törmä, Matthias Troyer, Felix Werner, Wilhelm Zwerger, and my co-examinator Manfred Sigrist.

Before starting my PhD in Zurich, I worked at the LKB/ENS in Paris on the “Rb2” (atom guide) experiment during one year. I would like to thank Jean Dalibard and David Guéry-Odelin for having given me this opportunity which was a very valuable experience.

My most profound thanks go to my family who has always supported me. Much of what I am and of what I have achieved I owe to my parents. My sisters, Sandy and Jennifer, are always there for me, thanks so much.

Finally, I would like to thank Catarine for all her love and support as well as for her comprehension when physics was taking some of our time.

Curriculum vitae

Kenneth John Günter

E-mail ken@kenneth.ch, web www.kenneth.ch

Personal information

Date of birth: 10th of April 1978
Place of birth: Zurich, Switzerland
Native place: Thörigen BE, Switzerland
Nationality: Switzerland and Great Britain

Education

1985 – 1991	Primary school	Schulhaus Apfelbaum, Zurich
Aug. 1991 – Jan. 1998	High school	Kantonsschule Oerlikon, Zurich
Oct. 1998 – Jul. 2000	Undergrad. studies in Physics	ETH Zurich
Oct. 2000 – Jul. 2001	ERASMUS scholarship	Universidad de Granada (Spain)
Oct. 2001 – Jul. 2002	Studies in Physics	ETH Zurich
Apr. 2003	Diploma in Physics	ETH Zurich

Research activity

Nov. 2002 – Mar. 2003	Quantum Optics Group at ETH Zurich: Diploma thesis under the supervision of Prof. T. Esslinger, <i>Frequenz- und Phasenstabilisierung von Diodenlasern.</i>
May 2003 – Mar. 2004	Cold Atoms Group at the Laboratoire Kastler Brossel, Ecole Normale Supérieure, Paris: 1 st year of PhD under the supervision of Dr. D. Guéry-Odelin and Prof. J. Dalibard.
Mar. 2004 – Sep. 2007	Quantum Optics Group at ETH Zurich: PhD under the supervision of Prof. T. Esslinger.
Nov. 2007 –	Laboratoire Kastler Brossel, Ecole Normale Supérieure, Paris: Postdoc in the group of Prof. J. Dalibard.

